

國 立 中 央 大 學

物 理 研 究 所
碩 士 論 文

Overdamped Brownian dynamics in Inhomogeneous
Temperature Field: Effective Potential, Transition Rate,
Landauer Limit, and Gyration in two-dimensions

研 究 生：潘勤華
指 導 教 授：黎壁 賢

中 華 民 國 一 百 一 十 四 年 六 月

國立中央大學圖書館學位論文授權書

填單日期：2025/5/30

2019.9 版

授權人姓名	潘勤華	學號	113222039
系所名稱	物理學系碩士班	學位類別	<input checked="" type="checkbox"/> 碩士 <input type="checkbox"/> 博士
論文名稱	Overdamped Brownian Dynamics in Inhomogeneous Temperature Field: Effective Potential, Transition Rate, Landauer Limit, and Gyration in two-dimensions	指導教授	黎璧賢

學位論文網路公開授權

授權本人撰寫之學位論文全文電子檔：

- 在「國立中央大學圖書館博碩士論文系統」

同意立即網路公開

同意 於西元_____年_____月_____日網路公開

不同意網路公開，原因是：_____

- 在國家圖書館「臺灣博碩士論文知識加值系統」

同意立即網路公開

同意 於西元_____年_____月_____日網路公開

不同意網路公開，原因是：_____

依著作權法規定，非專屬、無償授權國立中央大學、台灣聯合大學系統與國家圖書館，不限地域、時間與次數，以文件、錄影帶、錄音帶、光碟、微縮、數位化或其他方式將上列授權標的基於非營利目的進行重製。

學位論文紙本延後公開申請 (紙本學位論文立即公開者此欄免填)

本人撰寫之學位論文紙本因以下原因將延後公開

• 延後原因

- 已申請專利並檢附證明，專利申請案號：_____
- 準備以上列論文投稿期刊
- 涉國家機密
- 依法不得提供，請說明：_____

• 公開日期：西元_____年_____月_____日

※繳交教務處註冊組之紙本論文(送繳國家圖書館)若不立即公開，請加填「國家圖書館學位論文延後公開申請書」

研究生簽名：潘勤華

指導教授簽名：黎璧賢

國立中央大學碩士班研究生
論文指導教授推薦書

物理學系碩士班 學系/研究所 潘勤華 研究生
所提之論文 Overdamped Brownian dynamics in
Inhomogeneous Temperature Field: Effective Potential,
Transition Rate, Landauer Limit, and Gyration in two-
dimensions

係由本人指導撰述，同意提付審查。

指導教授

黎隆煥

(簽章)

114 年 6 月 3 日

國立中央大學碩士班研究生
論文口試委員審定書

物理學系碩士班 學系/研究所 潘勤華 研究生
所提之論文 Overdamped Brownian dynamics in
Inhomogeneous Temperature Field: Effective Potential,
Transition Rate, Landauer Limit, and Gyration in two-
dimensions

經由委員會審議，認定符合碩士資格標準。

學位考試委員會召集人

委

員

潘勤華

蔡陸波

田濬權

陳宣毅

中 華 民 國

114 年 6 月 23 日

1140619

摘要

我們透過解析法和朗之萬動力學模擬研究了非均勻溫度場中的過阻尼布朗動力學。在一維系統中，單軸溫度分佈和單勢阱陷阱可以產生單峰或雙峰穩態分佈，這些分佈可以用有效位勢來表徵。當有效勢具有雙勢阱結構時，我們推導出躍遷速率的一般近似公式。結果表明，躍遷速率越過有效勢壘遵循通常的 Kramers 指數行為。我們也考慮了雙勢阱的情況，所有理論和近似公式與數值模擬結果一致。

另一個主題是非均勻溫度場下的蘭道爾極限。這是一個具有時間相關勢的一維非平衡系統。我們的目標是找出與蘭道爾極限相關的有效溫度 \tilde{T} ，即 $k_B \tilde{T} \ln 2$ 。結果表明， \tilde{T} 可能無法表示為空間溫度分佈的簡單加權平均值。在某些情況下， \tilde{T} 可能會超出整個溫度範圍。這種偏差可能源自於熱流沿溫度梯度所引起的耗散。我們進一步推廣了蘭道爾極限，應用 Jarzynski 恆等式，並以有效位勢來表徵系統。

在二維系統中，我們研究了粒子通量場的空間行為。特別地，我們給出了無粒子通量的條件以及粒子通量旋度消失的位置。此外，我們推導出了高維零通量條件下有效勢的顯式表達式。研究發現，單個非均勻溫度場可以誘導布朗粒子發生平均旋轉運動，這是由於通量場中兩對渦旋強度的不對稱所造成的，較強的渦旋決定了平均粒子旋轉的主導方向。與雙溫度系統的布朗旋轉子不同，我們提出了一種更簡單的方法來實現布朗粒子的轉動，即使轉動速率低於雙溫度系統。

Overdamped Brownian Dynamics in Inhomogeneous Temperature Field: Effective Potential, Transition Rate, Landauer Limit, and Gyration in two-dimensions

by

Cin-Hua PAN

Abstract

We study overdamped Brownian dynamics in non-uniform temperature fields analytically and by Langevin dynamics simulations. In a one-dimensional system, a uniaxial temperature profile and a single-well trap can give rise to either unimodal or bimodal steady-state distributions, which can be characterized by an effective potential. We derive the general approximate formulas for the transition rate when the effective potential possesses a double-well structure. The results show that the transition rate over the effective barrier follows the usual Kramers' exponential behavior. We also consider the double-well potential case, and all theoretical and approximate formulas are consistent with numerical simulations.

Another topic is the Landauer limit under a non-uniform temperature field. This is a one-dimensional non-equilibrium system with a time-dependent potential. We aim to find the effective temperature \tilde{T} associated with the Landauer limit, which is $k_B \tilde{T} \ln 2$. The results show that \tilde{T} may not be expressed as a simple weighted average of the spatial temperature profile. In some situations, \tilde{T} can exceed the entire temperature range. This deviation arises from the dissipation induced by heat flow across the temperature gradient. We further generalized the Landauer limit by applying the Jarzynski equality to characterize the system using an effective potential.

In a two-dimensional system, we studied the spatial behavior of the particle flux field. In particular, we give the conditions that there is no particle flux and the locations where the curl of the particle flux vanishes. In addition, we derived an explicit expression for the effective potential under the zero-flux condition in higher dimensions. It is found that a non-uniform temperature field can induce a mean rotational motion for the Brownian particle, which is caused by the asymmetry in the strength of two vortex pairs in the flux field, and the stronger vortex pair determines the dominant direction of mean particle rotation. Different from the Brownian rotator of the two-temperature system, we propose a simpler method to realize the Brownian particle rotation even if the rotation rate is lower than the two-temperature system.

NATIONAL CENTRAL UNIVERSITY

Department of Physics

Master thesis

**Overdamped Brownian Dynamics in
Inhomogeneous Temperature Field:
Effective Potential, Transition Rate,
Landauer Limit, and Gyration in
two-dimensions**

研究生: Cin-Hua PAN

指導教授: Pik-Yin LAI

2025 年 6 月

CONTENTS

1	Introduction	1
2	Overdamped Langevin Equation Model with Multiplicative Noise	5
2.1	Overview of the Langevin Equation in Uniform Temperature Field	5
2.2	From the Einstein Relation Under a Non-uniform Temperature Field Deduces the Fokker-Planck Equation and the Langevin Equation	6
2.3	Stochastic Calculus Approach	10
2.4	Multiplicative Noise Models and Unit of Numerical Simulation	12
2.5	Entropy and Information in Stochastic Process	13
3	One-Dimensional System in Inhomogeneous Temperature Field	15
3.1	Non-Boltzmann Distribution under Harmonic Potential $\frac{1}{2}kx_1^2$	15
3.2	Transition Rate (K) in Non-Uniform Temperature Field	18
3.3	Generalization of Transition rate for y-axis symmetric single-well $U(x)$ and a unimodal $T(x)$	23
3.3.1	An example: Single-well potential and Gaussian temperature field	25
3.3.2	Another example: Transition rate correction for the double- well potential	31
3.4	Diffusion field reconstruction using steady-state position and diffu- sion constant distributions	35
3.4.1	An Example: Symmetrical diffusion field with a single peak .	36
4	Landauer Limit under a Non-uniform Temperature Field	39

5 Two-dimensional autonomous Brownian gyrator	48
5.1 The most general two-dimensional system	48
5.2 $T_{12} = T_{21} = 0$ but T_{11} and $T_{22} \neq 0$	49
5.2.1 The case of $T_{11}(x_1, x_2) = T_{22}(x_1, x_2) = T(x_1, x_2)$	50
6 Conclusion and Outlook	68
A Some Derivations	71
A.1 Overview of the Stochastic Wiener Process	71
A.2 Derivation of the Itô Lemma	72
A.3 Derivation of the Mean First Passage Time	72
A.4 Table of Integrals	73
Bibliography	74

LIST OF FIGURES

1.1 (a) The Brownian ratchet [9], where the ratchet on the right limits the direction of gear rotation, and the fan on the left is rotated by particle impact. (b) Büttiker-Landauer engine [2], where the potential well is periodic and has two temperatures T_1 (high temperature) and T_2 (low temperature).	2
2.1 N Brownian particles diffuse under the pressure difference on both sides, where the virtual cross-sectional area is A (blue area).	7
3.1 (a) The temperature field ($T_0 = 1$) varies with x_1 and a . (b) Under an inhomogeneous temperature field, the harmonic potential well can have two position states similar to a double-well potential. (c) Theoretical (solid curves) and numerical (circles) comparison of the probability density distribution shape varies with z . The theoretical critical value ($z = 1$) for unimodal ($z < 1$) and bimodal ($z > 1$) distributions is the green solid curve. In the bimodal distribution, the maximum well distance w occurs at $z = 2$, which is denoted by the blue solid curve, and its value is $\sqrt{\sigma^2/2}$. The distribution of P_{eqm} is derived using the bin quantities $x_{\text{bin}} = 316$ ($N_{\text{sample}} = 10^6$).	17
3.2 (a) The dwell-time distribution $P_{\text{dwell}}(t)$ is fitted to an exponential distribution. The solid lines are the exponential fitting lines, where τ is obtained by averaging the data. The symbols are the numerical results. Note that the sampling time $\Delta t = dt$ here, that is, only the iteration time $dt = 10^{-3}$ is used, while the number of samples is $N_{\text{sample}} = 10^5$	19

- 3.3 (a) Integral range of the function $G(x, y)$ (purple area). (b) The transition rate under harmonic potential and non-uniform temperature field $T(x_1) = 1/(1 + ax_1^2)$, where w is the width of the effective potential energy well composed of the potential energy and the temperature field. The solid curves are the results of solving the backward Fokker-Planck equation through numerical integration, and the circles are measured through the numerical solution of the Langevin equation. In contrast, the dashed curves are the Kramers rate formula solution, that is, use U_{eff} directly as the potential energy and the temperature field is a constant 1. The dotted curves represent the approximation of K . Note that the sampling time $\Delta t = dt$ here, while the number of samples is $N_{sample} = 10^5$

22

3.4 (a) Double-well effective potentials (dashed curves) experienced by a Brownian particle under a Gaussian temperature field $T(x)$ (dotted curve) and various single-well harmonic and anharmonic potential traps (solid curves). $\sigma = 0.5$ and $\Delta = 1$. The effective potentials measured from simulations of the Langevin dynamics are also shown (symbols). (b)-(d) Contour plots of the effective barrier height as a function of σ and Δ for different trapping potentials of $n = 2, 4, 6$. . .

29

3.5 Transition rate in the double-well effective potential under different heating profiles. (a) K vs. Δ for given values of σ , where dotted straight lines represent the convergence approximation line we calculated for $n = 2$ (Eq. (3.51)). (b) K vs. σ for given values of Δ . The symbols denote results from the Langevin simulations. The curves depict the theoretical results from numerical integration using (3.33).

30

3.6 The results of transition rate varies with E_{eff} . E_{eff} is changed by varying ε while fixing σ . The hollow symbols denote results from the Langevin simulation, the solid curves depict results from numerical integration, and the dashed curves present the approximation results. The red, blue, and black colors represent $n = 2, 4, 6$ respectively. (a) Taking the ambient temperature as the unit, the temperature T_0 of each data point is different. (b) After removing the influence of T_0 , the effective barrier height returns to a form similar to the Kramers rate. Both figures are fixed with $T_\infty = 1$ and $\sigma = 0.5$

30

3.7 (a) The double-well potential and the Gaussian temperature field. Transition rate K of a Brownian particle in a double-well trap under different heating profiles. Theoretical results (curves) are obtained using (3.57). K measured from the Langevin simulation is denoted by the symbols. (b) K vs. Δ for given E_b and σ . (c) K vs. σ for given E_b and Δ . (d) K vs. E_b for various values of σ and $\Delta = 0.5$. The transition rates for the cases of uniform temperatures of T_0 and T_∞ are also shown for comparison.	34
3.8 The two case $\sigma = 0.5$ ((a)-(b)) and $\sigma = 1.5$ ((c)-(d)) of steady-state position and diffusion distribution, where $D_0 = 2$, $D_\infty = 1$, and $\alpha = 0.5$ are fixed. We measure 100,000 trajectories, and the bin size is 316.	37
3.9 Reconstructed and real diffusion field, where the reconstructed diffusion field is obtained by solving Eq. (3.62) and the real diffusion field is described by Eq. (3.63).	38
4.1 (a) The control protocol. The red solid line represents the control function modulating the potential barrier, while the blue solid line adjusts the potential tilt. The dashed lines are the change rate of the control function. (b) The erase process. The left and right figures represent not erased and fully erased, respectively.	43
4.2 (a) The Landauer limit, as predicted by Eq. (4.21), aligns with the dotted line. (b) The Landauer limit can be higher than the entire temperature field. The circles, solid lines, and dashed lines represent the Langevin simulation, fitting curve, and the Landauer limit, taking T_0 as the temperature, respectively. (c) The Landauer limit varies with ε . The upper bound corresponds to the peak value shown in (b), and the thick and thin solid lines represent the 1st and 2nd-order theories, respectively, in Eq. (4.22). When σ is small, the 2nd-order coefficient is more important than when σ is large. (d) The Landauer limit varies with σ . The yellow region represents the normal Landauer limit (between T_0 and T_∞), while the blue region denotes the anomalous Landauer limit (exceeding the entire temperature field).	45
5.1 The definition of tilted angle is the σ_{i1} axis, where $i = U$ or T , starts counterclockwise from the first quadrant.	56

5.2 (a) Under the uniaxial Gaussian temperature field, the relative angle Ψ (purple solid curve) between two straight lines ($\nabla \times \vec{J} = 0$) vary with $\theta_T - \theta_U$ in a period. Note that when $\sigma_{T2} \rightarrow \infty$, Ψ is independent of σ_{T1} and σ_{T2} . We fixed $\theta_U = 0$, $\sigma_{U1} = \sqrt{2}$, $\sigma_{U2} = 1$, $\sigma_{T2} \rightarrow \infty$ and $a = 0$. (b) Under the uniaxial Gaussian temperature field and fixing the harmonic potential, the Langevin simulation of the mean angular velocity of the Brownian particle varies with θ_T . For all $\theta_T - \theta_U = 0$, $\pi/2$ and π , $\langle \omega \rangle = 0$. The fixed parameters are the same as (a). (c) Under the biaxial Gaussian temperature field, Ψ varies with $\theta_T - \theta_U$ in a period. The different σ_{T1} effects the waveform of Ψ . We fixed $\theta_U = 0$, $\sigma_{U1} = \sqrt{2}$, $\sigma_{U2} = \sigma_{T2} = 1$ and $a = 0$. (d) Under the biaxial Gaussian temperature field, the mean rotation angular velocity varies with θ_T . The direction of rotation is related to the relative sizes of σ_{T1} and σ_{T2} . It does not rotate when $\sigma_{T1} = \sigma_{T2}$. We fixed parameters that are the same as (c). (b) and (d) are obtained from $N_{sample} = 10^4$ trajectories and the time of each trajectory is $\tau = 10^3$.	60
5.3 Under the uniaxial Gaussian temperature field, the Langevin simulation of the steady-state probability density P_{ss} (color map) and the probability flux \vec{J} (vector field) under the fixed harmonic potential and the uniaxial Gaussian temperature field, while black solid curves represent the equipotential curve and the blue solid lines represent the points satisfying $\nabla \times \vec{J} = 0$. The grid size of P_{ss} is $x_{bin} = \frac{4}{99}$ ($N_{sample} = 10^7$) and the grid size of \vec{J} is $x_{bin} = \frac{4}{29}$ ($N_{sample} = 10^4$). We fixed $\sigma_{U1} = \sigma_{T1} = \sqrt{2}$, $\sigma_{U2} = 1$ and $a = 0$.	61
5.4 (a) The Langevin simulation of the total average entropy rate varies with θ_T under the uniaxial Gaussian temperature field (fixed $\sigma_{T2} = \infty$) and the harmonic potential well. (b) The Langevin simulation of the total average entropy rate varies with θ_T under the biaxial Gaussian temperature field (fixed $\sigma_{T2} = 1$) and the harmonic potential well. Both the samples of the figures are $N_{sample} = 10^5$, and $\sigma_{U1} = \sqrt{2}$ and $\sigma_{U2} = 1$.	63

5.5	\vec{J} varies with the tilted angle of temperature $T(x_1, x_2) = a + \exp\left(-\frac{x_1'^2}{\sigma_{T1}^2} - \frac{x_2'^2}{\sigma_{T2}^2}\right)$ under the non-tilted harmonic potential $U(x_1, x_2) = \frac{x_1^2}{\sigma_{U1}^2} + \frac{x_2^2}{\sigma_{U2}^2}$. The color map represents the probability density of the Brownian particle, and the black curves represent the equipotential curves. The vector field is \vec{J} , and the blue lines are the positions where $\nabla \times \vec{J} = 0$. The grid size of P_{ss} is $\frac{4}{99}$ ($N_{sample} = 10^7$) and \vec{v}_{av} is $\frac{4}{29}$ ($N_{sample} = 10^4$). We set $\theta_U = 0$, $a = 0$, $\sigma_{T1} = \sigma_{U1} = \sqrt{2}$ and $\sigma_{T2} = \sigma_{U2} = 1$	65
5.6	$E_b = 1$ and under the Mexican hat potential U_{hat} , the steady-state distribution of a Brownian particle through Langevin simulation. The black and blue curves represent $\nabla \times \vec{J} = 0$ and the lowest points of the potential. The orange dots represent the center of the vortices. Note that the \vec{J} vector field (white arrow) is amplified seven times relative to the harmonic potential well.	67

LIST OF TABLES

- | | |
|---|----|
| 4.1 The coefficients table of the first-order and second-order terms of two cases $\sigma = 0.65$ and $\sigma = 0.25$, where the numerical integral is obtained by integrating Eq. (4.20). | 46 |
|---|----|

INTRODUCTION

3 The Brownian heat engine has been studied by many groups in the past decade.
4 There are many studies about the Brownian heat engine of active particles and pas-
5 sive particles, which are considered theoretically feasible [1, 5, 11, 21]. We know that
6 the model of the classical heat engine is the Carnot engine, while most of the Brow-
7 nian gyrators discussed rely on changing the external potential energy to achieve
8 the four-stage heat engine cycle, thus turning the Brownian gyrator into a Brownian
9 heat engine. This type of heat engine is referred to as a non-autonomous active or
10 passive cyclic heat engine. Achieving a net directional motion of Brownian particles
11 typically requires the implementation of a time-dependent potential or a tempera-
12 ture field that varies in space or time. Among them, it is an interesting problem
13 to orient the average trajectory of Brownian particles only through the temperature
14 gradient. In many situations, spatially nonuniform temperature is characterized by a
15 time-independent temperature field in which temperature reservoirs can be created
16 at different temperatures or by localized heating sources. The temperature gradi-
17 ent can often give rise to a spatially non-uniform diffusion field or, in some cases,
18 give rise to thermophoretic effects [30] that result in a net particle flux due to the
19 non-uniform thermal fluctuations, manifesting the non-equilibrium nature [22].

20 An interesting question is whether we can build a device that can perform work
21 solely by harnessing thermal fluctuations. As early as 1962, the physicist Feynman
22 proposed a famous thought experiment, the Feynman ratchet (see Fig. 1.1). The
23 device has two heat reservoirs connected by a paddle. A gear in one of the reservoirs
24 can only rotate in one direction due to a ratchet constraint. In the other reservoir, due
25 to Brownian motion, molecules can only turn in a single direction as they randomly
26 hit the paddles. As long as there is a temperature difference between the two heat

27 reservoirs, the work done by rotating the gear does not violate the second law of
 28 thermodynamics. However, because the thermal fluctuations are very small, it is
 29 difficult to implement such a mechanical device directly.

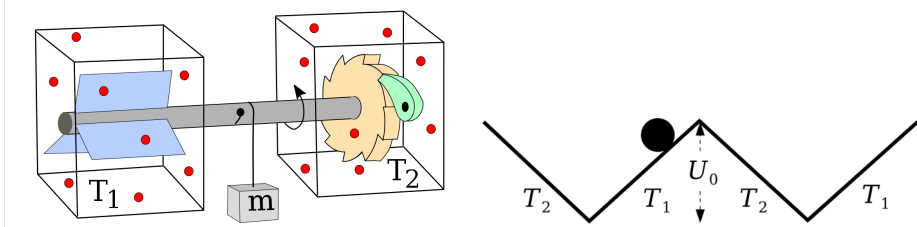


FIGURE 1.1: (a) The Brownian ratchet [9], where the ratchet on the right limits the direction of gear rotation, and the fan on the left is rotated by particle impact. (b) Büttiker-Landauer engine [2], where the potential well is periodic and has two temperatures T_1 (high temperature) and T_2 (low temperature).

30 One of the best-known methods for achieving directed motion of particles with
 31 average trajectories via thermal fluctuations is the Büttiker-Landauer engine.[2, 19].
 32 As shown in 1.1 (right), the system consists of a one-dimensional periodic potential
 33 landscape and two different temperature staggered arrangements. It is called a heat
 34 engine because it can extract work. In some papers, the overdamped model calcu-
 35 lates that its efficiency can reach the Carnot limit [22]. However, this calculation is
 36 invalid because the overdamped model directly ignores the inertia term, and heat
 37 is related to momentum transfer. In addition, when the underdamped Brownian
 38 model is considered, the result of taking the overdamped limit is different from that
 39 of using the overdamped model directly [2]. This means that the inertia effect leads
 40 this system not to achieve the Carnot limit. It is also important to note that an over-
 41 damped Brownian model with a temperature gradient will be underestimated when
 42 calculating heat or entropy. In the limit of extremely small but finite inertia, entropy
 43 generation is dominated by an anomalous contribution that has no corresponding
 44 contribution in the overdamped approximation [4]. This is also caused by directly
 45 ignoring inertia, and this problem only occurs when calculating heat; other physical
 46 quantities can be well described by the damping system.

47 Another system that can achieve orienteering is a two-dimensional Brownian gy-
 48 rator. Recently, the autonomous Brownian gyrator has been demonstrated experi-
 49 mentally and theoretically under two uniform temperature fields, but it cannot ex-
 50 tract work [6–7]. Experimentally, the Brownian gyrator is realized by an RC circuit

51 and observes the fluctuation of its voltage under the tilted harmonic potential and
52 two heat reservoirs. The working principle for this autonomous Brownian gyrator
53 rotation is the mean probability density flow generated by the non-thermal equilib-
54 rium system. Therefore, studying the characteristics of mean probability density
55 flow can help us develop the possibility of realizing the Brownian engine. The ro-
56 tation modes of this type of mean probability density flow usually rotate around
57 equiprobability contours. However, under the non-harmonic potential, extra cur-
58 rents will be generated, so that the mean probability density flow will not rotate
59 around the equiprobability contour. A year later, in [20], they experimentally used
60 an optical feedback trap to confirm that a Brownian gyrator of a colloidal particle
61 confined in a two-dimensional harmonic potential, a non-conservative force, and
62 two different effective temperatures on orthogonal axes can work as an autonomous
63 heat engine.

64 On the other hand, in the one-dimensional system with a non-uniform temper-
65 ature field, both the transition rate and the Landauer limit are also of interest. The
66 transition rate, which concerns the problem of escape dynamics, is widely applied
67 in fields such as chemistry, biophysics, and others [15, 17, 32]. The seminal work
68 of Kramers [14] laid the foundation for understanding the escape rate of a Brown-
69 ian particle from a metastable state under thermal fluctuations. Recently, people
70 have also been interested in the transition rate of self-propelled particles [31]. In
71 their experiment, a one-dimensional periodic potential landscape was produced on
72 a microgroove-patterned PDMS substrate, on which a self-propelled particle was
73 placed. Since the potential is an open boundary, the probability density function in
74 the steady state is non-equilibrium. Once the self-propulsion force is incorporated
75 into the potential energy, the escape dynamics of slowly rotating self-propulsion
76 particles in the potential landscape can be described by the effective potential. We
77 note that the transition rate under non-uniform temperature does not seem to be
78 mentioned (at least in [14]). However, many real-world systems exhibit spatially
79 varying temperature or diffusion profiles [28], which can lead to modifications in
80 noise characteristics and consequently in escape dynamics. On the other hand, the
81 Landauer limit (or Landauer’s principle) describes the minimum energy required to
82 irreversibly erase a bit, which is $k_B T \ln 2$, where k_B is the Boltzmann constant and T
83 is a constant temperature [3]. Landauer’s principle may seem simple, but there are
84 subtleties involved in understanding when thermodynamic irreversibility results. If

85 logically speaking, when an irreversible operation, such as erasure, is applied to ran-
86 dom data, the operation may still be thermodynamically reversible because it repre-
87 sents a transfer of entropy from the data to the environment. But if in computation, a
88 logically irreversible operation is usually applied to known data, this operation is ir-
89 reversible from a thermodynamic point of view, because the decrease in the entropy
90 of the ambient entropy data does not offset this increase. The most important point
91 of Landauer's principle is that measuring physical information does not necessar-
92 ily lead to energy loss, but the destruction of information will have an unavoidable
93 thermodynamic cost. There are many rigorous experimental or simulation results to
94 support this principle [8, 16, 24]. Since it is impossible for real-life systems to achieve
95 quasi-static processes, people have recently given a formula for the finite-time Lan-
96 dauer limit [25] at uniform temperature.

97 In this thesis, the main topics discussed can be divided into one-dimensional sys-
98 tems and two-dimensional systems. We first review the most general overdamped
99 Langevin equation and the corresponding Fokker-Planck equation in Chapter 2, and
100 also review stochastic energetics. In one-dimensional systems, following Kramers's
101 footsteps, we derived an approximate expression for the transition rate under a non-
102 uniform temperature field. Among them, special attention is paid to the transition
103 rate of the system with only effective (virtual) barriers in Chapter 3. On the other
104 hand, we try to derive the Landauer limit of the double-well potential under non-
105 uniform temperature in Chapter 4. In two-dimensional systems, we propose that
106 the passive Brownian particle under a non-uniform temperature field can also be a
107 Brownian gyrator in Chapter 5. Even though the rotation speed of this kind of Brow-
108 nian gyrator is lower than that of the two-temperature system Brownian gyrator, it
109 provides an easier experimental control for the Brownian engine. We only briefly in-
110 troduced how Brownian particles in non-uniform temperature fields become Brow-
111 nian cyclotrons and studied the behavior of particle fluxes. More in-depth energetic
112 studies are awaited in the future. Finally, the conclusion of this thesis is found in
113 Chapter 6.

114

2

115

116

OVERDAMPED LANGEVIN EQUATION MODEL WITH MULTIPLICATIVE NOISE

117

118

2.1 Overview of the Langevin Equation in Uniform Temperature Field

119 Brownian motion obeys the Langevin equation, which is a stochastic differential
 120 equation (SDE). The equation describes the position of the mesoscopic particle's ran-
 121 dom walk due to the collision of water molecules. The solution we care about is
 122 the ensemble average of an observable physical quantity H , written $\langle H \rangle$. The 1-
 123 dimensional Langevin equation is given by

$$\frac{dp}{dt} = -\frac{dU(x)}{dx} - \gamma \frac{p}{m} + \eta(t), \quad \frac{dx}{dt} = \frac{p}{m}, \quad (2.1)$$

124 where $U(x)$ is the potential energy, $-\gamma$ is the friction coefficient and η is the fluc-
 125 tuation force, that is, a white Gaussian process with the average 0 , $\langle \eta(t) \rangle = 0$ and
 126 $\langle \eta(t)\eta(t') \rangle = 2k_B T \delta(t-t')$. If we focus on the time scale $\Delta t \gg \frac{m}{\gamma}$, we can replace (2.1)
 127 approximately without the inertia term, called the overdamped Langevin equation.
 128 We only focus on the overdamped Langevin equation in this article, that is,

$$0 = -\frac{dU(x)}{dx} - \gamma \frac{dx}{dt} + \eta(t). \quad (2.2)$$

129 **2.2 From the Einstein Relation Under a Non-uniform**
 130 **Temperature Field Deduces the Fokker-Planck Equa-**
 131 **tion and the Langevin Equation**

132 Einstein's relation describes the relation between the diffusion coefficient D and mo-
 133 bility (the ratio between the terminal velocity of the particle and the force) at constant
 134 temperature T . In overdamped Brownian motion (low Reynolds number), the mo-
 135 bility is the reciprocal of the friction coefficient γ . The friction coefficient is defined
 136 as

$$\vec{F}_f = -\gamma \vec{v}, \quad (2.3)$$

137 where \vec{F}_f is the friction force and \vec{v} is the velocity of the particle. It is not difficult
 138 to derive the Einstein relation. First, let us assume that the N Brownian particles
 139 ($N \rightarrow \infty$) are not interacting and they are in a fluid (maybe a liquid or a gas). At
 140 a certain moment, assume that the particle concentration on the left is greater than
 141 the particle concentration on the right, as shown in Fig. 2.1. Then the left and right
 142 pressure on the middle particles are different (thus $p(x) > p(x + \Delta x)$). The pressure
 143 gradient (take $\Delta x \rightarrow 0$ limit) can be expressed as

$$\frac{\partial p(x)}{\partial x} \hat{i} = - \lim_{\Delta x \rightarrow 0} \frac{N F \hat{i}}{A \Delta x} = -\rho F \hat{i}, \quad (2.4)$$

144 where \hat{i} is the unit vector point to the x direction, ρ is the number density of Brownian
 145 particles at position x and time t , and F is the force exerted upon each Brownian
 146 particle. Assume that the Reynolds number of the fluid is less than 1, that is, the
 147 impact of fluid viscosity on particles is greater than the inertial effect, then F is equal
 148 to the negative resistance force F_f by a single particle, i.e., dynamic equilibrium.

$$-\vec{F} = \vec{F}_f = -\gamma \vec{v}, \quad (2.5)$$

149 where v is the velocity of a particle due to the force F . Note that this assumption
 150 ignores the effect of inertia. The Van't Hoff law for osmotic pressure is given by

2.2. From the Einstein Relation Under a Non-uniform Temperature Field Deduces the Fokker-Planck Equation and the Langevin Equation

¹⁵¹ (Einstein's derivation cf. [10])

$$p = \rho k_B T, \quad (2.6)$$

¹⁵² where p is the pressure. Taking the derivative of (2.6), we get

$$\frac{\partial p(x)}{\partial x} = k_B T \frac{\partial \rho(x)}{\partial x}. \quad (2.7)$$

¹⁵³ Combining equation (2.4), (2.5) and (2.7), one get

$$k_B T \frac{\partial \rho}{\partial x} = -\rho \gamma v. \quad (2.8)$$

¹⁵⁴ However, Fick's first law tells us

$$\rho v = -D \frac{\partial \rho}{\partial x}. \quad (2.9)$$

¹⁵⁵ Comparing (2.8) and (2.9), we get

$$D = \frac{k_B T}{\gamma} = \text{const.} \quad (2.10)$$

¹⁵⁶ This is called the Einstein relation.

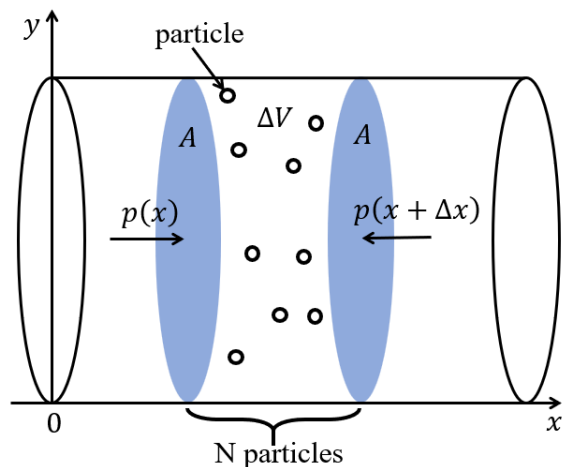


FIGURE 2.1: N Brownian particles diffuse under the pressure difference on both sides, where the virtual cross-sectional area is A (blue area).

¹⁵⁷ For liquids, when the Reynolds number is small, the resistance of a sphere with
¹⁵⁸ radius r satisfies Stokes' law.

$$\vec{F}_f = -\gamma \vec{v} = -6\pi r \eta \vec{v}, \quad (2.11)$$

¹⁵⁹ where η is the viscosity coefficient of the liquid. Substituting (2.11) into (2.10), we get

$$D = \frac{k_B T}{6\pi r \eta}. \quad (2.12)$$

¹⁶⁰ This is called the Stokes-Einstein formula. Next, we will use the same method to de-
¹⁶¹ rive the Einstein relation under the non-uniform temperature field and the presence
¹⁶² of external force \vec{F}_{ex} . Taking the derivative of (2.6) and using (2.3) again, we get

$$\frac{\partial p(x)}{\partial x} = k_B \frac{\partial T(x)}{\partial x} \rho(x) + k_B T(x) \frac{\partial \rho(x)}{\partial x} = -\rho(x) F. \quad (2.13)$$

¹⁶³ Now, the total force on the particle becomes (written in the form of Fick's law)

$$\begin{aligned} F + F_{ex} &= -k_B T_x(x) - k_B T(x) \frac{\rho'(x)}{\rho(x)} + F_{ex} = \gamma(x) v \\ &= -\tilde{D}(x) \frac{\partial \rho(x)}{\partial x} \frac{\gamma(x)}{\rho(x)}, \end{aligned} \quad (2.14)$$

¹⁶⁴ where ($\rho(x) \neq \text{const.}$)

$$\begin{aligned} \tilde{D}(x) &= \frac{k_B T(x)}{\gamma(x)} + \frac{k_B T'(x)}{\gamma(x)} \frac{\rho(x)}{\rho'(x)} - \frac{F_{ex}(x)}{\gamma(x)} \frac{\rho(x)}{\rho'(x)} \\ &= D(x) \left(1 + \frac{T'(x)}{T(x)} \frac{\rho(x)}{\rho'(x)} - \frac{F_{ex}(x)}{k_B T(x)} \frac{\rho(x)}{\rho'(x)} \right), \end{aligned} \quad (2.15)$$

¹⁶⁵ the superscript "prime" represents the derivative for x and $D(x) = \frac{k_B T(x)}{\gamma(x)}$. We can
¹⁶⁶ see that the functional form of the diffusion coefficient under a non-uniform temper-
¹⁶⁷ ature field is different from that of the constant temperature field. It has the physical
¹⁶⁸ meaning in the second term in (2.15). One is the velocity v_p caused by the particle
¹⁶⁹ concentration gradient, that is, if T is a constant, the equation (2.13) can be written
¹⁷⁰ as

$$v_p \equiv -\frac{k_B T}{\gamma(x)} \frac{\rho'(x)}{\rho(x)}. \quad (2.16)$$

2.2. From the Einstein Relation Under a Non-uniform Temperature Field Deduces the Fokker-Planck Equation and the Langevin Equation

- ¹⁷¹ The other is the velocity v_t caused by the temperature gradient, that is, if $\rho(x)$ is a
¹⁷² constant, the equation (2.17) can be written as

$$v_t \equiv -\frac{k_B}{\gamma(x)} T'(x). \quad (2.17)$$

- ¹⁷³ Thus, substituting (2.16) and (2.17) into (2.15), we get

$$\tilde{D}(x) = D(x) \left(1 + \frac{v_t}{v_p} - \frac{F_{ex}(x)}{k_B T(x)} \frac{\rho(x)}{\rho'(x)} \right). \quad (2.18)$$

- ¹⁷⁴ This means if v_p is fixed and $F_{ex} = 0$, the temperature gradient will change the diffusion speed (\tilde{D} can be greater than D or less than D). Now we will derive the Fokker-
¹⁷⁵ Planck equation and the Langevin equation. Note that the number density of the
¹⁷⁶ particles $\rho(x)$ should be conserved, which directly gives the Fokker-Planck equation

$$\frac{\partial \rho(x, t)}{\partial t} + \nabla \cdot (-\tilde{D} \nabla \rho(x, t)) = 0. \quad (2.19)$$

- ¹⁷⁸ Substituting \tilde{D} into (2.19), using the product rule of calculus and the fact that the
¹⁷⁹ probability density function $P(x, t) \equiv \frac{\rho(x, t)}{N}$, we get the Fokker-Planck equation

$$\frac{\partial P(x, t)}{\partial t} = -\frac{\partial}{\partial x} \left\{ \left[\frac{F_{ex}(x)}{\gamma(x)} + k_B T(x) \frac{\partial}{\partial x} \left(\frac{1}{\gamma(x)} \right) \right] P(x, t) \right\} + \frac{\partial^2}{\partial x^2} \left(\frac{k_B T(x)}{\gamma(x)} P(x, t) \right) \quad (2.20)$$

$$= -\frac{\partial}{\partial x} (\mu(x) P(x, t)) + \frac{\partial^2}{\partial x^2} (D(x) P(x, t)), \quad (2.21)$$

- ¹⁸⁰ where $\mu(x)$ is the drift caused by the external forces, the non-uniform temperature,
¹⁸¹ and the non-uniform friction coefficient. Of course, if force is a potential force, then
¹⁸² $F_{ex} = -\frac{\partial U(x)}{\partial x}$ in (2.20). Whether T or γ in (2.20) is a constant affects the form of
¹⁸³ the equation. The intuitive understanding is that temperature actively transports
¹⁸⁴ energy, but friction does not. This formula is mentioned in K. Sekimoto's book [27],
¹⁸⁵ but it is derived using different methods (we will do a brief review later). The effect
¹⁸⁶ of temperature on the friction coefficient is different in air and liquid. In the gas,
¹⁸⁷ the effect is called the Enskog-Chapman effect; in the liquid, the effect is called the
¹⁸⁸ Ludwig-Soret effect (see [23]). Now, if the stochastic process is considered to be a
¹⁸⁹ Markov process, equation (2.21) can be written in the form of a stochastic differential

¹⁹⁰ equation (SDE) using the Itô lemma.

$$dX_t = \mu(X_t)dt + \sqrt{2D(X_t)} \cdot dB_t, \quad (2.22)$$

¹⁹¹ where the subscript t represents a random process that varies over time, X_t is the
¹⁹² trajectory of the particle, and B_t is the standard Wiener process. Equation (2.22) is
¹⁹³ the Itô form of SDE, and note that it is the Langevin equation written using rigorous
¹⁹⁴ mathematical form.

¹⁹⁵ 2.3 Stochastic Calculus Approach

¹⁹⁶ The form of the Langevin equation (2.1) with the Markov process is not rigorous
¹⁹⁷ due to the poor mathematical differential properties of $\langle \eta(t)\eta(t') \rangle = \delta(t - t')$, i.e., not
¹⁹⁸ differentiable; therefore, the stochastic calculus was developed. The standard form
¹⁹⁹ of a stochastic differential equation is written rigorously in mathematics as (2.22),
²⁰⁰ and there are different product methods for the product before dB_t . Those different
²⁰¹ product methods are called the α convention written as " \times_α " in the book [29]. For
²⁰² some special values of α , there are some special names. If $\alpha = 0$, it is called Itô-type
²⁰³ calculus and written as " \cdot ", such as the product symbol form of equation (2.22). If
²⁰⁴ $\alpha = 1/2$, it is called Stratonovich-type calculus and written as " \circ ". If $\alpha = 1$, it is called
²⁰⁵ anti-Itô-type calculus and written as " \odot ". All different calculus product types can be
²⁰⁶ written in Itô type through the Itô lemma, such as (2.22), but the different conventions
²⁰⁷ can generate new terms in the drift $\mu(X_t)$. The Itô lemma for any function $f(X_t)$ is
²⁰⁸ given by (see [27] or Appendix A)

$$df(X_t) = [\mu(X_t, t)f'(X_t) + D(X_t, t)f''(X_t)] dt + \sqrt{2D(X_t, t)} \cdot dB_t. \quad (2.23)$$

²⁰⁹ And the α convention is defined by

$$[\alpha f(s + \Delta s) + (1 - \alpha)f(s)] (B_{s+\Delta s} - B_s) \rightarrow f(s) \times_\alpha dB_s. \quad (2.24)$$

²¹⁰ These conventions can simplify our writing of μ in (2.22) into only the forces like the
²¹¹ Langevin equation (2.1), but the price paid is that different situations have different
²¹² conventions. For example, in equation (2.22), if only γ is a constant (should use $\alpha =$

2.3. Stochastic Calculus Approach

²¹³ 0), it can be written as

$$dX_t = \frac{F_{ex}(x)}{\gamma} dt + \sqrt{2D(X_t)} \cdot dB_t, \quad (2.25)$$

²¹⁴ and if only T is a constant (should use $\alpha = 1$), it should be written

$$dX_t = \frac{F_{ex}(x)}{\gamma(x)} dt + \sqrt{2D(X_t)} \odot dB_t. \quad (2.26)$$

²¹⁵ Let us verify that the equation (2.26) satisfies the equation (2.21). Using (2.23) and
²¹⁶ (2.24), we get the method of converting a convention to Itô

$$f(s) \times_{\alpha} dB_t = f(s) \cdot dB_t + \alpha \sqrt{2D(s)} f'(s) dt, \quad (2.27)$$

²¹⁷ where we use $dBdt = 0$ and $(dB)^2 = dt$. This is because the order dB is \sqrt{dt} (Wiener
²¹⁸ process), and we can ignore all infinitesimal amounts greater than dt (see [27]). Sub-
²¹⁹ stituting $f(X_t) = \sqrt{2D(X_t)}$ into (2.27), (2.26) becomes

$$dX_t = \left(\frac{F_{ex}(X_t)}{\gamma(X_t)} + k_B T \frac{\partial}{\partial X_t} \left(\frac{1}{\gamma(X_t)} \right) \right) dt + \sqrt{2D(X_t)} \cdot dB_t. \quad (2.28)$$

²²⁰ Obviously, (2.25) (when only γ is a constant) or (2.28) (when only T is a constant) is
²²¹ the same as equation (2.22) with different $\mu(X_t)$ respectively.

²²² Now let us generalize the Fokker-Planck equation (2.21) to d-dimensional space.
²²³ Start from SDE (2.22) but $\vec{\mu}$ is a d-dimensional vector and $\overset{\leftrightarrow}{D}$ is a $d \times d$ tensor. Then,
²²⁴ (2.21) can be written as

$$\frac{\partial P(\vec{r}, t)}{\partial t} = - \sum_i^d \frac{\partial}{\partial x_i} (\mu_i P(\vec{r}, t)) + \sum_{i,j}^d \frac{\partial^2}{\partial x_i \partial x_j} (D_{ij} P(\vec{r}, t)). \quad (2.29)$$

²²⁵ Using the ∇ operator and considering the potential force in $\mu(x)$, it can be written as

$$\frac{\partial P(\vec{r}, t)}{\partial t} = \nabla \cdot \left\{ \frac{1}{\gamma(\vec{r})} \left[P(\vec{r}, t) \nabla U(\vec{r}) + k_B \nabla \cdot \left(\overset{\leftrightarrow}{T}(\vec{r}) P(\vec{r}, t) \right) \right] \right\} = -\nabla \cdot \vec{J}, \quad (2.30)$$

²²⁶ where \vec{J} is probability flux, $\overset{\leftrightarrow}{T}$ is temperature tensor field (> 0) and $P(\vec{r}, t)$ is the space-
²²⁷ time probability density of a Brownian particle. Here, the local Einstein relation
²²⁸ $\overset{\leftrightarrow}{D}(x) = \frac{k_B T(x)}{\gamma(x)}$ is assumed.

2.4 Multiplicative Noise Models and Unit of Numerical Simulation

In numerical simulations, we typically do not directly solve the Fokker-Planck equation but instead use a method similar to the Monte Carlo method, namely the Langevin equation. It is convenient to make the units dimensionless for numerical simulations. x in a unit of some length scale of the potential (sig), t in a unit of $\gamma \cdot sig^2/k_B T$ (i.e., the unit of potential energy $U(\vec{r})$ is $k_B T$), and we set $\gamma = 1$. From now on, if there is no special mention, the time step, $dt = 10^{-3}$ is used. Using the Einstein summation convention, the d-dimensional overdamped Langevin equation with the diffusion tensor $D_{\mu\nu}(\vec{r})$ and the potential force is given by

$$\dot{x}_\mu = \frac{1}{\gamma(\vec{r})} \frac{\partial U(\vec{r})}{\partial x_\mu} + \sqrt{2D_{\mu\nu}(\vec{r})} \times_\alpha \xi_\nu(t), \quad (2.31)$$

where $\langle \xi_\mu(t) \xi_\nu(t') \rangle = \delta(t - t')$, that is standard zero-mean Gaussian white noise. Note that Euler's method (say Itô form) is often used to solve the Langevin equation numerically. As mentioned before if γ is a constant ($\alpha = 0$, i.e., Itô), (2.31) written as

$$\dot{x}_\mu = \frac{1}{\gamma} \frac{\partial U(\vec{r})}{\partial x_\mu} + \sqrt{2D_{\mu\nu}(\vec{r})} \cdot \xi_\nu(t). \quad (2.32)$$

If $T_{\mu\nu}$ is a constant ($\alpha = 1$, i.e., anti-Itô), (2.31) written as

$$\dot{x}_\mu = \frac{1}{\gamma(\vec{r})} \frac{\partial U(\vec{r})}{\partial x_\mu} + \frac{\partial D_{\mu\nu}(\vec{r})}{\partial x_\nu} + \sqrt{2D_{\mu\nu}(\vec{r})} \cdot \xi_\nu(t). \quad (2.33)$$

The steady-state solution of equation (2.33) is boring in a one-dimensional system. Because the steady-state solution at constant temperature has nothing to do with $\gamma(\vec{r})$. This can be seen from the equation (2.30) because one-dimensional steady-state should $\vec{J}(\vec{r}) = \text{const.} = 0$, i.e., no particle flux (we will give a proof in chapter 5). In this thesis, we only focus on the equation (2.32) (Itô form), that is, the multiplicative noise is caused by the spatial variation of the temperature field.

2.5 Entropy and Information in Stochastic Process

250 In the macroscopic world, heat can be felt indirectly, such as melting ice cubes. But
 251 there is no concept of heat in the microscopic world; everything is the movement
 252 of particles. We can define the energy given to Brownian particles by the thermal
 253 environment as heat, while work is the energy given to the Brownian particle by an
 254 external agent (e.g., change in potential energy over time, more broadly defined as en-
 255 ergy other than heat). This can be given by the Langevin equation. The heat flowing
 256 into the system from the μ -th thermal environment is defined as (no summation)

$$d'Q_\mu \equiv \left(-\gamma(\vec{r}) \frac{dx_\mu}{dt} + \eta_\mu(t) \right) \circ dx_\mu(t) = -\frac{\partial U(\vec{r})}{\partial x_\mu} \circ dx_\mu, \quad (2.34)$$

257 where “ \circ ” represents the Stratonovich type. The reason for using Stratonovich-type
 258 products is based on the perspective of energy conservation in K. Sekimoto’s book
 259 [27]. The work is defined as

$$d'W \equiv \frac{\partial U(\vec{r}, a)}{\partial a} \circ da, \quad (2.35)$$

260 where a is the external time-varying parameter. In a broader definition, work is
 261 energy other than heat; that is, if there is a non-conservative force, there are also con-
 262 tributions from conservative forces [20]. In addition, generalized entropy is called
 263 Shannon entropy, and it can be defined by the probability, $P, \langle S \rangle \equiv -k_B \sum_i P_i \ln P_i$,
 264 where $\sum_i \ln P_i$ is called surprise. In information theory, the higher the Shannon
 265 entropy, the more information can be transmitted, and the higher the uncertainty
 266 about something. Generally, the contribution of total entropy changes consists of
 267 the system and the thermal environment entropy changes. The heat of thermal envi-
 268 ronments with non-uniform temperature fields can be seen as extracting or releasing
 269 heat from a series of many different constant-temperature environments. The most
 270 general total entropy production rate along a non-equilibrium-steady-state trajectory
 271 can be expressed as ($k_B = 1$)

$$\left(\frac{dS}{dt} \right)_{\text{ssf}} = \vec{v}_{av}^\top(\vec{r}) \cdot \overset{\leftrightarrow}{D}^{-1}(\vec{r}) \cdot \vec{v}_{av}(\vec{r}), \quad (2.36)$$

272 where \vec{v}_{av} is the average probability density flow velocity, that is $\vec{J} = P\vec{v}_{av}$, and $\overset{\leftrightarrow}{D}$ is
 273 the diffusion tensor. “ssf” represents along a steady-state path. This conclusion can
 274 be derived from the Fokker-Planck equation. In numerical simulations, we also use
 275 the following method to calculate $\vec{v}_{av}(\vec{r})$ as in [6].

$$\vec{v}_{av}(\vec{r}) \approx \frac{1}{2\Delta t} \{ \langle [\vec{r}(t + \Delta t) - \vec{r}(t)] | \vec{r}'(t) = \vec{r} \rangle + \langle [\vec{r}(t) - \vec{r}(t - \Delta t)] | \vec{r}'(t) = \vec{r} \rangle \}, \quad (2.37)$$

276 that is, the average of inflow and outflow $\vec{v}_{av}(\vec{r})$ over all spatial grids. Moreover,
 277 Frisman and Ronceray combined information theory to define the information on
 278 Brownian particle trajectories [13]. The information rate along a trajectory can be
 279 written as

$$\left(\frac{dI}{dt} \right)_{ssf} = \vec{F}^\top(\vec{r}) \cdot \overset{\leftrightarrow}{D}^{-1}(\vec{r}) \cdot \vec{F}(\vec{r}), \quad (2.38)$$

280 where $\vec{F}(\vec{r})$ is the force field. As mentioned before, the higher information rate
 281 means that the system is more difficult to predict.

282

283

284

ONE-DIMENSIONAL SYSTEM IN INHOMOGENEOUS TEMPERATURE FIELD

3.1 Non-Boltzmann Distribution under Harmonic Potential $\frac{1}{2}kx_1^2$

287 In the one-dimensional case, the diffusion field competes with the potential energy.
 288 Therefore, we can expect to find an effective potential energy that maps into an
 289 isothermal system description. The one-dimensional-steady-state solution of equa-
 290 tion (2.30) is $\vec{J} = \text{const}$. However, since the potential limits the particle to infinity, a
 291 reasonable assumption for the harmonic potential is $\vec{J} = 0$ at the boundary; therefore,
 292 $\vec{J} = 0$ everywhere (there is no particle flux condition for high-dimensional systems,
 293 which we will give in [chapter 5](#)). From equation (2.30) (set $k_B = 1$), we get

$$T(x_1) \frac{dP(x_1)}{dx_1} + \left(\frac{d}{dx_1} (U(x_1) + T(x_1)) \right) P(x_1) = 0. \quad (3.1)$$

294 The solution of equation (3.1) is

$$P(x_1) = \frac{1}{Z} \exp \left(- \int \frac{\frac{d}{dx_1} (U(x_1) + T(x_1))}{T(x_1)} dx_1 \right) \equiv \frac{1}{Z} \exp (-U_{eff}(x_1)), \quad (3.2)$$

295 where Z is the partition function, and $U_{eff}(x_1)$ is the effective potential. It is easy to
 296 see that when T is a constant, $P(x_1)$ obeys the Boltzmann distribution form. First,
 297 we consider the Lorentzian temperature profile $T(x_1) = T_0/(1 + ax_1^2)$, where T_0 is

298 a constant, and $a > 0$. In this situation, the diffusion force pushes the Brownian
 299 particle away from $x_1 = 0$ due to the temperature gradient field (see Fig. 3.1(a)).
 300 However, the harmonic potential constrains particles to diffuse outward. Therefore,
 301 the distribution we expected to be bimodal. The effective potential in this case can
 302 be derived to be (using (3.2))

$$U_{eff}(x_1) \equiv \frac{k}{T_0} \left(\frac{1}{2}x_1^2 + \frac{1}{4}ax_1^4 \right) - \ln(1 + ax_1^2), \quad (3.3)$$

303 where T_0 is a constant. Thus, the equilibrium distribution, $P_{eqm}(x_1)$ is given by

$$P_{eqm} \propto \exp(-U_{eff}(x_1)) = (1 + ax_1^2) \exp\left(-\left(\frac{1}{2}\frac{x_1^2}{\sigma^2} + \frac{a}{4}\frac{x_1^4}{\sigma^2}\right)\right), \quad (3.4)$$

304 where $\sigma^2 = T_0/k$ is the width of the distribution when $a = 0$, i.e., constant tem-
 305 perature (Gaussian distribution). The distribution shape of P_{eqm} is determined by σ
 306 and a . We are interested in the transition rate in a bimodal distribution because this
 307 is “similar” to a double-well distribution. As shown in Fig. 3.1(c), even if the har-
 308 monic potential only has a single well, we can also turn it into a bimodal distribution
 309 through the temperature field. The effective barrier height E_{eff} of U_{eff} is given by

$$|E_{eff}(a\sigma^2)| = \ln\left((2a\sigma^2)^{\frac{1}{2}} \exp\left(\frac{1}{4a\sigma^2} - \frac{1}{2}\right)\right), \quad (2a\sigma^2 > 1). \quad (3.5)$$

310 It is an unimodal distribution when $a\sigma^2 \leq \frac{1}{2}$. The critical point between unimodal
 311 and bimodal distributions is when the equal sign holds. If we fix σ and vary a , the
 312 barrier height diverges as $\ln(a)$. In addition, the distance of the well from the origin
 313 of U_{eff} , w , is not constant when we fixed σ and vary a . w^2 can be written as (recall
 314 bimodal distribution requires $a\sigma^2 > \frac{1}{2}$)

$$w^2 = \sqrt{\frac{2\sigma^2}{a}} - \frac{1}{a}. \quad (3.6)$$

315 Therefore, the extreme value of w occurs at $a\sigma^2 = 2$ (see Fig. 3.1). At this point, the
 316 maximum value is $w^2 = \frac{\sigma^2}{2}$. In other words, it is not that the larger the temperature
 317 gradient, say large a , is near the origin, the wider the distribution will be. This is be-
 318 cause when a is large, the diffusion field far away from the origin attenuates rapidly,
 319 that is, the particle does not move very much (the thermal fluctuation is small). For

3.1. Non-Boltzmann Distribution under Harmonic Potential $\frac{1}{2}kx_1^2$

320 simplicity, we can represent (3.3) by two independent parameters E_{eff} and w , which
 321 is written as

$$U_{eff}(x) = \frac{z-1}{z^2} \left(\left(\frac{x}{w} \right)^2 + \frac{z-1}{2} \left(\frac{x}{w} \right)^4 \right) - \ln \left(1 + (z-1) \left(\frac{x}{w} \right)^2 \right), \quad (3.7)$$

322 where $z^2 \equiv 2a\sigma^2$ in (3.5) which only related to E_{eff} is the curvature ratio of $U(x_1 = 0)$
 323 and $T(x_1 = 0)$. Note that in numerical simulation, we use the parameters a and σ to
 324 vary w and E_{eff} . Before Section 3.3, we choose the unit in terms of

$$[\text{length}] = \left(\frac{k_B T_0}{k} \right)^{1/2}; \quad [\text{energy}] = k_B T_0; \quad [\text{time}] = \frac{\gamma[\text{length}]}{k_B T_0}.$$

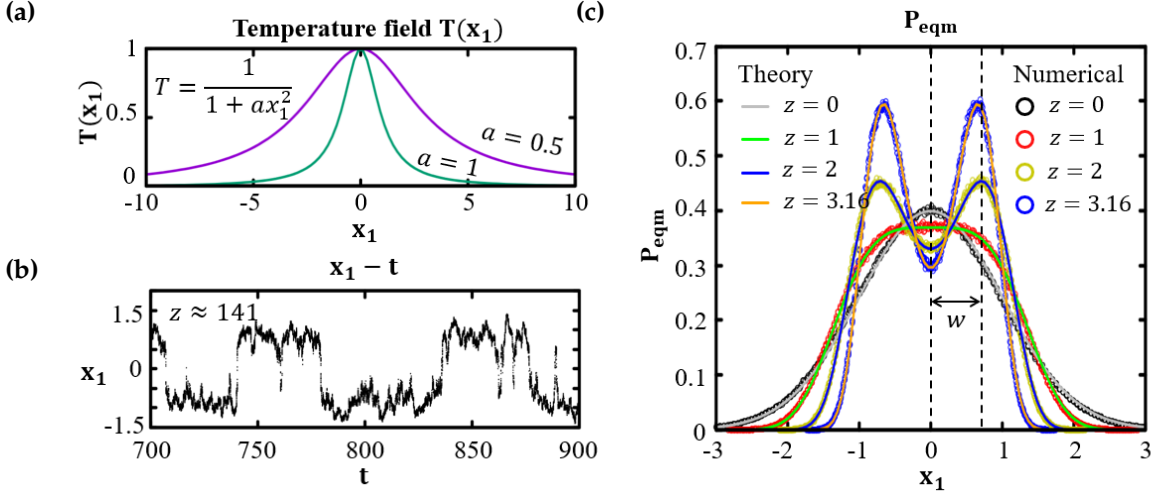


FIGURE 3.1: (a) The temperature field ($T_0 = 1$) varies with x_1 and a . (b) Under an inhomogeneous temperature field, the harmonic potential well can have two position states similar to a double-well potential. (c) Theoretical (solid curves) and numerical (circles) comparison of the probability density distribution shape varies with z . The theoretical critical value ($z = 1$) for unimodal ($z < 1$) and bimodal ($z > 1$) distributions is the green solid curve. In the bimodal distribution, the maximum well distance w occurs at $z = 2$, which is denoted by the blue solid curve, and its value is $\sqrt{\sigma^2/2}$. The distribution of P_{eqm} is derived using the bin quantities $x_{bin} = 316$ ($N_{sample} = 10^6$).

3.2 Transition Rate (K) in Non-Uniform Temperature Field

We can see that bimodal systems have two position states (see Fig. 3.1(b)). What is the transition rate between these two states? The transition time means how long a Brownian particle stays on average in one of the wells before it jumps to the other. We define the transition state as completed when the particle touches the barrier (at $x_1 = 0$). The transition rate is the reciprocal of the mean dwell time in the well. In chemistry, a barrier is the activation energy of a chemical reaction. The relation between the reaction rate constant (K) and the barrier height follows the Arrhenius equation. It is given by

$$K \propto \exp(-E_{eff}), \quad (3.8)$$

where E_{eff} is the activation energy or the barrier height. The transition rate (1/dwell-time) is like the reaction rate constant. A faster reaction rate occurs at higher temperatures. We will see later that the proportional constant in (3.8) is related to the curvature of the barrier and the well.

1. Dwell-Time Distribution $P_{dwell}(t)$

If the escape of particles from a potential well follows a Poisson process, then the dwell time, the time a particle spends inside the well before escaping, should follow an exponential distribution. This can be understood through queuing theory. Imagine particles as customers waiting in line to be "served" by the system, i.e., to escape the well. In a Poisson process, the number of escape events in a fixed time interval follows the Poisson distribution. The time between successive escape events, or the dwell time of each particle, follows an exponential distribution. This illustrates the fundamental relationship between the Poisson distribution (event count over time) and the exponential distribution (time between events). The timing of the events in the Poisson process is random and does not affect each other. The exponential distribution is given by

$$P_{dwell}(t) = \frac{1}{\tau} \exp\left(\frac{-t}{\tau}\right), \quad (3.9)$$

where τ is the average time of $P_{dwell}(t)$. Fig. 3.2 shows the logarithmic transition time distribution for a particle escaping from the left potential well (fixed $w = 1$, vary

3.2. Transition Rate (K) in Non-Uniform Temperature Field

353 E_{eff}), and we compare the measured dwell time in the numerical solution with the
 354 theoretical fitting (solid line). As we expected, the waiting time distribution of the
 355 particles is exponential. We observed that the higher E_{eff} , the longer the mean dwell
 356 time τ . From a probabilistic perspective, a higher barrier means that the particle
 357 needs to wait for large thermal fluctuations to escape the well; therefore, the chance
 358 of escape is reduced.

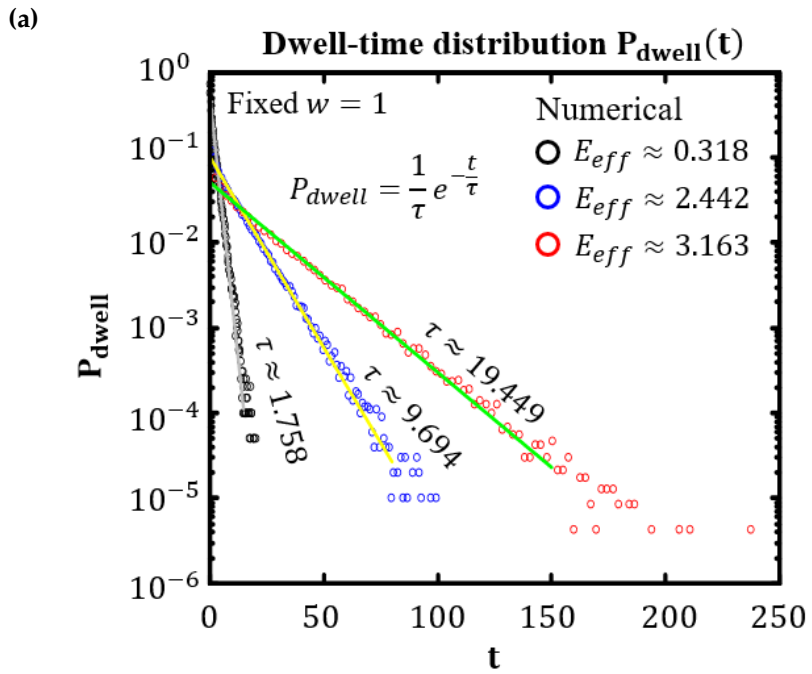


FIGURE 3.2: (a) The dwell-time distribution $P_{dwell}(t)$ is fitted to an exponential distribution. The solid lines are the exponential fitting lines, where τ is obtained by averaging the data. The symbols are the numerical results. Note that the sampling time $\Delta t = dt$ here, that is, only the iteration time $dt = 10^{-3}$ is used, while the number of samples is $N_{sample} = 10^5$.

359 2. Mean First Passage Time, $\tau(x)$

360 Kramers has long completed the description of the transition rate in a uniform tem-
 361 perature field. However, when the temperature field is non-uniform, can we use
 362 U_{eff} to describe the transition rate equivalently? If not, what is the difference be-
 363 tween the actual values and the U_{eff} description? The mean first passage time is the
 364 function that, given an initial position, we can predict how long it will take on aver-
 365 age to reach the specified position. It can be solved by the one-dimensional backward

³⁶⁶ Fokker-Planck equation [14, 27],

$$\mathcal{L}^\dagger \tau(x) \equiv \left[\left(-\frac{\partial U}{\partial x} + k_B T(x) \frac{\partial}{\partial x} \right) \frac{1}{\gamma(x)} \frac{\partial}{\partial x} \right] \tau(x) = -1, \quad (3.10)$$

³⁶⁷ where $\tau(x)$ is the mean first page time and \mathcal{L}^\dagger is the adjoint operator of the Fokker-
³⁶⁸ Planck operator \mathcal{L} . Note that the second term in parentheses must differentiate to
³⁶⁹ the right, and U is the original potential. We derived the equation in [Appendix A](#).
³⁷⁰ The solution of (3.10) with the boundary absorption condition can be written as (set
³⁷¹ $k_B, \gamma = 1$)

$$\tau(-x) = \int_{-x}^0 \exp \left(\int^y \frac{U'(x)}{k_B T(x)} dx \right) dy \int_{-\infty}^y \exp \left(- \int^{x'} \frac{U'(x)}{k_B T(x)} dx \right) \frac{\gamma}{k_B T(x')} dx', \quad (3.11)$$

³⁷² where $U'(x)$ is the derivative of U with respect to x . With $U(x)$ and $T(x)$ as in Sec.
³⁷³ 3.1 and using the effective potential description (3.7), we get

$$\tau(-w) \equiv K^{-1} = \int_{y=-w}^0 \int_{x=-\infty}^y \exp(G(x, y)) dx dy, \quad (3.12)$$

³⁷⁴ where $G(x, y)$ can be written as (using (3.7))

$$G(x, y) \equiv \frac{z-1}{z^2} \left(\left(\frac{y}{w} \right)^2 + \frac{z-1}{2} \left(\frac{y}{w} \right)^4 \right) - U_{eff}(x) \equiv U_1(y) - U_{eff}(x), \quad (3.13)$$

³⁷⁵ where U_{eff} is given by (3.7). Note that U_1 can be written in U_{eff} as

$$U_1(y) = U_{eff}(y) + \ln \left((1 + (z-1) \left(\frac{y}{w} \right)^2) \right). \quad (3.14)$$

³⁷⁶ We shall apply the steepest descent approximation in the integral range shown in Fig.
³⁷⁷ 3.3 (a). Expand the function $G(x, y)$ about the saddle point $(-w, 0)$ in the integration
³⁷⁸ interval, we get (the first-order differential term is 0 at the extreme point, and the
³⁷⁹ cross term of the second derivative of G also vanishes.)

$$K^{-1} \approx \int_{y=-w}^0 \int_{x=-\infty}^y \exp \left(G(-w, 0) + \frac{1}{2} G_{xx}(-w, 0)(x + w)^2 + \frac{1}{2} G_{yy}(-w, 0)y^2 \right) dx dy, \quad (3.15)$$

3.2. Transition Rate (K) in Non-Uniform Temperature Field

³⁸⁰ where the subscripts represent the derivatives. We note that

$$G(-w, 0) = U_1(0) - U_{eff}(-w) = U_{eff}(0) - U_{eff}(-w) = \frac{|E_{eff}|}{k_B T_0}, \quad (3.16)$$

$$G_{xx}(-w, 0) = -U''_{eff}(-w) = -\frac{8(z-1)^2}{z^2 w^2}, \quad (3.17)$$

$$G_{yy}(-w, 0) = U''_1(0) = \frac{2(z-1)}{z^2 w^2}. \quad (3.18)$$

³⁸¹ Substitute G , G_{xx} and G_{yy} in (3.15) with the above formulas, we get

$$K^{-1} \approx \exp\left(\frac{|E_{eff}|}{k_B T_0}\right) \int_{y=-w}^0 \int_{x=-\infty}^y \exp\left(-\frac{1}{2}U''_{eff}(-w)(x+w)^2 + \frac{1}{2}U''_1(0)y^2\right) dx dy. \quad (3.19)$$

³⁸² The integration along the x direction gives the error function, that is

$$K^{-1} \approx \frac{\exp(|E_{eff}|/k_B T_0)}{\sqrt{U''_{eff}(-w)}} \sqrt{\frac{\pi}{2}} \int_{y=-w}^0 \exp\left(\frac{1}{2}U''_1(0)y^2\right) \left[\operatorname{erf}\left(\sqrt{\frac{U''_{eff}(-w)}{2}}(y+w)\right) + 1 \right] dy. \quad (3.20)$$

³⁸³ Note that

$$\exp\left(\frac{1}{2}U''_1(0)y^2\right) \left[\operatorname{erf}\left(\sqrt{\frac{U''_{eff}(-w)}{2}}(y+w)\right) + 1 \right] \approx \operatorname{erf}\left(\sqrt{\frac{U''_{eff}(-w)}{2}}(y+w)\right) + 1, \quad (3.21)$$

³⁸⁴ when $U''_1(0) \rightarrow 0$ (w or E_{eff} is large in (3.18)) in the integral range. Therefore, the ³⁸⁵ result can be written as

$$K^{-1} \approx \frac{bw \cdot \operatorname{erf}(bw) + \exp\left(\frac{-(bw)^2}{2}\right) + bw\sqrt{\pi} - 1}{U''_{eff}(-w)} \exp\left(\frac{|E_{eff}|}{k_B T_0}\right), \quad (3.22)$$

³⁸⁶ where $b \equiv \sqrt{\frac{U''_{eff}(-w)}{2}} = \frac{2(z-1)}{wz}$. Since we only care about the transition rate when ³⁸⁷ $|E_{eff}|$ is large, the product bw can be approximated as 2. Finally, our approximate ³⁸⁸ result is

$$K \approx \frac{U''_{eff}(-w)}{2\sqrt{\pi}(\operatorname{erf}(2) + 1) + e^{-4} - 1} \exp\left(-\frac{|E_{eff}|}{k_B T_0}\right) = \frac{1}{A} \frac{8(z-1)^2}{z^2 w^2} \exp\left(-\frac{|E_{eff}|}{k_B T_0}\right), \quad (3.23)$$

³⁸⁹ where the coefficient $A \approx 6.0915$. This result shows that K does not depend on ³⁹⁰ the curvature of U_{eff} at the origin when E_{eff} is large. Since the effective potential ³⁹¹ is bimodal, we want to know how far this differs from the Kramers transition rate

392 prediction. The Kramers rate formula for the double-well potential approximation
 393 under the uniform temperature field is given by (we called K_{eff})

$$K_{eff} \approx \frac{\sqrt{|U''_{eff}(0)| \cdot U''_{eff}(-w)}}{2\pi} \exp\left(-\frac{|E_{eff}|}{k_B T_0}\right) = \frac{2(z-1)^2 \sqrt{(z+1)}}{w^2 z^2 \pi} \exp\left(-\frac{|E_{eff}|}{k_B T_0}\right), \quad (3.24)$$

394 Note that this formula also holds when E_{eff} is large. The ratio of K_{eff} and K is

$$\frac{K_{eff}}{K} = \frac{A\sqrt{(z+1)}}{4\pi}. \quad (3.25)$$

395 As z increases, K and K_{eff} differs by a factor of \sqrt{z} .

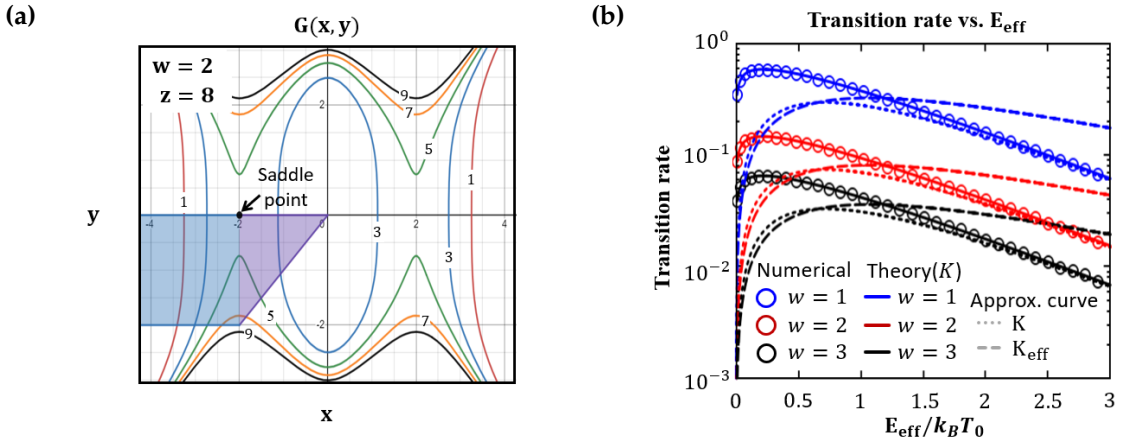


FIGURE 3.3: (a) Integral range of the function $G(x, y)$ (purple area). (b) The transition rate under harmonic potential and non-uniform temperature field $T(x_1) = 1/(1 + ax_1^2)$, where w is the width of the effective potential energy well composed of the potential energy and the temperature field. The solid curves are the results of solving the backward Fokker-Planck equation through numerical integration, and the circles are measured through the numerical solution of the Langevin equation. In contrast, the dashed curves are the Kramers rate formula solution, that is, use U_{eff} directly as the potential energy and the temperature field is a constant 1. The dotted curves represent the approximation of K . Note that the sampling time $\Delta t = dt$ here, while the number of samples is $N_{sample} = 10^5$.

396 Fig. 3.3 (b) shows the results of the transition rate, where formula (3.23) is a better ap-
 397 proximation than the Kramers rate formula in our case discussed. The temperature
 398 field of K_{eff} ($T = 1$) is larger than K ($T = (1/(1 + ax_1^2))$), hence the reaction speed
 399 (transition rate) of K_{eff} is faster than K . Through the above analysis, we know that
 400 the transition rate of the non-uniform temperature field can be obtained by correct-
 401 ing the Kramers rate. Of course, the so-called transition rate is only available when

3.3. Generalization of Transition rate for y-axis symmetric single-well $U(x)$ and a unimodal $T(x)$

402 a bimodal distribution is produced. In fact, if the potential is a single-well potential
 403 and the temperature field is uniaxial, they may generate a bimodal distribution. This
 404 depends on the curvature of both at the extreme values.

405 **3.3 Generalization of Transition rate for y-axis symmet-
 406 ric single-well $U(x)$ and a unimodal $T(x)$**

407 Inspired by the previous section, we want to generalize the transition rate in this
 408 section. The shape of a y-axis symmetry single-well potential and a unimodal tem-
 409 perature are shown in Fig. 3.4(a). It means $T(x) > 0$ for all x ; $T''(0) < 0$; $T'(0) = 0$;
 410 $U''(0) \geq 0$ and $U'(0) = 0$. The effective potential U_{eff} can be described by Eq. (3.2).

$$U_{eff}(x) \equiv \tilde{T} \int^x \frac{U'(x) + T'(x)}{T(x)} dx, \quad (3.26)$$

411 where \tilde{T} is some fixed constant temperature, for instance, one can choose $\tilde{T} = T(0)$
 412 or $T(\infty)$. For convenience, we choose the unit in terms of

$$[\text{length}] = \left(\frac{k_B T_\infty}{k} \right)^{1/n}; \quad [\text{energy}] = k_B T_\infty; \quad [\text{time}] = \frac{\gamma [\text{length}]^2}{k_B T_\infty}. \quad (3.27)$$

413 In this section. Hence, Eq. (3.26) can be rewritten as

$$U_{eff}(x) = \int_0^x \frac{U(s)}{T(s)} ds + \ln \left[\frac{T(x)}{1 + \Delta} \right], \quad (3.28)$$

414 where the prime represents the derivative of x and

$$\Delta \equiv \frac{T_0 - T_\infty}{T_\infty}. \quad (3.29)$$

415 Take the derivative of x in Eq. (3.28).

$$U'_{eff}(x) = \frac{U'(x) + T'(x)}{T(x)} = 0. \quad (3.30)$$

⁴¹⁶ Since $T(x) \neq 0$,

$$U'(x) + T'(x) = 0. \quad (3.31)$$

⁴¹⁷ The extreme points of U_{eff} must satisfy Eq. (3.31). Obviously, $x = 0$ is a solution, and ⁴¹⁸ the other solutions are $\pm w$, where w is the width of the effective potential as dashed ⁴¹⁹ curves in Fig. 3.4(a). The second derivative of $U_{eff}(x)$ at the extreme point is

$$U''_{eff}(x) = \frac{U''(x) + T''(x)}{T(x)} - \frac{U'(x) + T'(x)}{T^2(x)} T'(x) \Big|_{x=0, \pm w} = \frac{U''(x) + T''(x)}{T(x)} \Big|_{x=0, \pm w}. \quad (3.32)$$

⁴²⁰ Since $T(x)$ is always positive and $T''(0)$ is always negative therefore a double well ⁴²¹ cannot form if $U''(0) \geq |T''(0)|$ according to Eq. (3.32). Now, we place the Brown- ⁴²² ian particle at $x = -w$ and wait for it to reach $x = 0$ for the first time. Again, the ⁴²³ mean first-passage time of the particle τ can be written by solving Eq. (3.10). The ⁴²⁴ dimensionless solution of τ at $x = -w$ is given by

$$K^{-1} \equiv \tau(-w) = \frac{1}{1 + \Delta} \int_{-w}^0 dy \int_{-\infty}^y \exp[G(x, y)] dx \equiv \frac{1}{1 + \Delta} K_0^{-1}, \quad (3.33)$$

⁴²⁵ where K is referred to as the transition rate, K_0 represents the transition rate that ⁴²⁶ eliminates the influence of temperature difference, and

$$G(x, y) \equiv \int_0^y \frac{U'(s)}{T(s)} ds - U_{eff}(x). \quad (3.34)$$

⁴²⁷ It can be shown that $(\pm w, 0)$ are always the saddle points of $G(x, y)$ if the temperature ⁴²⁸ is a spatial function,

$$\frac{\partial^2 G}{\partial x^2} \Big|_{x=\pm w} = -\frac{\partial^2 U_{eff}(x)}{\partial x^2} \Big|_{x=\pm w} \geq 0, \quad (3.35)$$

⁴²⁹ and

$$\frac{\partial^2 G}{\partial y^2} \Big|_{y=0} = \frac{U''(y)}{T(y)} \Big|_{y=0} \leq 0. \quad (3.36)$$

3.3. Generalization of Transition rate for y-axis symmetric single-well $U(x)$ and a unimodal $T(x)$

⁴³⁰ Using the saddle-point approximation as in the previous section, we obtain

$$K^{-1} \approx \frac{w}{1 + \Delta} \left[\sqrt{\frac{\pi}{2u''}} \left(\operatorname{erf} \left(\sqrt{\frac{u''}{2}} \right) + 1 \right) + \frac{1}{u''} \left(1 - e^{-\frac{u''}{2}} \right) \right] \exp(E_{eff}), \quad (3.37)$$

⁴³¹ where E_{eff} is the effective barrier height, and $u'' \equiv U''_{eff}(-\omega)$. The square bracket in
⁴³² Eq. (3.37) only depends on the curvature of the effective potential at $x = \pm w$, which
⁴³³ is different from the classical Kramers rate. In the following section, we give two
⁴³⁴ examples to verify our calculation results.

⁴³⁵ **3.3.1 An example: Single-well potential and Gaussian temperature
⁴³⁶ field**

⁴³⁷ Now, consider the dimensionless potential is a power function

$$U(x) = \frac{1}{2} kx^n, \quad x = 2, 4, 6, \dots, \quad (3.38)$$

⁴³⁸ where k is a constant controlling the potential strength. The dimensionless tempera-
⁴³⁹ ture is given by

$$T(x) = 1 + \Delta \exp \left(-\frac{x^2}{2\sigma^2} \right), \quad (3.39)$$

⁴⁴⁰ where $\Delta \equiv \frac{T_0 - T_\infty}{T_\infty}$ and σ represents the width of the temperature. Using Eq. (3.28),
⁴⁴¹ we obtain the representation of the effective potential.

$$\begin{aligned} U_{eff}(x; n, \sigma, \Delta) &= \frac{1}{2} \int_0^x \frac{nu^{n-1}}{1 + \varepsilon \exp \left[\frac{-u^2}{2\sigma^2} \right]} du + \ln \left[\frac{1 + \Delta \exp \left[\frac{-x^2}{2\sigma^2} \right]}{1 + \Delta} \right] \\ &= \frac{n\sigma^n}{2} \left[I_n \left(\frac{x}{\sigma}; \Delta \right) - I_n(0; \Delta) \right] + \ln \left[\frac{1 + \Delta e^{-\frac{x^2}{2\sigma^2}}}{1 + \Delta} \right], \end{aligned} \quad (3.40)$$

⁴⁴² where

$$I_n(s; \Delta) = \sum_{k=1}^{n/2} (-1)^k \frac{(n-2)!!}{(n-2k)!!} s^{n-2k} \text{Li}_k \left(-\frac{e^{\frac{s^2}{2}}}{\Delta} \right) \quad n = 2, 4, 6, \dots \quad (3.41)$$

$$I_n(0, \Delta) = (-1)^{\frac{n}{2}} \text{Li}_{\frac{n}{2}} \left(\frac{-1}{\Delta} \right). \quad (3.42)$$

⁴⁴³ Then, the effective barrier can be written as

$$|E_{eff}(n, \sigma, \Delta)| = \frac{n\sigma^2}{2} \left[I_n(0; \Delta) - I_n \left(\frac{w(\sigma, \Delta)}{\sigma}; \Delta \right) \right] + \ln \left[\frac{1 + \Delta \exp \left(-\frac{w^2(\sigma, \Delta)}{2\sigma^2} \right)}{1 + \Delta} \right], \quad (3.43)$$

⁴⁴⁴ where $w(\sigma, \Delta)$ satisfies (using Eq. (3.31))

$$\frac{n\sigma^2}{2\Delta} = w^{2-n} \exp \left(-\frac{w^2}{2\sigma^2} \right). \quad (3.44)$$

⁴⁴⁵ $w(\sigma, \Delta)$ can further be solved explicitly from Eq. (3.44):

$$w(\sigma, \Delta) = \sigma \sqrt{2 \ln \left(\frac{\Delta}{\sigma^2} \right)}, \quad n = 2 \quad (3.45)$$

$$= \sigma \sqrt{(n-2) W \left(\frac{(\frac{2\Delta}{n\sigma^n})^{\frac{2}{n-2}}}{n-2} \right)}, \quad n = 4, 6, 8 \dots, \quad (3.46)$$

⁴⁴⁶ where W is the Lambert W function. Notice that $\Delta > \sigma^2$ for $n = 2$ is the condition
⁴⁴⁷ for forming an effective barrier for the case of a harmonic trap, which translates back
⁴⁴⁸ to the dimensional form, reads $k_B T''(0) > k_{sp}$ (k_{sp} is the stiffness of the harmonic
⁴⁴⁹ trap), i.e. the local heating profile must be strong enough for the formation of the
⁴⁵⁰ double-well structure in the effective potential. On the other hand, there is no such
⁴⁵¹ a condition for $n \geq 4$, and a double-well always exists in U_{eff} . The potential traps
⁴⁵² for $n = 2, 4, 6$ (solid curves) and the corresponding $U_{eff}(x)$ (dashed curves) for $T(x)$
⁴⁵³ given by Eq. (3.39) (dotted curve) are shown in Fig. 3.4(a) for $\sigma = 0.5$ and $\Delta = 1$,
⁴⁵⁴ displaying the pronounced double-well features of $U_{eff}(x)$. The location of the wells
⁴⁵⁵ in the effective potential (distance from the origin to the minimum potential) will
⁴⁵⁶ vary as n, σ , or Δ , which is described in Eq. (3.44). The effective barrier varies with
⁴⁵⁷ σ and Δ for different n as shown in Fig. 3.4(b)-3.4(c). For smaller σ or larger Δ ,

3.3. Generalization of Transition rate for y-axis symmetric single-well $U(x)$ and a unimodal $T(x)$

458 the effective barrier increases. As shown in the figure, the maximum E_{eff} can be
 459 achieved is determined by Δ .

460 Next, we proceed to compute the transition rate between the double wells in
 461 $U_{eff}(x)$ using Eqs. (3.33) and (3.34). Using the U_{eff} in (3.40), one obtains

$$G(x, y) = \frac{n\sigma^n}{2} \left[I_n\left(\frac{y}{\sigma}; \Delta\right) - I_n\left(\frac{x}{\sigma}; \Delta\right) \right] - \ln \left(\frac{1 + \Delta e^{-\frac{x^2}{2\sigma^2}}}{1 + \Delta} \right), \quad (3.47)$$

462 and the transition rate can be computed by numerically by evaluating the double
 463 integral in (3.33), and the steepest descent (saddle-point) results is shown in Eq. (3.37),
 464 where E_{eff} is the effective barrier height given by (3.43), and $u'' \equiv U''_{eff}(w(\sigma, \Delta)) > 0$
 465 is the curvature of the wells.

466 The square bracket in Eq. (3.37) only depends on the curvature of the effective
 467 potential at $x = \pm w$. The exponential dependence of the transition rate on the barrier
 468 height is similar to the usual Kramers rate formula, albeit the dependence of the
 469 prefactor on the well curvature is significantly different. Using Eq. (3.40), one gets

$$u'' = \frac{2}{1+\sigma^2} \ln \frac{\Delta}{\sigma^2} \quad \text{for } n = 2 \quad (3.48)$$

$$= \frac{\sigma^{n-2} n(n-2)^{\frac{n}{2}} \left\{ 1 + W \left[\frac{1}{n-2} \left(\frac{2\Delta}{n\sigma^n} \right) \right]^{\frac{2}{n-2}} \right\}}{\sigma^n n(n-2)^{\frac{n-2}{2}} + 2W \left[\frac{1}{n-2} \left(\frac{2\Delta}{n\sigma^n} \right)^{\frac{2}{n-2}} \right]^{\frac{2-n}{2}}}, \quad n = 4, 6, 8, \dots \quad (3.49)$$

470 To verify the above theoretical results, we carry out a Langevin dynamics simulation
 471 by numerically solving the Langevin equation using the Euler-Maruyama scheme
 472 with a time step of 10^{-4} . The transition rate is measured from the first-passage times
 473 by averaging over 20,000 trajectories. The steady-state position distribution is then
 474 measured, which in turn gives the effective potential. Fig. 3.4(a) (symbols) shows the
 475 effective potential measured in the simulations, which is in good agreement with the
 476 theoretical formula (3.40).

477 The mean first-passage time, whose inverse gives the transition rate between the
 478 wells in U_{eff} , can also be measured in the simulations. Fig. 3.5 shows the measured
 479 transition rates from simulations (symbols) for various trapping potentials of differ-
 480 ent values of n . As shown in Fig. 3.5(a), K decreases monotonically with the heating
 481 strength Δ for the $n = 2$ harmonic trap for a fixed value of σ , but displays a minimum
 482 with Δ for anharmonic traps. This can be understood as the competition between the

483 effective barrier U_{eff} and the temperature difference Δ . The higher the temperature,
 484 the faster the transition rate. However, increasing Δ will lead to an increase in E_{eff} .
 485 For example, for the $n = 2$ case, the effective is written as

$$|E_{eff}(n = 2, \Delta, \sigma)| = \ln \left[\frac{1 + \Delta}{1 + \sigma^2} \left(\frac{\sigma^2}{\Delta} \frac{1 + \Delta}{1 + \sigma^2} \right)^{\sigma^2} \right]. \quad (3.50)$$

486 Then, we can calculate the transition rate of the $n = 2$ case when $\Delta \rightarrow \infty$.

$$K^{-1}(\Delta \rightarrow \infty) \approx \frac{\sigma \sqrt{2\pi(1 + \sigma^2)} \left(\frac{\sigma^2}{1 + \sigma^2} \right)^{\sigma^2}}{1 + \sigma^2}, \quad (3.51)$$

487 which is convergent. If $n > 2$, the transition rate will diverge when $\Delta \rightarrow \infty$. On
 488 the other hand, K is non-monotonic with σ and shows a minimum as σ increases
 489 for a fixed value of Δ for harmonic and anharmonic traps, as shown in Fig. 3.5(b).
 490 It can be understood as the competition between the effective barrier and the width
 491 of the effective potential. As σ increases, the effective barrier height decreases, lead-
 492 ing to a faster transition rate. On the contrary, as σ decreases, although the effective
 493 barrier height increases, the effective potential width decreases, increasing the trans-
 494 sition rate. The measured transition rates all agree well with the theoretical formula
 495 (curves) given by (3.37).

3.3. Generalization of Transition rate for y -axis symmetric single-well $U(x)$ and a unimodal $T(x)$

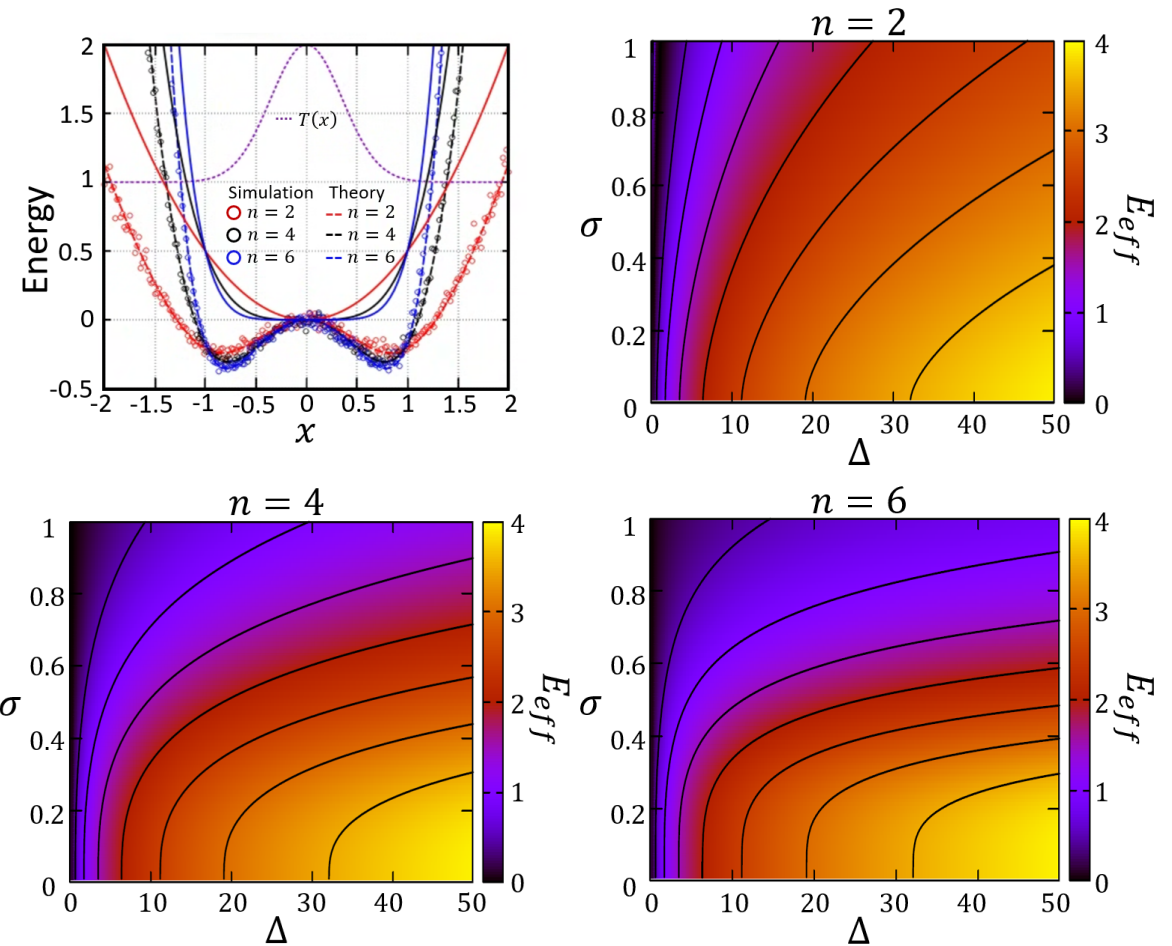


FIGURE 3.4: (a) Double-well effective potentials (dashed curves) experienced by a Brownian particle under a Gaussian temperature field $T(x)$ (dotted curve) and various single-well harmonic and anharmonic potential traps (solid curves). $\sigma = 0.5$ and $\Delta = 1$. The effective potentials measured from simulations of the Langevin dynamics are also shown (symbols). (b)-(d) Contour plots of the effective barrier height as a function of σ and Δ for different trapping potentials of $n = 2, 4, 6$.

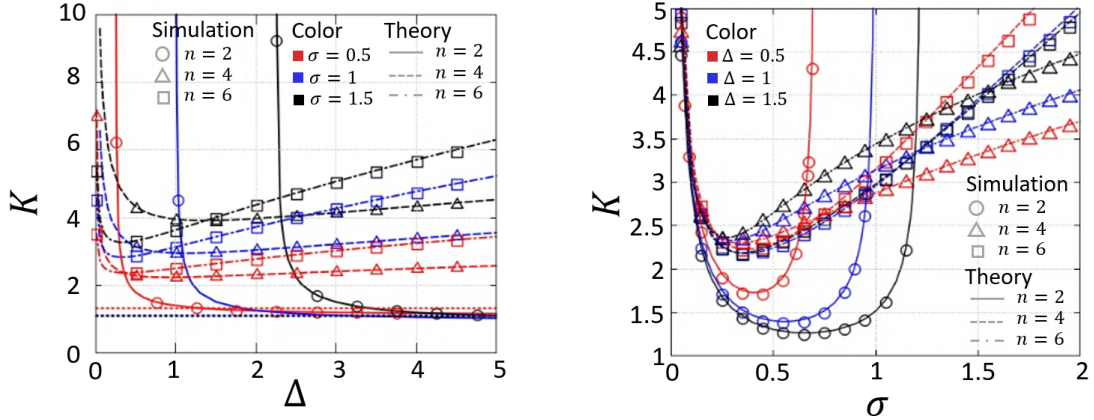


FIGURE 3.5: Transition rate in the double-well effective potential under different heating profiles. (a) K vs. Δ for given values of σ , where dotted straight lines represent the convergence approximation line we calculated for $n = 2$ (Eq. (3.51)). (b) K vs. σ for given values of Δ . The symbols denote results from the Langevin simulations. The curves depict the theoretical results from numerical integration using (3.33).

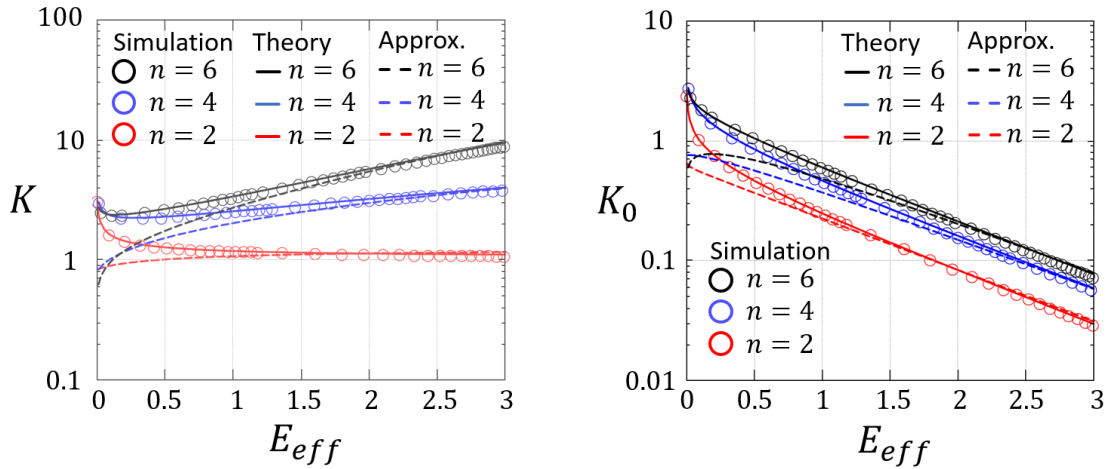


FIGURE 3.6: The results of transition rate varies with E_{eff} . E_{eff} is changed by varying ε while fixing σ . The hollow symbols denote results from the Langevin simulation, the solid curves depict results from numerical integration, and the dashed curves present the approximation results. The red, blue, and black colors represent $n = 2, 4, 6$ respectively. (a) Taking the ambient temperature as the unit, the temperature T_0 of each data point is different. (b) After removing the influence of T_0 , the effective barrier height returns to a form similar to the Kramers rate. Both figures are fixed with $T_\infty = 1$ and $\sigma = 0.5$.

496 The effective barrier varies with σ or Δ , but Δ dominates the possible maximum

3.3. Generalization of Transition rate for y -axis symmetric single-well $U(x)$ and a unimodal $T(x)$

value of E_{eff} as previously mentioned. Therefore, we select to fix $\sigma = 0.5$. The results are shown in Fig. 3.6(a). It is worth noting that for the well-studied situation of a uniform temperature in a double-well potential trap, the Kramers rate formula indicates that the higher the potential barrier, the longer the escape time. However, in the present case of a double-well effective potential induced by a localized heating profile, the transition rate does not appear to follow an exponential decrease with the effective barrier height, in contrast with the usual Kramers rate result. This apparent disagreement is due to the fact that E_{eff} arises from the nonuniform temperature field and increases with Δ , but at the same time, a larger Δ implies a higher temperature at $x = 0$, making the Brownian particle easier to escape from the trap. This effect is reflected in the prefactor $(1 + \Delta)$ in Eq. (3.37), and the results are shown in Fig. 3.6(a). When $n = 4$ and $n = 6$, the E_{eff} required for the minimum transition rate is much smaller than when $n = 2$. Moreover, the larger n is, the larger the transition rate will be. To understand the effect of the induced barrier caused by the temperature gradient on the transition rate, we divide K by the factor $(1 + \Delta)$, and the result is shown in Fig. 3.6(b). The scaled transition rate effective barrier follows the usual Kramers' behavior of exponential decrease with the barrier height. This once again verifies our previous discussion of the competitive relationship between effective barrier height and temperature difference in Eq. (3.5). In addition, the explicit approximation formula (3.37) (dashed curves) is a good approximation when E_{eff} is large ($\gtrsim 1$), as shown in Fig. 3.6.

3.3.2 Another example: Transition rate correction for the double-well potential

In this section, we choose the double-well length w (from the origin to the lowest point) for the unit, and the unit of energy is also $k_B T_\infty$. The dimensionless double-well potential is given by

$$U(x) = 4E_b \left(-\frac{1}{2}x^2 + \frac{1}{4}x^4 \right), \quad (3.52)$$

where E_b is the (dimensionless) barrier height. In the case of uniform temperature, the Brownian particle spends most of the time residing in one of the double wells

and occasionally makes transitions to the other well under stochastic thermal fluctuations. In the presence of a nonuniform temperature field, the location of the wells of the effective potential and the effective barrier (and hence the transition rate between the wells) will be modified. For further calculations, we consider the Gaussian temperature profile also given by Eq. (3.39).

In this case, using (3.40), one can derive

$$U_{eff}(x; E_b, \sigma, \Delta) = 4E_b \int_0^x \frac{u^3 - u}{1 + \Delta \exp\left[-\frac{u^2}{2\sigma^2}\right]} du + \ln \left(\frac{1 + \Delta e^{-\frac{x^2}{2\sigma^2}}}{1 + \Delta} \right) \quad (3.53)$$

$$= 4E_b \left[\sigma^4 \left(I_4\left(\frac{x}{\sigma}; \Delta\right) - I_4(0; \Delta) \right) - \sigma^2 \left(I_2\left(\frac{x}{\sigma}; \Delta\right) - I_2(0; \Delta) \right) \right] + \ln \left(\frac{1 + \Delta e^{-\frac{x^2}{2\sigma^2}}}{1 + \Delta} \right), \quad (3.54)$$

and the effective energy barrier is given by

$$|E_{eff}(E_b, \sigma, \Delta)| = 4E_b \left[\sigma^2 \left(I_2\left(\frac{1}{\sigma}; \Delta\right) - I_2(0; \Delta) \right) - \sigma^4 \left(I_4\left(\frac{1}{\sigma}; \Delta\right) - I_4(0; \Delta) \right) \right] - \ln \left(\frac{1 + \Delta e^{\frac{-1}{2\sigma^2}}}{1 + \Delta} \right). \quad (3.55)$$

Under the heating profile, the location of the double wells shifted from $x = \pm 1$ to $\pm w(E_b, \sigma, \Delta)$, which is given by

$$w(E_b, \sigma, \Delta) = \sqrt{2\sigma^2 W \left[\frac{\Delta}{8E_b \sigma^4} e^{-\frac{1}{2\sigma^2}} \right] + 1}. \quad (3.56)$$

Note that $w \rightarrow 1$ if $\sigma \rightarrow 0$ or ∞ , or $E_b \rightarrow \infty$. We then proceed to derive the transition rate and investigate how the rate K is affected by the spatial temperature profile. Similar to the case of a single well $U(x)$ in the previous section, the mean first-passage time and hence the inverse transition rate can be obtained by solving the backward Fokker-Planck equation. We obtain

$$K^{-1} \approx \exp(E_{eff}) \sqrt{\frac{\pi}{2U''(1)}} \frac{1}{1 + \Delta} \int_{-1}^0 \exp \left[\frac{-|U''(0)|}{2T_0} y^2 \right] \left(1 + \operatorname{erf} \left(\sqrt{\frac{U''_{eff}(1)}{2}} (y + w) \right) \right) dy, \quad (3.57)$$

3.3. Generalization of Transition rate for y-axis symmetric single-well $U(x)$ and a unimodal $T(x)$

539 where $U''(0) = -4E_b$. We further employ the steepest-descent approximation for
 540 large E_b to get

$$K^{-1} \approx \exp(E_{eff}) \sqrt{\frac{\pi}{2U''(1)}} \frac{2}{1+\Delta} \int_{-\infty}^0 \exp\left[\frac{-|U''(0)|}{2}y^2\right] dy \quad (3.58)$$

$$\Rightarrow K \approx \frac{1+\Delta}{\pi} \sqrt{U''_{eff}(1)|U''(0)|} \exp(-E_{eff}) \propto \exp(-E_b). \quad (3.59)$$

541 where E_{eff} is the effective barrier given by (3.55). Eq. (3.59) is very similar to the ex-
 542 pression of the Kramers rate, but the prefactor and exponent depend on the effective
 543 potential. Since E_{eff} depends linearly on E_b , $K \sim e^{-E_b}$ as given by the r.h.s of (3.59).

544 The dependences of the transition rate on the Δ , σ , and E_b are shown in Fig.
 545 3.8, for both the theoretical results (curves) from (3.57) and those measured from
 546 Langevin simulations (symbols). Again, the theoretical formula agrees accurately
 547 with the simulation results. As shown in Fig. 3.8(b), the transition rate increases
 548 with the temperature difference Δ for fixed values of σ and E_b . This is expected
 549 since a stronger localized heating at the center will effectively lower the barrier of the
 550 double-well trap. Fig. 3.8(c) indicates that a smaller temperature gradient (larger σ
 551 for a fixed value of Δ) results in a higher transition rate, which saturates for $\sigma \gtrsim 2$.
 552 The transition rates as a function of the barrier of the double-well trap are displayed
 553 in Fig. 3.8(d), verifying the exponential decrease with E_b for $E_b \gtrsim 1$.

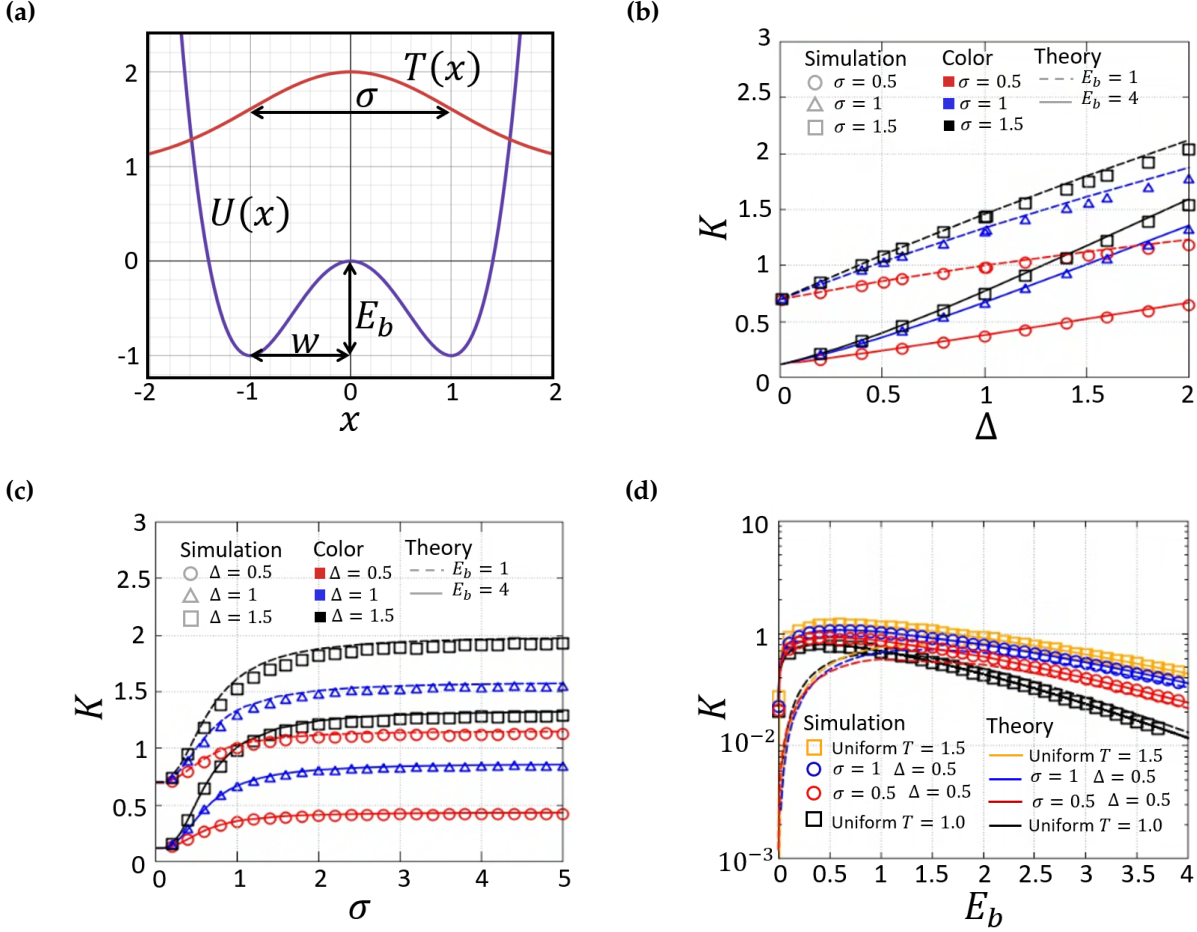


FIGURE 3.7: (a) The double-well potential and the Gaussian temperature field. Transition rate K of a Brownian particle in a double-well trap under different heating profiles. Theoretical results (curves) are obtained using (3.57). K measured from the Langevin simulation is denoted by the symbols. (b) K vs. Δ for given E_b and σ . (c) K vs. σ for given E_b and Δ . (d) K vs. E_b for various values of σ and $\Delta = 0.5$. The transition rates for the cases of uniform temperatures of T_0 and T_∞ are also shown for comparison.

At the end of this subsection, we would like to emphasize that this system, consisting of a Gaussian temperature field and a single-well trap, is not in thermal equilibrium even if the total particle flux is zero, because of the presence of a temperature gradient. The way to form a non-equilibrium steady state is that the particles absorb kinetic energy and quickly release it from high temperature to low temperature, and then slowly climb to high temperature to form a cycle. This velocity inversion asymmetry can lead to abnormal entropy production. Even if it is small, it will dominate the entropy production in the overdamped limit [4]. In the future, we will discuss

3.4. Diffusion field reconstruction using steady-state position and diffusion constant distributions

562 the energetics of this system.

563 In summary, we use the effective potential to describe the steady-state distribution
564 of a one-dimensional non-uniform temperature field system, and use this effective
565 potential to quantitatively describe the transition rate of this system. We then
566 discussed the transition rates of two different potential energy landscapes, and the
567 results were consistent with our theoretical expectations. We also give an approxi-
568 mate expression for the transition rate when E_{eff} is large, where the single-well trap
569 is determined by (3.37) and the double-well potential is determined by (3.59).

570 **3.4 Diffusion field reconstruction using steady-state po- 571 sition and diffusion constant distributions**

572 In the last small section of this chapter, we try to reconstruct the entire diffusion
573 field by knowing the steady-state position and diffusion constant distributions, be-
574 cause in experiments, the diffusion field is usually more difficult to measure than
575 the steady-state position and diffusion constant distributions. Given a potential well
576 and temperature field, the steady-state position distribution is given by Eq. (3.2)

$$P(x) = \frac{1}{Z} \frac{\exp\left(-\frac{U'(s)}{D(s)}ds\right)}{D(x)}, \quad (3.60)$$

577 where Z is the partition function, $D(x)$ is the diffusion field, and $U'(x)$ is the deriva-
578 tive of potential with respect to x . On the other hand, the steady-state diffusion
579 constant distribution can be written as

$$\begin{aligned} P_D(\mathcal{D}) &= \int P(x) \delta(\mathcal{D} - D(x)) dx \\ &= \int P(x) \sum_i \frac{\delta(x - x_i^*)}{|D'(x_i^*)|} dx \\ &= \sum_i \frac{P(x_i^*)}{|D'(x_i^*)|}, \end{aligned} \quad (3.61)$$

580 where x_i^* are roots of $D(x^*) = \mathcal{D}$. If the system has a unimodal and symmetrical
 581 diffuse field, Eq. (3.61) can be simply written as

$$\frac{dD(x)}{dx} = \frac{2P(x)}{P_D(\mathcal{D})}. \quad (3.62)$$

582 $D(x)$ can be obtained by solving this differential equation. It may be necessary to
 583 note that $P_D(\mathcal{D})$ may have singular points when $D'(x) = 0$.

584 3.4.1 An Example: Symmetrical diffusion field with a single peak

585 Consider the temperature field (we will reconstruct this field later)

$$\frac{1}{D(x)} = \frac{1}{D_\infty} - \left(\frac{1}{D_\infty} - \frac{1}{D_0} \right) \exp \left(-\frac{x^2}{2\sigma^2} \right) \equiv \frac{1}{D_\infty} \left(1 - \alpha \exp \left(-\frac{x^2}{2\sigma^2} \right) \right), \quad (3.63)$$

586 where $\alpha \equiv \frac{1}{D_\infty} - \frac{1}{D_0}$ and the harmonic potential is

$$U(x) = \frac{1}{2} kx^2. \quad (3.64)$$

587 In this case, the steady-state probability density is given by

$$P(x) = \frac{1}{Z} \left[1 - \alpha \exp \left(-\frac{x^2}{2\sigma^2} \right) \right] \exp \left[-\frac{k\sigma^2}{D_\infty} \left(\frac{x^2}{2\sigma^2} + \alpha e^{-\frac{x^2}{2\sigma^2}} \right) \right], \quad (3.65)$$

588 where Z is the partition function. Using Eq. (3.61), we get

$$P_D(\mathcal{D}) = \frac{2\sigma}{Z} \cdot \frac{T_\infty^2}{\mathcal{D}^3} \cdot \frac{\exp \left[-\frac{k\sigma^2}{T_\infty} \left(\ln \left(\frac{\alpha}{1 - \frac{T_\infty}{\mathcal{D}}} \right) + 1 - \frac{T_\infty}{\mathcal{D}} \right) \right]}{\left(1 - \frac{T_\infty}{\mathcal{D}} \right) \sqrt{2 \ln \left(\frac{\alpha}{1 - \frac{T_\infty}{\mathcal{D}}} \right)}}, \quad (3.66)$$

589 where $P_D(\mathcal{D})$ is only defined in the interval $\mathcal{D} = (D_\infty, D_0)$. We verify that the expressions
 590 of $P(x)$ and $P_D(\mathcal{D})$ are correct in Fig. 3.8.

3.4. Diffusion field reconstruction using steady-state position and diffusion constant distributions

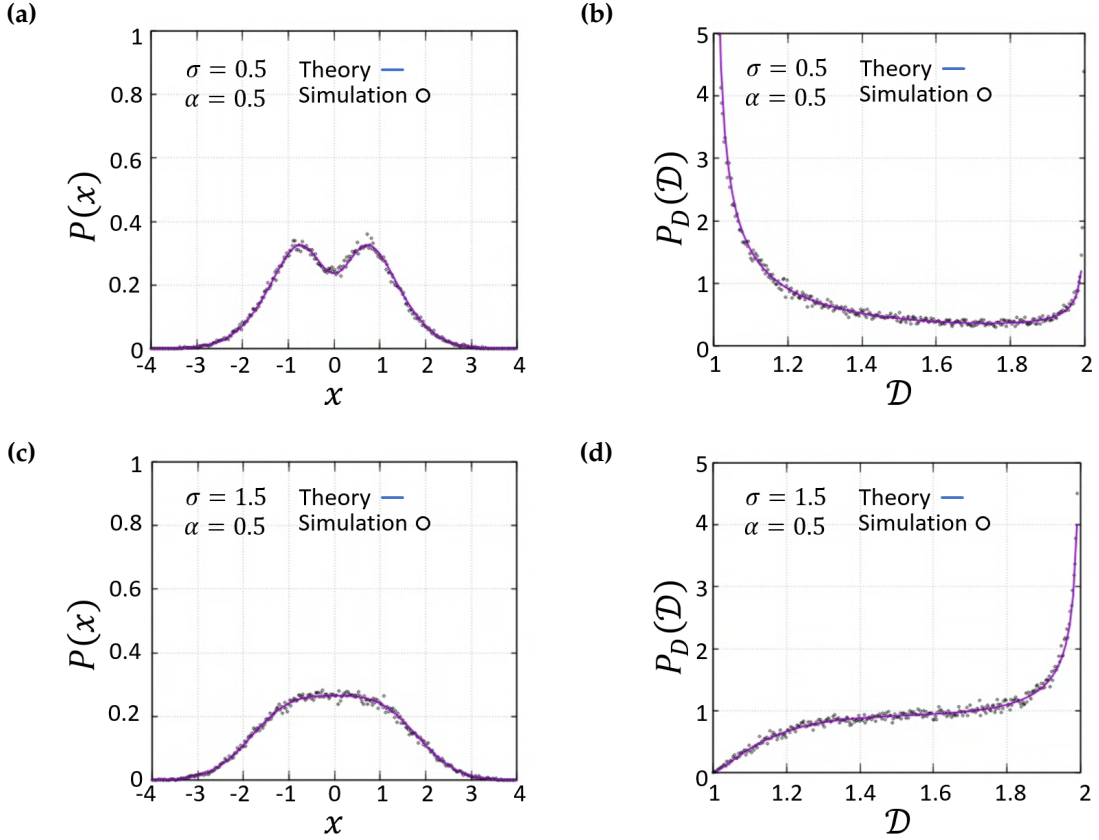


FIGURE 3.8: The two case $\sigma = 0.5$ ((a)-(b)) and $\sigma = 1.5$ ((c)-(d)) of steady-state position and diffusion distribution, where $D_0 = 2$, $D_\infty = 1$, and $\alpha = 0.5$ are fixed. We measure 100,000 trajectories, and the bin size is 316.

591 The divergence in $P_D(D)$ at D_∞ and D_0 in Fig. 3.8(b) and 3.8(d) follows from
 592 Eq. (3.61). The $D(x)$ reconstructed by measuring $P_D(D)$ and $P(x)$ and numerically
 593 solving Eq. (3.62) is shown in Fig. 3.9, where the reconstructed field is close to the
 594 real diffusion field. For a more general situation, say directly solve Eq. (3.61), we
 595 may first solve the monotonic interval of D . This issue will be investigated in future
 596 research.

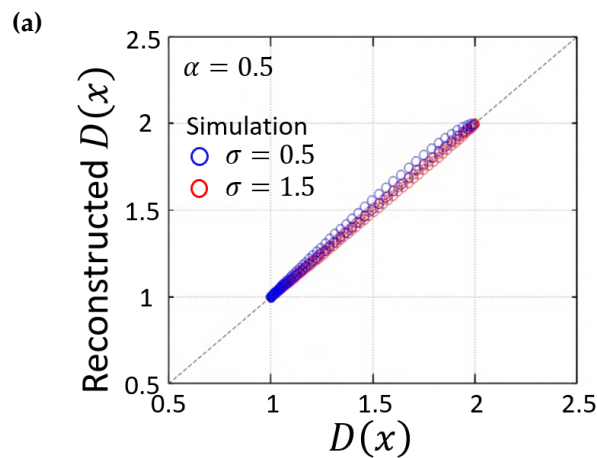


FIGURE 3.9: Reconstructed and real diffusion field, where the reconstructed diffusion field is obtained by solving Eq. (3.62) and the real diffusion field is described by Eq. (3.63).

LANDAUER LIMIT UNDER A NON-UNIFORM TEMPERATURE FIELD

600 The Landauer limit describes the minimum amount of energy required to erase one
 601 bit of information at a uniform temperature. Brownian heat engines are usually real-
 602 ized by changing the shape of the potential energy or by changing the temperature.
 603 Therefore, the minimum energy cost can help us understand the limit of the effi-
 604 ciency of the heat engine.

605 Essentially, the Landauer limit represents the information entropy of the system
 606 that is transferred to the environment. Consider a logic gate with two inputs and one
 607 output, and the number of possible states is $\Omega = 2^2$. Therefore, the entropy is $S_i =$
 608 $k_B \ln \Omega = 2k_B \ln 2$. After the logic operation, the output can take only two values,
 609 and the entropy of the gate becomes $S_f = k_B \ln 2$. The entropy difference before
 610 and after is $\Delta S = S_f - S_i = -k_B \ln 2$. However, the second law of thermodynamics
 611 requires that the sum of the entropy of the logic gate and the external entropy change
 612 be greater than zero. Therefore, the external entropy must be supplemented by at
 613 least $k_B \ln 2$. If the system is immersed in a constant temperature bath at temperature
 614 T , the heat the logic gate releases is $Q \geq k_B T \ln 2$.

615 In this section, we generalize the system to a non-uniform temperature field and
 616 investigate the possible modification in the Landauer limit of the system. The core
 617 question is whether we can find an effective temperature T_{eff} to describe the Lan-
 618 dauer limit, that is, $k_B T_{eff} \ln 2$. First, we need to design two wells on the left and
 619 right to represent the two-state storage. The most direct way is to directly give a
 620 double-well potential (however, in the previous section, it was also possible to cre-
 621 ate a virtual barrier through the effective barrier). Now, let us consider the system

under a Gaussian temperature field (Eq. (3.39) and the time-dependent double-well potential

$$U(x, f(t), g(t)) \equiv 4E_b \left(-\frac{1}{2}g(t)x^2 + \frac{1}{4}x^4 - Af(t)x \right), \quad (4.1)$$

where f and g are time-dependent protocols. The following erasure protocol is considered for $f(t)$ and $g(t)$, which are shown in Fig. 4.1(a).

$$f(t) = \begin{cases} 1 - \frac{4}{\tau}t, & 0 \leq t < \frac{\tau}{4} \\ 0, & \frac{\tau}{4} \leq t < \frac{\tau}{2} \\ \frac{4}{\tau}(t - \frac{\tau}{2}), & \frac{\tau}{2} \leq t < \frac{3\tau}{4} \\ 1, & \frac{3\tau}{4} \leq t \leq \tau \end{cases}, \quad (4.2)$$

and

$$g(t) = \begin{cases} 0, & 0 \leq t < \frac{\tau}{4} \\ \frac{4}{\tau}(t - \frac{\tau}{4}), & \frac{\tau}{4} \leq t < \frac{\tau}{2} \\ 1, & \frac{\tau}{2} \leq t < \frac{3\tau}{4} \\ 1 - \frac{\tau}{4}(t - \frac{3\tau}{4}), & \frac{3\tau}{4} \leq t \leq \tau \end{cases}. \quad (4.3)$$

The work in the stochastic process is defined in Eq. (2.35).

$$W = \int_0^\tau \dot{W}(x(t), t) dt = \int_0^\tau \frac{\partial U(x, f(t), g(t))}{\partial a} \frac{da}{dt} dt = -4E_b \int_0^\tau \left(\frac{\dot{g}(t)}{2}x^2 + A\dot{f}(t)x \right) dt, \quad (4.4)$$

where $a = f, g$ are the erasure protocols. The former controls the barrier height of the potential, and the latter controls the tilt of the potential. We initially placed the Brownian particle at $x = 0$ in the double-well potential, and then the particle randomly fell into the left or right wells. After the erasure protocol of f and g , if all particles are in the right well at time $t = \tau$, it is called fully erased. Otherwise, it is not erased. The definition and erasure process of the protocol are shown in Fig. 4.1(a) and 4.1(b).

We try to map the nonuniform temperature field into a uniform effective temperature T_0 system. The dimensionless Langevin equation under a non-uniform system

⁶³⁷ is given by

$$dx = -\frac{\partial U}{\partial x} dt + \sqrt{2T(x)} \cdot dB_t, \quad (4.5)$$

⁶³⁸ where B_t is the Wiener process. Now, consider another system with a constant tem-
⁶³⁹ perature $T_0 \equiv T_\infty + \varepsilon$ (set $T_\infty = 1$ as unit) and an effective potential $\Phi(y, t)$ as in paper
⁶⁴⁰ [12].

$$dy = -\frac{\partial \Phi(y, t)}{\partial y} dt + \sqrt{2T_0} \cdot dB_t. \quad (4.6)$$

⁶⁴¹ Using the change of variable

$$\frac{dy}{dx} = \sqrt{\frac{T_0}{T(x)}}, \quad \text{then} \quad \frac{d^2y}{dx^2} = -\frac{1}{2} \frac{dT(x)}{dx} \frac{T_0^{1/2}}{2T(x)^{3/2}}. \quad (4.7)$$

⁶⁴² Apply the Itô lemma (Eq. (2.23)) to Eq. (4.6), and using Eqs. (4.7), we obtain

$$\begin{aligned} dy(x) &= \left(-\frac{\partial U}{\partial x} \frac{dy}{dx} + T(x) \frac{d^2y}{dx^2} \right) dt + \left(\sqrt{2T(x)} \frac{dy}{dx} \right) \cdot dB_t \\ &= \left(-\frac{\partial U}{\partial x} - \frac{1}{2} \frac{dT(x)}{dx} \right) \sqrt{\frac{T_0}{T(x)}} dt + \sqrt{2T_0} \cdot dB_t. \end{aligned} \quad (4.8)$$

⁶⁴³ Therefore, we obtain the effective potential

$$\begin{aligned} \Phi(y, t) &= \int_0^y \left(\frac{\partial U(s, t)}{\partial s} + \frac{1}{2} \frac{dT(s)}{ds} \right) \left(\frac{T_0}{T(s)} \right)^{\frac{1}{2}} ds \\ &= \int_0^{x(y)} \left(\frac{\partial U(s, t)}{\partial s} + \frac{1}{2} \frac{dT(s)}{ds} \right) \left(\frac{T_0}{T(s)} \right) ds. \end{aligned} \quad (4.9)$$

⁶⁴⁴ The relationship between the original (non-uniform temperature) and the effective
⁶⁴⁵ (constant temperature) work can be derived from the definition of stochastic work

⁶⁴⁶ (Eq. (2.35)).

$$\begin{aligned}
 W_{eff}(y, t) &= \int_0^\tau \frac{\partial \Phi(x, t)}{\partial t} dt = \int_0^\tau \dot{W}_{eff}(x(t), t) dt \\
 &= \int_0^\tau \left[\int_0^{x(y)} \frac{T_0}{T(s)} \frac{\partial}{\partial t} \left(\frac{\partial U(s, t)}{\partial s} \right) ds \right] dt \\
 &= \int_0^\tau \left[\int_0^{x(y)} \frac{T_0}{T(s)} \frac{\partial}{\partial s} \left(\frac{\partial U(s, t)}{\partial t} \right) ds \right] dt \\
 &= \int_0^\tau \left[\int_0^{x(y)} \frac{T_0}{T(s)} \frac{\partial}{\partial s} (\dot{W}(s(t), t)) ds \right] dt,
 \end{aligned} \tag{4.10}$$

⁶⁴⁷ where the last equation is because we use Eq. (4.4). Thus,

$$\frac{\dot{W}_{eff}(y(t), t)}{k_B T_\infty} = \int_0^{x(y)} \frac{T_0}{k_B T(s)/T_\infty} \frac{\partial \dot{W}(s(t), t)}{\partial s} ds, \tag{4.11}$$

⁶⁴⁸ Henceforth, we shall express the work in units of $k_B T_\infty$, and all energies are in dimensionless form. On the other hand, the Jarzynski equality [26] in the effective system
⁶⁴⁹ ($T_0 = 1 + \varepsilon$ constant temperature) is given by
⁶⁵⁰

$$\left\langle \exp \left(-\frac{W_{eff}}{1 + \varepsilon} \right) \right\rangle = \exp \left(-\frac{\Delta F_{eff}}{1 + \varepsilon} \right) = \frac{1}{2}, \tag{4.12}$$

⁶⁵¹ where F_{eff} is the effective free energy and $\varepsilon \equiv \frac{T_0}{T_\infty} - 1$. The r.h.s. of Eq. (4.10) uses
⁶⁵² the partition function of F_{eff} for complete erasure when $t = \tau$ is half that of when
⁶⁵³ $t = 0$. Obviously, if there is no temperature difference (i.e. $\varepsilon = 0$), then $W_{eff} \rightarrow W$
⁶⁵⁴ and $\Delta F_{eff} \rightarrow \Delta F$, Eq. (4.10) returns to

$$\langle \exp(-W) \rangle = \frac{1}{2}, \tag{4.13}$$

⁶⁵⁵ where T is a constant temperature. Using Jensen's inequality, we obtain

$$\langle W \rangle \geq \ln 2. \tag{4.14}$$

⁶⁵⁶ Eq. (4.14) represents the minimum energy required to completely erase one bit of
⁶⁵⁷ information at a uniform temperature, i.e., the Landauer limit. Eq. (4.11) and Eq.
⁶⁵⁸ (4.12) connect the effective system to the original system.

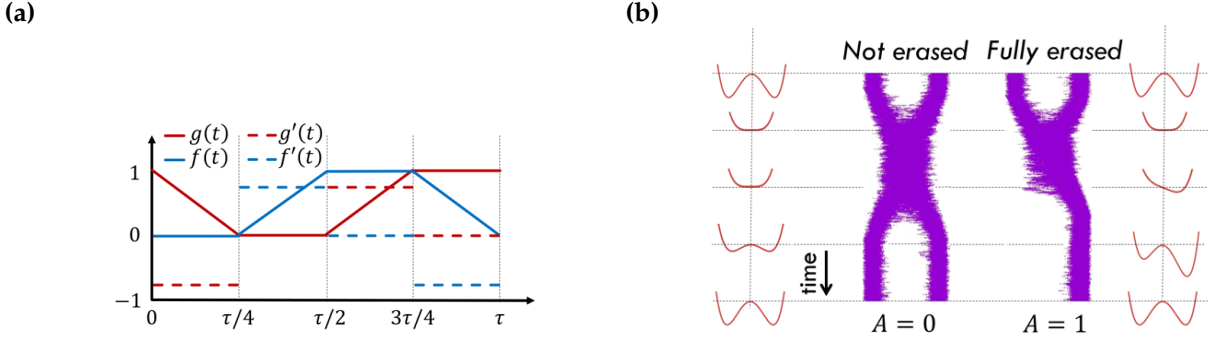


FIGURE 4.1: (a) The control protocol. The red solid line represents the control function modulating the potential barrier, while the blue solid line adjusts the potential tilt. The dashed lines are the change rate of the control function. (b) The erase process. The left and right figures represent not erased and fully erased, respectively.

659 For explicit calculations, we consider the Gaussian $T(x)$ (3.39). For convenience
 660 in notation, we use the symbol ε (instead of Δ) for the temperature difference in Eq.
 661 (3.39). The average effective work $\langle W_{eff} \rangle$ on the trajectory can be written as

$$\begin{aligned} \langle W_{eff}(y, \tau) \rangle &= -4E_b \int_0^\tau \left\langle \int_0^{x(y)} \frac{\dot{g}(t)x^2 + A\dot{f}(t)x}{1 + \varepsilon \exp\left(-\frac{x^2}{2\sigma^2}\right)} dx \right\rangle dt \\ &= -4E_b \left(\sigma^2 \int_0^\tau \dot{g}(t) \left\langle \ln \left(\varepsilon + \exp \left(\frac{+x^2}{2\sigma^2} \right) \right) \right\rangle dt + A \int_0^\tau \dot{f}(t) \left\langle \int_0^{x(y)} \frac{dx}{1 + \varepsilon \exp\left(-\frac{x^2}{2\sigma^2}\right)} \right\rangle dt \right). \end{aligned} \quad (4.15)$$

662 For small ε ($\ll 1$), we can expand Eq. (4.15) as

$$\frac{1}{T(x)} = 1 + \sum_{n=1}^{\infty} (-1)^n \exp\left(-\frac{nx^2}{2\sigma^2}\right) \varepsilon^n, \quad (4.16)$$

663

$$\sigma^2 \ln \left(\varepsilon + \exp \left(\frac{x^2}{2\sigma^2} \right) \right) = \frac{x^2}{2} - \sigma^2 \sum_{n=1}^{\infty} \frac{(-1)^n}{n} \varepsilon^n \exp\left(\frac{-nx^2}{2\sigma^2}\right), \quad (4.17)$$

⁶⁶⁴ and

$$\int_0^x \frac{ds}{1 + \varepsilon \exp\left(-\frac{s^2}{2\sigma^2}\right)} = x + \sqrt{\frac{\pi}{2}}\sigma \sum_{n=1}^{\infty} \frac{(-1)^n}{\sqrt{n}} \varepsilon^n \operatorname{erf}\left(\sqrt{\frac{n}{2}}\frac{x}{\sigma}\right). \quad (4.18)$$

⁶⁶⁵ Thus, Eq. (4.15) can be approximated as

$$\begin{aligned} \langle W_{eff}(y, \tau) \rangle &\approx -4E_b \left(\left\langle \int_0^\tau \dot{g}(t) \frac{x^2}{2} dt + A \int_0^\tau \dot{f}(t) x dt \right\rangle \right) \\ &- 4E_b \sum_{n=1}^{\infty} (-1)^{n+1} \left(\frac{\sigma^2}{n} \left\langle \int_0^\tau \exp\left(-\frac{nx^2}{2\sigma^2}\right) dt \right\rangle - A\sigma \sqrt{\frac{\pi}{2n}} \left\langle \int_0^\tau \operatorname{erf}\left(\sqrt{\frac{n}{2}}\frac{x}{\sigma}\right) dt \right\rangle \right) \varepsilon^n. \end{aligned} \quad (4.19)$$

⁶⁶⁶ Note that the first term in Eq. (4.19) is Eq. (4.4), and we define

$$\begin{aligned} F_n(\varepsilon, \sigma, \tau) &\equiv \\ &(-1)^{n+1} \frac{4E_b}{\ln 2} \left[\frac{\sigma^2}{n} \int_0^\tau \dot{g}(t) \left\langle \exp\left(-\frac{nx^2(t)}{2\sigma^2}\right) \right\rangle dt - \sigma \sqrt{\frac{\pi}{2n}} \int_0^\tau \dot{f}(t) \left\langle \operatorname{erf}\left(\sqrt{\frac{n}{2}}\frac{x(t)}{\sigma}\right) \right\rangle dt \right], \end{aligned} \quad (4.20)$$

⁶⁶⁷ where $\langle \cdot \rangle$ is the ensemble average with the probability density distribution under
⁶⁶⁸ ε . Substituting Eq. (4.15) into (4.12) and using Jensen's inequality to calculate Eq.
⁶⁶⁹ (4.12), we obtain

$$\langle W_{eff} \rangle = \langle W \rangle - \ln 2 \sum_{n=1}^{\infty} F_n(\varepsilon, \sigma, \tau) \varepsilon^n \geq (1 + \varepsilon) \ln 2. \quad (4.21)$$

⁶⁷⁰ Expanding $F_n(\varepsilon, \sigma, \tau)$ in Eq. (4.21) when ε is small, one gets

$$\frac{\langle W \rangle}{\ln 2} \geq 1 + \varepsilon \left(1 + F_1^{(0)}(0, \sigma, \tau) \right) + \varepsilon^2 \left(F_2^{(0)}(0, \sigma, \tau) + F_1^{(1)}(0, \sigma, \tau) \right) + O(\varepsilon^3), \quad (4.22)$$

⁶⁷¹ where the superscript indicates the number of times F_n is differentiated with respect
⁶⁷² to ε , and the equation holds when $\tau \rightarrow \infty$, i.e., Landauer limit, written as $\langle W \rangle_L$.
⁶⁷³ To have good information storage capabilities, E_b needs to be relatively large. As
⁶⁷⁴ mentioned in the previous section, the transition rate of the effective barrier also
⁶⁷⁵ satisfies the classical behavior. Here we choose $E_b = 10$. The simulation results of
⁶⁷⁶ the original and effective work are shown in Fig. 4.2(a) and 4.2(b), where the time
⁶⁷⁷ step of the Langevin simulation is $dt = 10^{-4}$, and we average over 10^5 trajectories.

⁶⁷⁸ In the effective system, it can be seen that the fitting line hits the predicted dashed

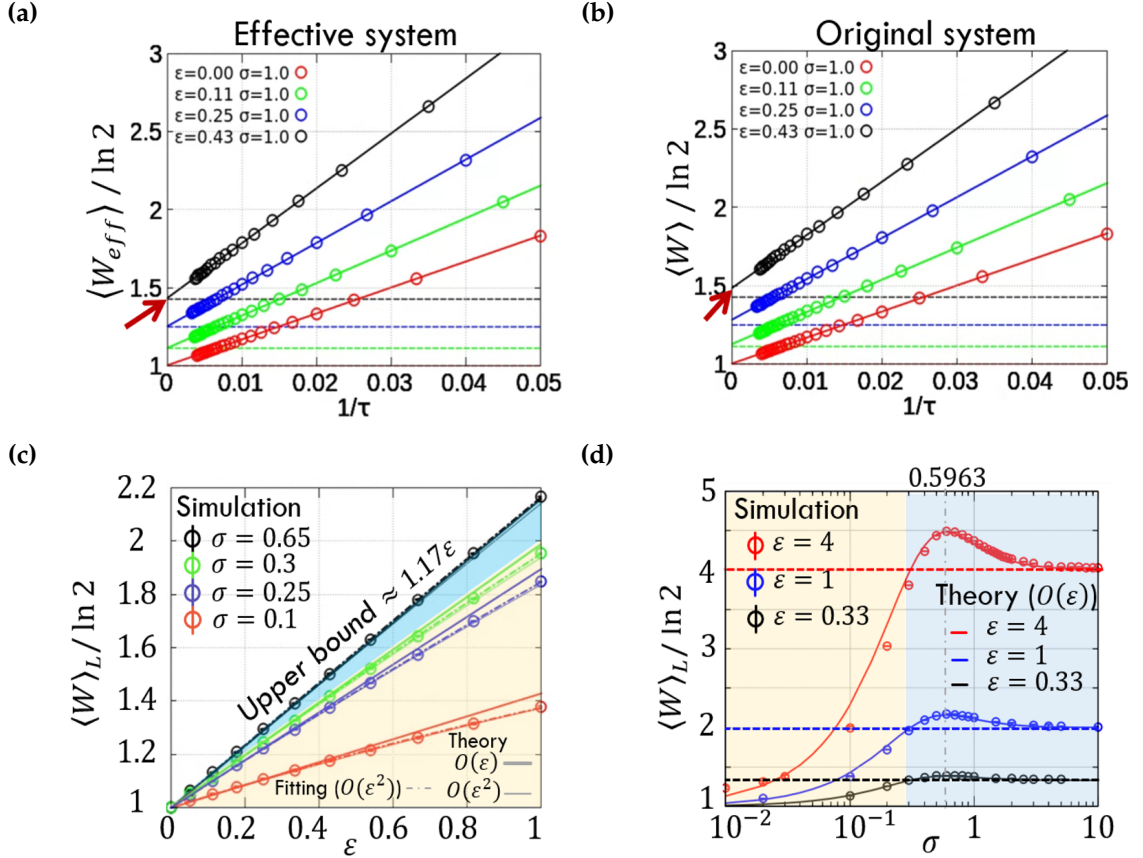


FIGURE 4.2: (a) The Landauer limit, as predicted by Eq. (4.21), aligns with the dotted line. (b) The Landauer limit can be higher than the entire temperature field. The circles, solid lines, and dashed lines represent the Langevin simulation, fitting curve, and the Landauer limit, taking T_0 as the temperature, respectively. (c) The Landauer limit varies with ϵ . The upper bound corresponds to the peak value shown in (b), and the thick and thin solid lines represent the 1st and 2nd-order theories, respectively, in Eq. (4.22). When σ is small, the 2nd-order coefficient is more important than when σ is large. (d) The Landauer limit varies with σ . The yellow region represents the normal Landauer limit (between T_0 and T_∞), while the blue region denotes the anomalous Landauer limit (exceeding the entire temperature field).

line at time $\tau \rightarrow \infty$ (Eq. (4.21)) for different ε cases. However, as shown in Fig. 4.2(b), the measured average work of the original system extrapolated to large τ appears to be higher than the predicted value of $1 + \varepsilon$ (marked by the dashed lines). This means that the leading temperature factor coefficient of the Landauer limit under the non-uniform temperature field may not be a weighted average of the position of particles. This conclusion should be able to be calculated from Eq. (4.22), and the results are shown in Fig. 4.2(c) and 4.2(d). For convenience, if the temperature coefficient of the Landauer limit exceeds the entire temperature field, it is referred to as the anomalous Landauer limit; otherwise, it is called the normal Landauer limit. In Fig. 4.2(c), for a fixed σ , the Landauer limit varies almost linearly with ε . The yellow region is the normal Landauer limit, and the blue region is the anomalous Landauer limit. In Fig. 4.2(d), for a fixed ε , it is obvious that the scale of σ affects the Landauer limit in the blue or yellow region. This can be understood as the fact that the double-well potential constrains the particles within a certain range; therefore, the temperature gradient within a certain range can increase the Landauer limit. The thin and thick curves in both figures are the first-order $O(\varepsilon)$ and the second-order $O(\varepsilon^2)$ approximation in Eq. (4.22). Clearly, those curves are good approximations. We also try to compare the first-order and second-order approximation curves, and the results are shown in Table 4.1. We calculate two cases, $\sigma = 0.65$ and $\sigma = 0.25$, where the second-order term is significantly smaller than the first-order term. Therefore, the first-order coefficients dominate the Landauer limit, and we can ignore the second-order term in our system.

Coefficients	σ	Numerical integral	Fitting Eq. (4.22) (up to ε^2)
$1 + F_1^{(0)}$	0.65	1.1571	1.1682 ± 0.0012
	0.25	0.8945	0.8982 ± 0.0031
$F_1^{(1)} + F_2^{(0)}$	0.65	-0.0167	-0.0143 ± 0.0050
	0.25	-0.0585	-0.0525 ± 0.0038

TABLE 4.1: The coefficients table of the first-order and second-order terms of two cases $\sigma = 0.65$ and $\sigma = 0.25$, where the numerical integral is obtained by integrating Eq. (4.20).

In summary, the Landauer limit can counterintuitively exceed the corresponding Landauer limit at uniform temperatures for the entire temperature range, with

703 a maximum at $\sigma \approx 0.6$. These results show that the coefficient of the Landauer
704 limit may not be the simple weighted average of the temperature experienced by the
705 particle. Further investigation of the relevant energetics could provide insight for
706 manipulating the dissipation.

707 In addition, in the previous chapter, we learned that a single-well trap and a
708 non-uniform temperature field can produce a bimodal distribution. This bimodal
709 effective potential can also store information as an ordinary double-well potential.
710 Theoretically, the system can also store information, but the storage stability is insuf-
711 ficient. An interesting question is whether we can use a time-varying temperature
712 field to erase information. This is the main research direction for the future.

TWO-DIMENSIONAL AUTONOMOUS BROWNIAN GYRATOR

716 In previous chapters, for Brownian motion in one dimension, the competition be-
 717 tween the diffusion field and the trapping potential can be mapped to an effective
 718 potential. In a two-dimensional system, it may not be possible to find the corre-
 719 sponding effective potential analytically, especially when the temperature field is a
 720 tensor field. The concept of temperature here can be understood as the amplitude of
 721 thermal fluctuations of Brownian particles. Through experiments and simulations,
 722 it has been discovered that for a two-dimensional system with two different uniform
 723 temperatures on the orthogonal axes and in a harmonic potential well, the average
 724 trajectory of the Brownian particle rotates autonomously, known as the autonomous
 725 Brownian gyrator [6–7]. It has also been observed from numerical simulations that
 726 the probability density flux \vec{J} is not perpendicular to the equiprobability contour un-
 727 der a non-harmonic potential trap, in contrast to the harmonic case. In this chapter,
 728 we discuss whether, for the case of a single spatially non-uniform temperature field,
 729 a Brownian gyrator can lead to a Brownian gyrator. Then we further discuss the
 730 conditions that can lead to the generation of the gyrating probability fluxes.

5.1 The most general two-dimensional system

732 Starting from the steady-state Fokker-Planck equation, (2.30), the i^{th} component of
 733 the equation (using Einstein summation convention) is written as ($k_B = 1$)

$$\partial_i(P(x_1, x_2)\partial_i U(x_1, x_2) + \partial_j(T_{ij}(x_1, x_2)P(x_1, x_2))) = -\partial_i J_i(x_1, x_2) = 0, \quad (5.1)$$

5.2. $T_{12} = T_{21} = 0$ but T_{11} and $T_{22} \neq 0$

⁷³⁴ where $T_{ij} \geq 0$ is the temperature tensor and ∂_i represents $\frac{\partial}{\partial x_i}$ T_{ij} is defined as

$$\hat{T} \equiv \begin{bmatrix} T_{11}(x_1, x_2) & T_{12}(x_1, x_2) \\ T_{21}(x_1, x_2) & T_{22}(x_1, x_2) \end{bmatrix}. \quad (5.2)$$

⁷³⁵ If we define $\phi = -\ln(P)$, the probability density flux can be rewritten as

$$J_i = P(-\partial_i U - \partial_j T_{ij} + T_{ij} \partial_j \phi) \equiv P v_{av,i}, \quad (5.3)$$

⁷³⁶ where $v_{av,i}$ is the i^{th} component of the drift (average) velocity of the Brownian particle,
⁷³⁷ J_i . Therefore, (5.1) can be simplified to

$$\partial_i v_{av,i} - v_{av,i} \partial_i \phi = 0. \quad (5.4)$$

⁷³⁸ Therefore, when \vec{v}_{av} is divergence-free, $\vec{v}_{av} \cdot \nabla \phi = 0$, i.e., \vec{v}_{av} is perpendicular to the
⁷³⁹ equiprobability curve. However, there is no clear stipulation that $\vec{v}_{av} \cdot \nabla \phi$ should be
⁷⁴⁰ 0. We will see that under a non-uniform temperature tensor field with $T_{11} = T_{22}$,
⁷⁴¹ $\vec{v}_{av} \cdot \nabla \phi$ is not 0 unless $\vec{v}_{av} = 0$. As will be demonstrated in the next section, \vec{v}_{av}
⁷⁴² must have a non-vanishing curl to produce a Brownian gyrator. The curl of \vec{v}_{av} can
⁷⁴³ be written as (using (5.3))

$$(\nabla \times \vec{v}_{av})_i = \epsilon_{ijk} \partial_j (T_{kl} \partial_l \phi - \partial_l T_{kl}), \quad (5.5)$$

⁷⁴⁴ where ϵ_{ijk} is Levi-Civita symbol. Generally, in physical systems, \hat{T} is a symmetric
⁷⁴⁵ tensor. To facilitate a better understanding, we first discuss the situation when the
⁷⁴⁶ off-diagonal terms are 0.

5.2 $T_{12} = T_{21} = 0$ but T_{11} and $T_{22} \neq 0$

⁷⁴⁷ This section will discuss the case where the off-diagonal terms of T_{ij} are 0. Using
⁷⁴⁹ (5.5), the curl of \vec{v}_{av} can be simplified to

$$\begin{aligned} \nabla \times \vec{v}_{av} &= [T_{22} - T_{11}] \partial_1 \partial_2 \phi + [\partial_1 (T_{22}) \partial_2 \phi - \partial_2 (T_{11}) \partial_1 \phi] + \partial_1 \partial_2 [T_{11} - T_{22}] \\ &= \nabla \times (\hat{T} \cdot \nabla \phi) - \nabla \times (\nabla \cdot \hat{T}), \end{aligned} \quad (5.6)$$

750 that is, three terms affect the curl of \vec{v}_{av} . If we directly solve the Fokker-Planck equa-
 751 tion for \vec{v}_{av} , we can determine the characteristics of \vec{v}_{av} . However, directly solving
 752 the Fokker-Planck equation is difficult. Therefore, we try to discuss some properties
 753 in some cases.

754 **5.2.1 The case of $T_{11}(x_1, x_2) = T_{22}(x_1, x_2) = T(x_1, x_2)$**

755 Since T degenerates into a scalar field ($T_{11} = T_{22}$), (5.6) further simplified to

$$\nabla \times \vec{v}_{av} = \nabla T \times \nabla \phi. \quad (5.7)$$

756 This implies that if T is a constant or ∇T is parallel (or anti-parallel) to $\nabla \phi$, then the
 757 curl of \vec{v}_{av} vanishes. First, we will explain why $\vec{v}_{av} \cdot \nabla \phi$ cannot be 0 unless $\vec{v}_{av} = 0$,
 758 that is, \vec{v}_{av} must be a field with sources. Using the definition of \vec{v}_{av} in (5.3), one has

$$\vec{v}_{av} = -\nabla(U + T) + T\nabla\phi. \quad (5.8)$$

759 Substituting \vec{v}_{av} into (5.4), one gets

$$\nabla \cdot \vec{v}_{av} = \vec{v}_{av} \cdot \nabla \phi = (-\nabla(U + T) + T\nabla\phi) \cdot \nabla\phi. \quad (5.9)$$

760 Suppose $\vec{v}_{av} \cdot \nabla \phi = 0$, then (5.9) implies \vec{v}_{av} is divergence-free, that is, $\nabla \cdot \vec{v}_{av} = 0$. If we
 761 consider a restricted potential trap (in an open boundary), since the particle cannot
 762 go to infinity, \vec{J} usually forms some closed loops. Since P is not 0, \vec{v}_{av} must also have
 763 at least one closed loop. Calculating the circulation of \vec{v}_{av} around such a loop (using
 764 the fact that the circulation of a gradient field is 0), one gets from the expression of
 765 \vec{v}_{av} in (5.8)

$$\oint_{\partial S} \vec{v}_{av} \cdot d\vec{\ell} = \oint_{\partial S} T\nabla\phi \cdot d\vec{\ell}. \quad (5.10)$$

766 Then, by selecting \vec{v}_{av} along the closed circulation path, we have

$$\oint_{\partial S} T(\nabla\phi \cdot \hat{v}_{av}) d\ell = \oint_{\partial S} |\vec{v}_{av}| d\ell \geq 0, \quad (5.11)$$

767 where \hat{v}_{av} is a unit vector of \vec{v}_{av} . But by the assumed condition of $\vec{v}_{av} \cdot \nabla \phi = 0$, the
 768 left integral is 0; the only possibility is that $\vec{v}_{av} = 0$ from the right integral. Hence,
 769 we have the following condition:

5.2. $T_{12} = T_{21} = 0$ but T_{11} and $T_{22} \neq 0$

Condition 1

For $T_{11}(\vec{x}) = T_{22}(\vec{x})$, it is impossible to have $\vec{v}_{av} \cdot \nabla \phi = 0$ unless $\vec{v}_{av} = 0$.

770

771 For the special case of a uniform T , one always has $\vec{v}_{av} = 0$. A non-uniform $T(x)$ al-
 772 lows an interesting possible non-trivial nonequilibrium steady state (NESS) scenario
 773 ($\vec{v}_{av} \neq 0$) with $\vec{v}_{av} \cdot \nabla \phi \neq 0$. This means that for non-trivial NESSs \vec{v}_{av} is always a
 774 vector field with sources (see (5.9)), but \vec{J} is always divergence-free. Note that this
 775 is different from the situation considered in [6] in which $T_{11} \neq T_{22}$. Since $T_{11} \neq T_{22}$
 776 and from (5.3), \vec{v}_{av} involves the term $\partial_j T_{ij}$, which is not a gradient field and does not
 777 vanish in the loop integral (5.10). This prevents one from supposing $\vec{v}_{av} \cdot \nabla \phi = 0$ to
 778 assert a vanishing \vec{v}_{av} circulation. Even if both T_{11} and T_{22} are two distinct constants
 779 (i.e., $\partial_j T_{ij} = 0$ in (5.3)), the circulation in (5.10) reads

$$\oint_{\partial S} T_{ij} \partial_j \phi \cdot \hat{v}_i \, d\mathbf{r}. \quad (5.12)$$

780 Obviously, due to the tensorial product of T_{ij} and $\partial_j \phi$, the assumption of $\vec{v}_{av} \cdot \nabla \phi = 0$
 781 cannot be applied directly to simplify the loop integral (5.10). In other words, the
 782 tensorial nature of T_{ij} leads to the possibility that even if \vec{v}_{av} is perpendicular to $\nabla \phi$,
 783 the circulation of \vec{v}_{av} may not be 0. In fact, for a Brownian particle under a harmonic
 784 potential and two distinct uniform temperatures along the axes, a NESS exists with
 785 non-vanishing \vec{v}_{av} but with \vec{v}_{av} perpendicular to $\nabla \phi$, which is the only such a spe-
 786 cial case observed so far as reported in [6]. The curl of \vec{v}_{av} is usually a constant in
 787 this special situation. The reason is that the potential well is a quadratic function,
 788 making ϕ also a quadratic function under two uniform temperatures. Note that, in
 789 general, ϕ and U have distinct functional forms, and the corresponding NESS has a
 790 non-vanishing \vec{v}_{av} that is not perpendicular to $\nabla \phi$.

791 Return to the $T_{11} = T_{22}$ case. We further examine possible relations between $\nabla \times \vec{J}$
 792 and $\nabla \times \vec{v}_{av}$. We claim that $\nabla \times \vec{J} = 0$ iff $\nabla \times \vec{v}_{av} = 0$. The argument goes as follows:
 793 For steady states, $\vec{J} = P_{ss} \vec{v}_{av}$, we have

$$\begin{aligned} \nabla \times \vec{J} &= \nabla P_{ss} \times \vec{v}_{av} + P_{ss} \nabla \times \vec{v}_{av} \\ &= P_{ss} \nabla \phi \times \nabla(U + T) + P_{ss} \nabla T \times \nabla \phi \\ &= P_{ss} (\nabla \phi \times \nabla U). \end{aligned} \quad (5.13)$$

794 Notice that ϕ is determined by U and T , i.e., $\phi(U, T)$. Using the chain rule, the gradi-
 795 ent of ϕ can be written as

$$\nabla\phi = \frac{\partial\phi}{\partial U}\nabla U + \frac{\partial\phi}{\partial T}\nabla T \equiv f_1\nabla U + f_2\nabla T, \quad (5.14)$$

796 where f_1 and f_2 are some scalar functions that are not equal to 0. Hence, equation
 797 (5.13) can be written as

$$\nabla \times \vec{J} = P_{ss}f_2\nabla T \times \nabla U. \quad (5.15)$$

798 On the other hand, substituting (5.14) into (5.7), one gets

$$f_1\nabla T \times \nabla U = \nabla \times \vec{v}_{av} = \nabla T \times \nabla\phi. \quad (5.16)$$

799 Therefore, combine (5.15) and (5.16), we get

$$\nabla \times \vec{J} = P_{ss} \frac{f_2}{f_1} (\nabla \times \vec{v}_{av}). \quad (5.17)$$

800 This tells us that the only difference between $\nabla \times \vec{J}$ and $\nabla \times \vec{v}_{av}$ is a scalar function.
 801 In addition, according to the equation (5.16), $\nabla\phi = 0$ implies $\nabla T \times \nabla U = 0$, but for
 802 those points satisfying $\nabla\phi = 0$ may not satisfy $\nabla T \times \nabla U = 0$. This conclusion can
 803 directly predict the points of $\nabla \times \vec{J} = 0$ in space and the possible location of the
 804 extreme point of ϕ , given only T and U . This is the second condition:

Condition 2

- (I) There are always some points in the $x_1 - x_2$ plane that satisfy the following equivalent conditions: $\nabla \times \vec{J} = 0 \iff \nabla \times \vec{v}_{av} = 0 \iff \nabla T \times \nabla U = 0$.
- (II) The local extrema of the effective potential ($\nabla\phi = 0$) satisfy the condition $\nabla T \times \nabla U = 0$.

805 It should be noted that the converse of (II) may not be true, i.e., some points sat-
 806 isfying $\nabla T \times \nabla U = 0$ may not be a local extremum of ϕ .

807 In addition to this, $\nabla T \times \nabla U$ determines the local vortex rotation direction. This
 808 can be derived from the second law of thermodynamics. The total entropy S_{tot} is
 809 composed of the system entropy S_{sys} plus the environment entropy S_Q . Since the
 810 system entropy S_{sys} is a state function, its change over any closed path is equal to

5.2. $T_{12} = T_{21} = 0$ but T_{11} and $T_{22} \neq 0$

812 zero fro NESS. Therefore,

$$\oint_{ssf} dS_{tot} = \oint_{ssf} dS_Q = - \oint_{ssf} \frac{\nabla U(\vec{r})}{T(\vec{r})} \cdot d\vec{r} = \int_{ssf} \frac{\nabla T \times \nabla U}{T^2} \cdot d\vec{A} \geq 0, \quad (5.18)$$

813 where “ssf” designates that the physical quantity is evaluated along a NESS flow
 814 path \vec{J} , and \vec{A} is the direction of the area covered by the loop. Thus, the direction of
 815 $\nabla T \times \nabla U$ in space is the same as the local vortex direction.

816 Note that Condition 2 only tells us that $\nabla T \times \nabla U = 0$ iff $\nabla \times \vec{v}_{av} = 0$. But how
 817 about the condition for $\vec{v}_{av} = 0$? We will discuss this condition and show that a
 818 system with non-vanishing flux is due to the breaking of the condition $\nabla T \times \nabla U = 0$
 819 somewhere. First, we consider $\vec{v}_{av} = 0$ which gives (from (5.8))

$$\nabla(U + T) = T\nabla\phi. \quad (5.19)$$

820 Using the curl identity, one obtains the relation between U and T ,

$$\nabla \times \nabla\phi = \nabla \frac{1}{T} \times \nabla(U + T) + \frac{1}{T} \nabla \times \nabla(U + T) = -\frac{\nabla T \times \nabla U}{T^2} = 0. \quad (5.20)$$

821 Therefore, one obtains the sufficient condition for $\vec{v}_{av} = 0$:

$$\vec{v}_{av} = 0 \Rightarrow \nabla T \times \nabla U = 0. \quad (5.21)$$

822 Next, we derive the sufficient condition of $\nabla T \times \nabla U = 0$. Use Condition 2,

$$\nabla T \times \nabla U = 0 \iff \nabla \times \vec{J} = 0, \quad (5.22)$$

823 and notice the steady-state condition of \vec{J} in the Fokker-Planck equation (5.1)

$$\nabla \cdot \vec{J} = 0. \quad (5.23)$$

824 Combining (5.22) and (5.23), and use the Helmholtz theorem that if a vector field \vec{J}
 825 convergence fast enough and the curl and divergence are 0 “in the entire space” ,
 826 this vector field is a 0 vector field. Of course, in general, the probability flux quickly
 827 converges to 0 at infinity because the potential energy limits where the particles can

828 go. Thus, the sufficient condition of $\nabla T \times \nabla U = 0$ is

$$\nabla T \times \nabla U = 0 \text{ (everywhere)} \Rightarrow \vec{J} = 0 \text{ (everywhere)}. \quad (5.24)$$

829 We emphasize that this is only true when the entire space is 0. Note that (5.21) holds
830 not only when the entire space is 0 but also locally.

831 In addition, we can use (5.24) to deduce $\vec{v}_{av} = 0$ because $\vec{J} = P_{ss}\vec{v}_{av}$ and $P_{ss} \neq 0$.
832 Combining (5.24) and (5.21), therefore, we get the third condition:

Condition 3

A system with particle flux is due to the breaking of $\nabla T \times \nabla U = 0$ somewhere.
In other words, $\nabla T \times \nabla U = 0$ everywhere $\iff \vec{v}_{av} = \vec{J} = 0$ everywhere.

833 Conditions 2 and 3 also tell us that for NESS with non-vanishing particle flux, \vec{v}_{av}
834 is not a gradient field. This is because if \vec{v}_{av} is a gradient field, then its curl will be 0
835 (i.e., $\nabla \times \vec{v}_{av} = 0$ everywhere). Then, according to Condition 2, we get $\nabla T \times \nabla U =$
836 0 everywhere. Thus, using Condition 3, \vec{v}_{av} must be 0. After understanding the
837 cause of particle flux, one may be interested in seeing if one can derive the effective
838 potential ϕ analytically in the same way as in the one-dimensional case with zero
839 particle flux? The answer is true, and we can also generalize the answer to high-
840 dimensional situations. The expression of P can be written when $\vec{v}_{av} = 0$. Using
841 (5.19) and the gradient theorem, we get (for no flux situation)

$$\phi(\vec{r}) - \phi(0) = \int_C \nabla \phi \cdot d\vec{r} = \int_0^{\vec{r}} \nabla \phi \cdot d\vec{r} = \int_0^{\vec{r}} \frac{\nabla(U + T)}{T(\vec{r})} \cdot d\vec{r}, \quad (5.25)$$

843 where C represents integration along a path, but the result of integration is only
844 related to the beginning and end due to the gradient theorem. Then, taking the
845 exponent, the equation (5.25) can be written as

$$P(\vec{r}) \propto \frac{1}{T(\vec{r})} \exp \left(- \int^{\vec{r}} \frac{\nabla U(\vec{r}')}{T(\vec{r}')} \cdot d\vec{r}' \right) \equiv \exp(-\phi(\vec{r})), \quad (5.26)$$

846 where $\phi(\vec{r})$ is the effective potential. Because the integration is only related to the
847 upper and lower bounds, it must be a path-independent function. Thus, if a system
848 has zero particle flux, an effective potential can be found. If $\vec{v}_{av} \neq 0$, then the integral
849 will depend on the path. In addition, since there is no restriction on the dimensions

5.2. $T_{12} = T_{21} = 0$ but T_{11} and $T_{22} \neq 0$

850 of \vec{r} , this result is applicable in high dimensions. Therefore, for high dimensions
 851 under the zero particle flux condition: $T(\vec{r}) = f(U(\vec{r}))$ (where f is some differentiable
 852 function), the effective potential is given by

$$\phi(\vec{r}) = \int^{U(\vec{r})} \left[\frac{1 + f'(V)}{f(V)} \right] dV. \quad (5.27)$$

853 This result can be derived by substituting $T(\vec{r}) = f(U(\vec{r}))$ into (5.19) and integrat-
 854 ing. In Chapter 3, equation (3.2) is the one-dimensional case in (5.26). In the one-
 855 dimensional case, since ∇T is always parallel to ∇U , it must satisfy Condition 3. This
 856 once again verifies our result in Chapter 3, that is, a one-dimensional non-uniform
 857 temperature system is a system with zero particle flux.

858 Next, we consider explicit functional forms of potentials and temperature fields
 859 to confirm the above-mentioned properties. For convenience, unless otherwise spec-
 860 ified, the temperature field is in the form of a Gaussian function.

$$T(x_1, x_2) = a + \exp \left(-\frac{x_1'^2}{\sigma_{T1}^2} - \frac{x_2'^2}{\sigma_{T2}^2} \right), \quad (5.28)$$

861 where x'_1 and x'_2 represent the coordinates after the rotation matrix, and a , σ_{T1} and
 862 σ_{T2} are constants. We define the rotation matrix for clockwise rotation, and the angle
 863 is defined starting from the first quadrant (see Fig. 5.1).

$$\begin{bmatrix} x'_1 \\ x'_2 \end{bmatrix} = \begin{bmatrix} \cos(\theta_i) & \sin(\theta_i) \\ -\sin(\theta_i) & \cos(\theta_i) \end{bmatrix} \begin{bmatrix} x_1 \\ x_2 \end{bmatrix}, \quad (5.29)$$

864 where $i = T, U$ represents the tilted angle of the temperature field T or potential
 865 energy U respectively as shown in Fig. 5.1.

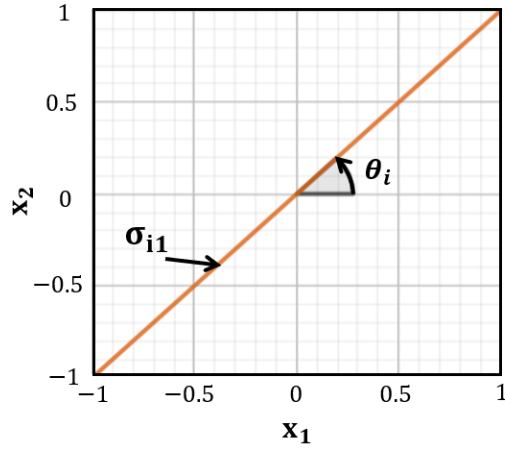


FIGURE 5.1: The definition of tilted angle is the σ_{i1} axis, where $i = U$ or T , starts counterclockwise from the first quadrant.

866 **A. Harmonic Potential**

867 First, we consider a Harmonic potential which is given by

$$U(x_1, x_2) = \frac{x_1'^2}{\sigma_{U1}^2} + \frac{x_2'^2}{\sigma_{U2}^2}, \quad (5.30)$$

868 where x'_1, x'_2 is defined in (5.29), and σ_{U1} and σ_{U2} are two constants. For $U(\vec{x})$ and $T(\vec{x})$
 869 given by (5.30) and (5.28) respectively, the loci of points that satisfy $\nabla T \times \nabla U = 0$ (or
 870 equivalently $\nabla \times \vec{J} = 0$) are two straight lines through the origin. These two lines
 871 cross at an angle that depends on θ_T and θ_U (we will see that this angle is a function
 872 of $\theta_T - \theta_U$). We can easily verify that if T has radial symmetry, then these two lines
 873 are perpendicular. This means that $\vec{J}(x_1, x_2)$ is mirror-symmetric, so the average
 874 rotation of the particles is 0. Thus, the necessary condition for the mean trajectory to
 875 be gyrating about the origin (potential minimum) is to break the mirror symmetry
 876 involving regions separated by these two lines. A simple way to verify our statement
 877 is to calculate the average angular gyration velocity of the particle around the origin,
 878 $\langle \omega \rangle$.

$$\langle \omega \rangle = \iint \frac{\vec{r} \times \vec{J}}{|\vec{r}|^2} d\vec{r} = \iint \frac{xJ_y - yJ_x}{x^2 + y^2} dx dy, \quad (5.31)$$

5.2. $T_{12} = T_{21} = 0$ but T_{11} and $T_{22} \neq 0$

879 where J_x and J_y are the components of the particle flux. The integral can be ex-
 880 pressed in polar coordinates as

$$\langle \omega \rangle = \int_0^\infty \int_0^{2\pi} J_\theta(r, \theta) dr d\theta, \quad (5.32)$$

881 where J_θ is the θ direction component of \vec{J} . If the integral is non-zero, the Brownian
 882 particle trajectory will gyrate around the origin on average. For convenience, we
 883 define two quantities

$$\Sigma_i \equiv \sigma_{i1}^2 + \sigma_{i2}^2; \quad \Delta_i \equiv \sigma_{i1}^2 - \sigma_{i2}^2,$$

884 where $i = U, T$ are the axes. Now, let us start with the simple case of a temperature
 885 field where T is a Gaussian function in only one direction.

$$T(x_1) = a + \exp\left(-\frac{x_1'^2}{\sigma_{T1}^2}\right) \quad (5.33)$$

886 This system always has a non-vanishing particle flux in this case because $\nabla T \times \nabla U \neq$
 887 0 for any values of θ_T or θ_U . The difference from the temperature field where both
 888 axes are Gaussian is that there is a straight line that remains stationary when we fix
 889 θ_T , that is, $\nabla T = 0$ is a line only depending on θ_T .

890 The loci of points satisfying of $\nabla T \times \nabla U = 0$ are two straight lines givne by

$$x_2 = -\cot(\theta_T)x_1, \quad (5.34)$$

$$x_2 = \frac{\Delta_U[-\cos(2(\theta_U - \theta_T)) + \cos(2\theta_U)] + \Sigma_U(\cos(2\theta_T) - 1)}{\Delta_U[\sin(2(\theta_U - \theta_T)) - \sin(2\theta_U)] - \Sigma_U \sin(2\theta_T)} x_1. \quad (5.35)$$

891 The two straight lines are independent of σ_{T1} . This means that σ_{T1} only shifts and
 892 scales the P along one line. In addition, the relative angle (we named $\Psi(\theta_T - \theta_U)$) of
 893 the two straight lines oscillates with $\theta_T - \theta_U$ instead of maintaining a fixed relative
 894 angle, which is shown in Fig. 5.2. Take the arctangent of the slope ((5.34) and (5.35))
 895 and use the fact

$$\arctan(f(x)) \bmod \pi = \frac{\pi}{2} - \arctan(f(x)^{-1}), \quad (5.36)$$

896 where $f(x)$ is arbitrary function. We obtain the relation

$$\Psi(\theta_T - \theta_U) = \frac{\pi}{2} + \arctan \left(\frac{\sin(2(\theta_T - \theta_U))}{\cos(2(\theta_T - \theta_U)) + \frac{\Sigma_U}{\Delta_U}} \right), \quad (5.37)$$

897 where the extrema of Ψ occur at

$$\theta_T - \theta_U = n\pi \pm \arctan \left(\frac{\sigma_{U1}}{\sigma_{U2}} \right); \quad n \in \mathbb{N}, \quad (5.38)$$

898 and the optimal relative angle is

$$\arctan \left(\frac{|\Delta_U|}{2\sigma_{U1}\sigma_{U2}} \right) + \frac{\pi}{2}. \quad (5.39)$$

899 It means if $\Delta_U = 0$, then the relative angle Ψ maintains at $\pi/2$.

900 Now, consider the potential U with parameters $\sigma_{U1} = \sqrt{2}$, $\sigma_{U2} = 1$ and $\theta_U = 0$.
901 The theoretical results are shown in Fig. 5.2. Fig. 5.2(a) shows that Ψ first increases
902 with θ_T and then decreases if θ_U is fixed to 0. This is verified by the Langevin simula-
903 tion shown in Fig. 5.2, where the angle between the two blue lines, Ψ , oscillates with
904 θ_T (with θ_U fixed at 0). The color and arrows represent the steady-state probability
905 density and particle flux fields, respectively. We confirm that the blue line indeed
906 passes through the $\nabla \times \vec{J} = 0$ position in Fig. 5.2 and distinguishes four spaces and
907 forms two pairs of vortices.

908 An interesting question is whether different sizes of these four vortices (that is, if
909 $\Psi \neq \pi/2$,) will cause the mean trajectory of the Brownian particles to gyrate around
910 the origin like a Brownian gyrator. The answer is true. The Brownian particle rotates
911 on average in the four small loops, but whether there is a net circulation about the
912 origin depends on $\langle \omega \rangle$ given by Eq. (5.31). In addition, the location of the two straight
913 lines can determine whether the \vec{J} field of the system has the required symmetry for
914 a vanishing $\langle \omega \rangle$. One can see from Fig. 5.2(b) that, if the relative angle $\Psi = \pi/2$, the
915 average angular velocity vanishes for different values of σ_{T1} .

916 A reasonable inference is that when $\Psi = \pi/2$, the four vortices of the same size
917 (distinguished by two lines) cancel with each other, thus causing the net circulation
918 ω to be 0 on average. Thus, the rotated direction of the Brownian particle can be seen
919 from the rotated direction of the larger pair of vortices, which dominates the overall
920 average rotated direction. According to (5.37), if $\Delta_U = 0$ or $\theta_T = \theta_U$, Ψ equals to $\pi/2$,

5.2. $T_{12} = T_{21} = 0$ but T_{11} and $T_{22} \neq 0$

which means that the two straight lines have mirror symmetry. Thus, the Brownian particle has a net circulation around the origin due to the breaking of the symmetry between the regions separated by the two straight lines satisfying $\nabla T \times \nabla U = 0$. The local direction of vortex rotation can be given by Eq. (5.18), so one can predict whether the Brownian particle will have a net gyration around the origin, for given T and U .

It is worth noting that since the gyration of the Brownian particle about the origin is determined by whether regions separated by the two lines have symmetry, the system may not have a net gyration around the origin even if it far from non-equilibrium (see Fig. 5.4(a) and Fig. 5.2(b) at $\theta = 0$ or π). According to Condition 3, if U and T have the same functional form, $\nabla T \times \nabla U = 0$ everywhere. Therefore, the degree of similarity between the two functions is related to the degree of non-equilibrium of the system, i.e., $\langle \dot{S} \rangle$. Since the temperature field is (5.33) (σ_{T2} tends to infinity), σ_{T1} plays the role of the minor axis and σ_{T2} is the infinitely long major axis. Note that σ_{U1} is the major axis and σ_{U2} is the minor axis for U . Thus, when the major and minor axes of T overlap with U , the two functional forms are most similar. This happens when $\theta_T = \pi/2$ because the major axis of the temperature field (σ_{T2}) will coincide with the major axis of the potential well (σ_{U1}) after rotating $\pi/2$. This is the reason why the minimum value of $\langle \dot{S} \rangle$ occurs at $\theta_T = \pi/2$ as shown in Fig. 5.4(a). As σ_{T1} increases, T tends to a constant like a uniform temperature field. Therefore, the larger σ_{T1} , the smaller $\langle \dot{S} \rangle$ in the uniaxial case.

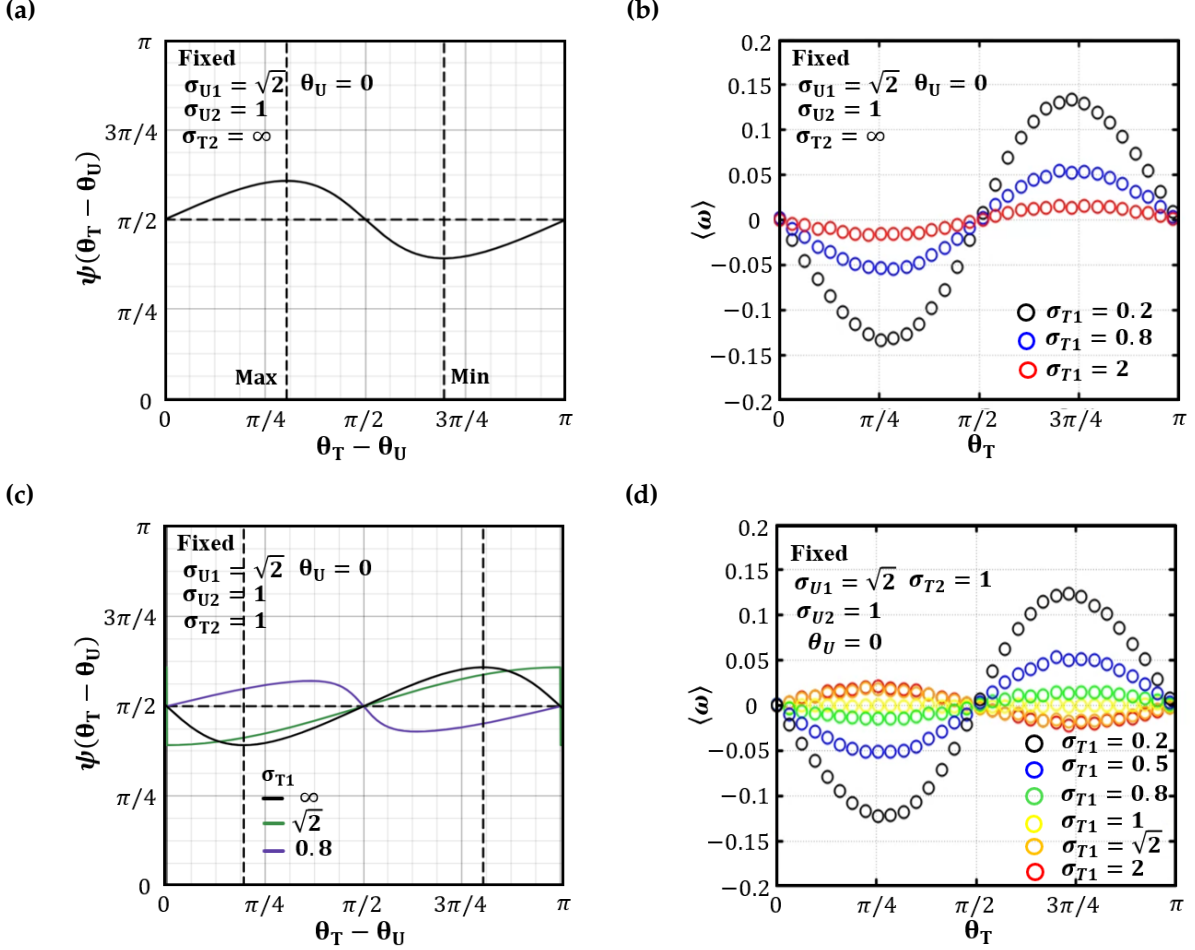


FIGURE 5.2: (a) Under the uniaxial Gaussian temperature field, the relative angle Ψ (purple solid curve) between two straight lines ($\nabla \times \vec{J} = 0$) vary with $\theta_T - \theta_U$ in a period. Note that when $\sigma_{T2} \rightarrow \infty$, Ψ is independent of σ_{T1} and σ_{T2} . We fixed $\theta_U = 0$, $\sigma_{U1} = \sqrt{2}$, $\sigma_{U2} = 1$, $\sigma_{T2} \rightarrow \infty$ and $a = 0$. (b) Under the uniaxial Gaussian temperature field and fixing the harmonic potential, the Langevin simulation of the mean angular velocity of the Brownian particle varies with θ_T . For all $\theta_T - \theta_U = 0, \pi/2$ and π , $\langle \omega \rangle = 0$. The fixed parameters are the same as (a). (c) Under the biaxial Gaussian temperature field, Ψ varies with $\theta_T - \theta_U$ in a period. The different σ_{T1} effects the waveform of Ψ . We fixed $\theta_U = 0$, $\sigma_{U1} = \sqrt{2}$, $\sigma_{U2} = \sigma_{T2} = 1$ and $a = 0$. (d) Under the biaxial Gaussian temperature field, the mean rotation angular velocity varies with θ_T . The direction of rotation is related to the relative sizes of σ_{T1} and σ_{T2} . It does not rotate when $\sigma_{T1} = \sigma_{T2}$. We fixed parameters that are the same as (c). (b) and (d) are obtained from $N_{sample} = 10^4$ trajectories and the time of each trajectory is $\tau = 10^3$.

5.2. $T_{12} = T_{21} = 0$ but T_{11} and $T_{22} \neq 0$

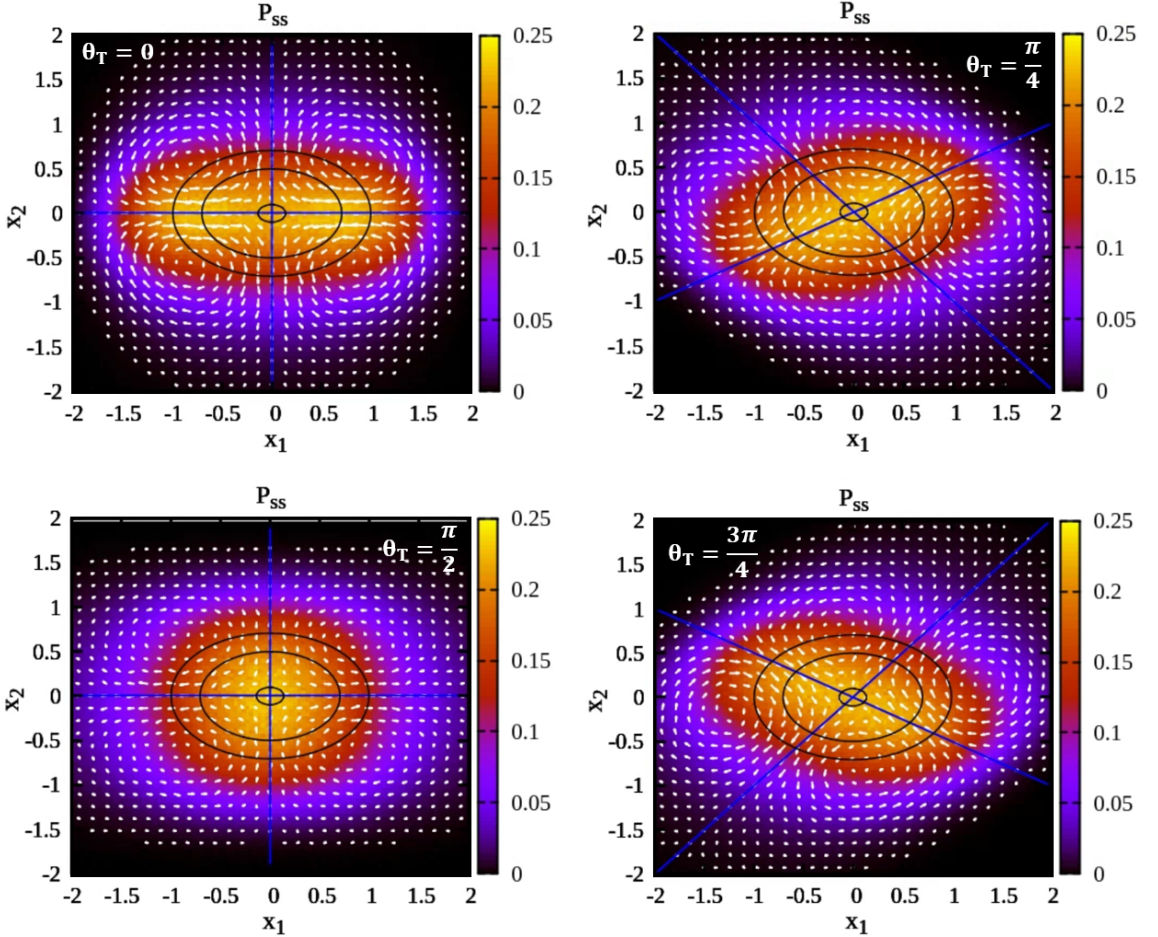


FIGURE 5.3: Under the uniaxial Gaussian temperature field, the Langevin simulation of the steady-state probability density P_{ss} (color map) and the probability flux \vec{J} (vector field) under the fixed harmonic potential and the uniaxial Gaussian temperature field, while black solid curves represent the equipotential curve and the blue solid lines represent the points satisfying $\nabla \times \vec{J} = 0$. The grid size of P_{ss} is $x_{bin} = \frac{4}{99}$ ($N_{sample} = 10^7$) and the grid size of \vec{J} is $x_{bin} = \frac{4}{29}$ ($N_{sample} = 10^4$). We fixed $\sigma_{U1} = \sigma_{T1} = \sqrt{2}$, $\sigma_{U2} = 1$ and $a = 0$.

942 In order to verify Condition 3, we consider the case where the temperature is
943 given by (5.28), i.e., the biaxial Gaussian temperature field. Obviously, the uniaxial
944 case is a special case of the biaxial case with $\sigma_T = \infty$. Comparing the uniaxial and
945 biaxial cases, the former has the curless \vec{J} straight line independent of θ_U , i.e., (5.34),
946 but the two lines in the latter case depend on θ_T and θ_U . The straight lines are given

⁹⁴⁷ by $(A \neq 0)$

$$x_2 = \frac{-B \pm \sqrt{B^2 - AC}}{A} x_1, \quad (5.40)$$

⁹⁴⁸ where

$$A \equiv \Delta_U \Sigma_T \sin(2\theta_U) - \Sigma_U \Delta_T \sin(2\theta_T) + \Delta_U \Delta_T \sin(2(\theta_U - \theta_T)), \quad (5.41)$$

$$B \equiv \Delta_U \Sigma_T \cos(2\theta_U) - \Sigma_U \Delta_T \cos(2\theta_T), \quad (5.42)$$

$$C \equiv -\Delta_U \Sigma_T \sin(2\theta_U) + \Sigma_U \Delta_T \sin(2\theta_T) + \Delta_U \Delta_T \sin(2(\theta_U - \theta_T)). \quad (5.43)$$

⁹⁴⁹ Note that in the above formula, if $\Delta_i = 0$, then the terms involving θ_i will also
⁹⁵⁰ disappear. This is because when $\Delta_i = 0$, it is a circle with no "tilted angles". Taking
⁹⁵¹ the arctangent of the slope and using (5.36) again, we get

$$\begin{aligned} & \Psi(\theta_T - \theta_U) \\ &= \frac{\pi}{2} - \arctan \left(\frac{\operatorname{sgn}(\Delta_T \Delta_U) \sin(2(\theta_T - \theta_U))}{\sqrt{\left(\frac{\Sigma_T}{\Delta_T}\right)^2 + \left(\frac{\Sigma_U}{\Delta_U}\right)^2 - 1 + 2 \left(\frac{\Sigma_T}{\Delta_T}\right) \left(\frac{\Sigma_U}{\Delta_U}\right) \cos(2(\theta_T - \theta_U)) + \cos^2(2(\theta_T - \theta_U))}} \right), \end{aligned} \quad (5.44)$$

⁹⁵² where $\operatorname{sgn}(x)$ is the sign function. This is the most general relative-angle formula
⁹⁵³ of the two $\nabla \times \vec{J} = 0$ lines for the Gaussian temperature field and the harmonic
⁹⁵⁴ potential well. We can check that if σ_{T2} tends to infinity, $\frac{\Sigma_T}{\Delta_T}$ reduces to unity, and
⁹⁵⁵ (5.44) degenerates to equation (5.37). It is worth noting that the formula (5.44) is also a
⁹⁵⁶ function with period π , and when $\theta_T - \theta_U = n\pi/2$ ($n \in \mathbb{N}$), the relative angle between
⁹⁵⁷ the two lines is $\pi/2$ as in the uniaxial case. The difference between the uniaxial and
⁹⁵⁸ the biaxial case is that when $\sigma_{U1} = \sigma_{T1}$ and $\sigma_{U2} = \sigma_{T2}$, Ψ does not exist for $\theta_T - \theta_U = 0$
⁹⁵⁹ or π . This is because in this case, T and U have the same functional form, so the
⁹⁶⁰ system achieves no flux according to Condition 3.

⁹⁶¹ In other words, except in the special case where $\sigma_{U1} = \sigma_{T1}$ and $\sigma_{U2} = \sigma_{T2}$ (making
⁹⁶² $\theta_T - \theta_U = 0$ or π undefined) the relative angle $\Psi = \frac{\pi}{2}$ at $\theta_T - \theta_U = n\pi/2$ for any
⁹⁶³ Gaussian temperature field and harmonic potential well. This is shown in Fig. 5.2(c).

5.2. $T_{12} = T_{21} = 0$ but T_{11} and $T_{22} \neq 0$

964 In the same way, we can calculate the extrema of Ψ . It is given by

$$\theta_T - \theta_U = \frac{1}{2} \arccos(R) \quad (R \leq 1) \quad (5.45)$$

$$\theta_T - \theta_U = \frac{1}{2} \arccos\left(\frac{1}{R}\right) \quad (R \geq 1), \quad (5.46)$$

965 where $R \equiv \frac{\Delta_T \Sigma_u}{\Sigma_T \Delta_u}$. It is not difficult to find that when the major and minor axes are
966 very different, slightly changing the lengths of the major and minor axes will have
967 little change in R . Thus, if σ_{T2} tends to infinity, the relative angle Ψ is independent
968 of the temperature. This explains why the two straight lines have nothing to do with
969 σ_{T1} in the uniaxial temperature field.

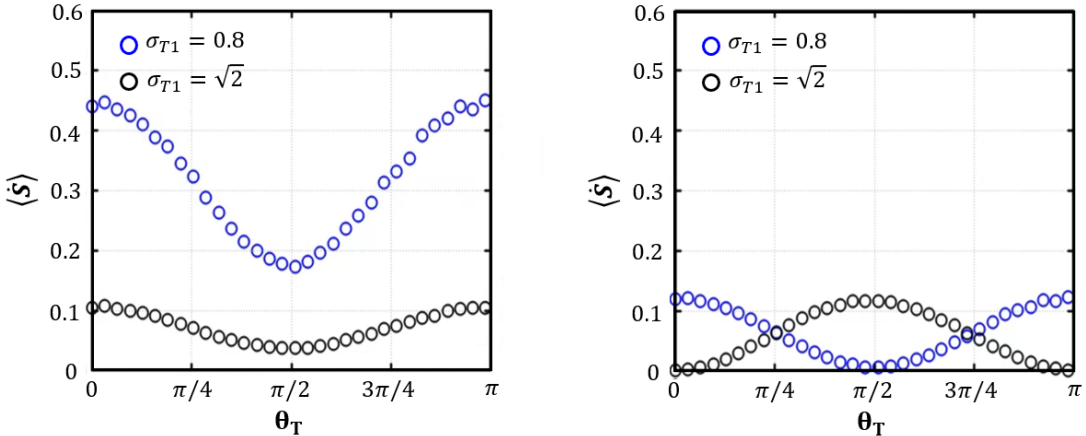


FIGURE 5.4: (a) The Langevin simulation of the total average entropy rate varies with θ_T under the uniaxial Gaussian temperature field (fixed $\sigma_{T2} = \infty$) and the harmonic potential well. (b) The Langevin simulation of the total average entropy rate varies with θ_T under the biaxial Gaussian temperature field (fixed $\sigma_{T2} = 1$) and the harmonic potential well. Both the samples of the figures are $N_{sample} = 10^5$, and $\sigma_{U1} = \sqrt{2}$ and $\sigma_{U2} = 1$.

970 Now, we consider $\sigma_{T1} = \sigma_{U1}$ and $\sigma_{T2} = \sigma_{U2}$. The \vec{J} field is shown in Fig. 5.5,
971 and it is verified that the two straight lines disappeared at $\theta_T = \theta_U$. Again, we also
972 see that \vec{J} does not surround the equiprobability density curve, which is consistent
973 with the prediction of Condition 1, and these two lines pass through $\nabla\phi = 0$, which
974 is Condition 2. The direction of rotation is closely related to Fig. 5.2(c). It can be
975 determined by (5.44), that is,

$$\operatorname{sgn} [\Delta_T \Delta_U \sin(2(\theta_T - \theta_U))]. \quad (5.47)$$

976 If the value is positive (negative), it gyrates counterclockwise (clockwise) around the
977 origin, and if the value is 0, the particle does not gyrate. In addition, when Ψ is at
978 an extreme value, it seems that a Brownian particle is not gyrating fastest, as can be
979 seen from Fig. 5.2. One may have the question: Is the entropy production rate largest
980 when the Brownian particle gyrates fastest around the origin? The answer is no, but
981 it is true for the local vortex rotation. We compare the $\langle \dot{S} \rangle$ of the uniaxial case and
982 the biaxial case as shown in Fig. 5.4. We can see that $\langle \dot{S} \rangle$ in Fig. 5.4(b) is obviously
983 lower than Fig. 5.4(a). This is because the functional form of biaxial T is more similar
984 to U than in the uniaxial T case. In Fig. 5.4(b), the maximum value of $\langle \dot{S} \rangle$ changes
985 when σ_{T1} is changed. This is because the major and minor axes are interchanged.
986 In fact, the entropy production rate calculated in Fig. 5.4 is underestimated. The
987 correct approach is to use the underdamped model to calculate the entropy at the
988 overdamped limit. Overdamped entropy is mainly contributed by the anomalous
989 entropy [4].

990 There may be another question: why is the direction of gyration different in the
991 uniaxial case when σ_{T1} is greater than 1 (Fig. 5.2(b) and 5.2(d))? It is because the
992 parameters tending to infinity are just the opposite. In Fig. 5.2(c), σ_{T2} tends to infinity,
993 but in Fig. 5.2(d), σ_{T1} becomes larger; therefore they will have a phase difference of
994 $\pi/2$. We also show that Ψ has a phase difference of $\pi/2$ when the σ_{T2} goes to infinity
995 (Fig. 5.2(a)) or σ_{T1} goes to infinity (Fig. 5.2(c)).

5.2. $T_{12} = T_{21} = 0$ but T_{11} and $T_{22} \neq 0$

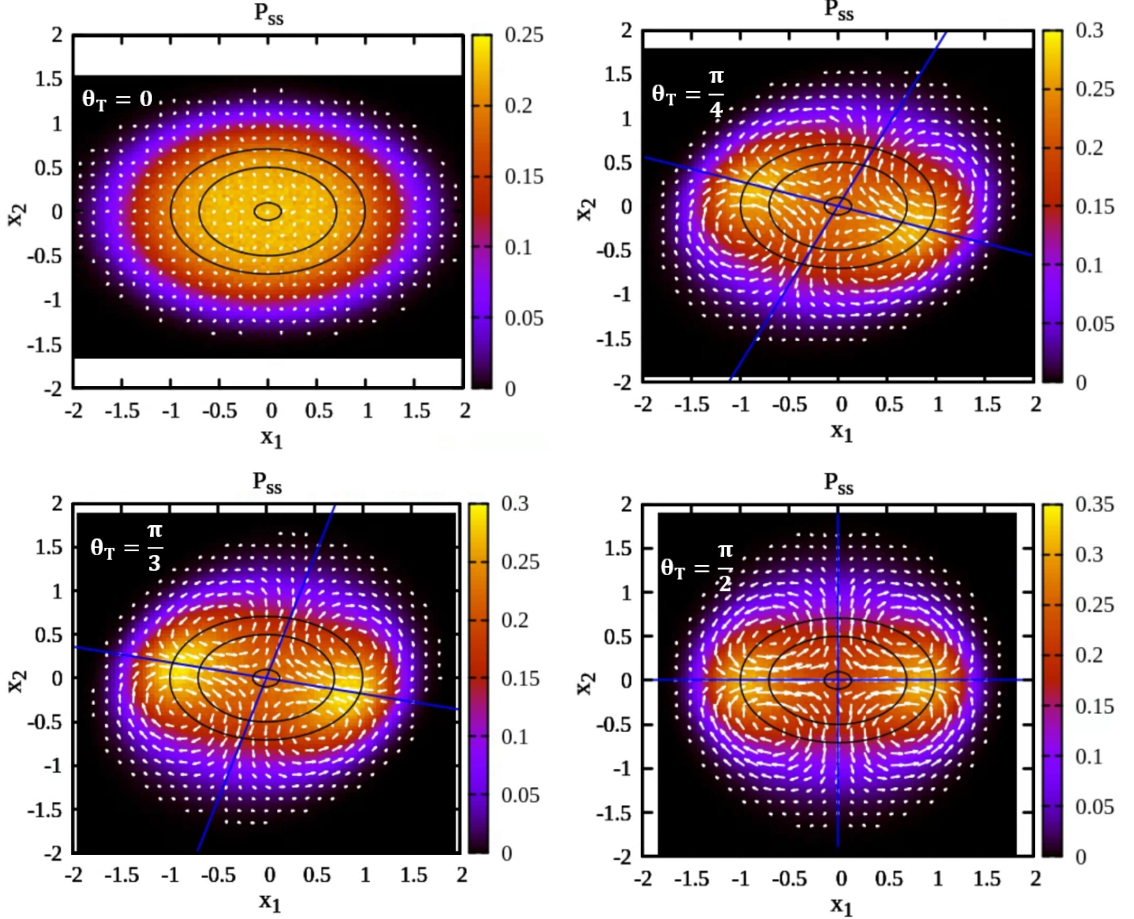


FIGURE 5.5: \vec{J} varies with the tilted angle of temperature $T(x_1, x_2) = a + \exp\left(-\frac{x_1'^2}{\sigma_{T1}^2} - \frac{x_2'^2}{\sigma_{T2}^2}\right)$ under the non-tilted harmonic potential $U(x_1, x_2) = \frac{x_1^2}{\sigma_{U1}^2} + \frac{x_2^2}{\sigma_{U2}^2}$. The color map represents the probability density of the Brownian particle, and the black curves represent the equipotential curves. The vector field is \vec{J} , and the blue lines are the positions where $\nabla \times \vec{J} = 0$. The grid size of P_{ss} is $\frac{4}{99}$ ($N_{sample} = 10^7$) and \vec{v}_{av} is $\frac{4}{29}$ ($N_{sample} = 10^4$). We set $\theta_U = 0$, $a = 0$, $\sigma_{T1} = \sigma_{U1} = \sqrt{2}$ and $\sigma_{T2} = \sigma_{U2} = 1$.

Now, we know that two pairs of different-sized vortices cause the rotation of the Brownian particle in \vec{J} , and we can check whether the points (x_1, x_2) that satisfy $\nabla T \times \nabla U = 0$ have mirror symmetry. If these points have mirror symmetry, then the Brownian particle does not gyrate about the origin because the contributions of the two pairs of vortices to the Brownian trajectory cancel out. This usually happens when the function $T(\vec{r})$ or $U(\vec{r})$ has radial symmetry. Two questions arise: (i) if the local positions solution that satisfies $\nabla \times \vec{J} = 0$ is connected into a loop, how will the flow field of \vec{J} be distributed? (ii) Will some given orbit make the Brownian

1004 particle gyrate better? These two questions can be answered through the Mexican
 1005 hat potential.

1006 **B. Mexican Hat Potential**

1007 Same as before, we designed the Mexican hat potential with a major axis and a minor
 1008 axis, which is given by

$$\begin{aligned} U_{\text{hat}}(x_1, x_2) &= 4E_b \left[-\frac{1}{2} \left(\frac{x_1'^2}{\sigma_{U1}^2} + \frac{x_2'^2}{\sigma_{U2}^2} \right) + \frac{1}{4} \left(\frac{x_1'^2}{\sigma_{U1}^2} + \frac{x_2'^2}{\sigma_{U2}^2} \right)^2 \right] \\ &= 4E_b \left[-\frac{1}{2}U(x_1, x_2) + \frac{1}{4}U(x_1, x_2)^2 \right], \end{aligned} \quad (5.48)$$

1009 where E_b is the barrier height (> 0) and U is defined in (5.30). Consider the temper-
 1010 ature field as (5.28), then the locations that satisfy $\nabla T \times \nabla U_{\text{hat}} = 0$ consist of two
 1011 lines as in the previous harmonic potential well given by (5.40) plus an elliptic curve
 1012 which is the lowest points (groove) in the Mexican hat potential, that is,

$$\frac{(x_1 \cos \theta_U + x_2 \sin \theta_U)^2}{\sigma_{U1}^2} + \frac{(-x_1 \sin \theta_U + x_2 \cos \theta_U)^2}{\sigma_{U2}^2} = 1. \quad (5.49)$$

1013 Note that the loci of $\nabla T \times \nabla U_{\text{hat}} = 0$ are independent of E_b . Now for Langevin
 1014 simulations, we set $\sigma_{T1} = \sigma_{U1} = \sqrt{2}$, $\sigma_{T2} = \sigma_{U2} = 1$, $\theta_U = 0$, and $E_b = 1$. In Fig.
 1015 5.6, we see that when $\theta_T = 0$, the entire system has zero particle flux as expected.
 1016 When $\theta_T = \pi/4$, the P_{ss} distribution has obvious splits and the extreme value of the
 1017 distribution falls on one of the lines, just like Condition 3. Since the elliptic curve and
 1018 the two lines divide the two-dimensional plane, 8 vortices are generated (the centers
 1019 of the vortices are marked by the orange dots in Fig. 5.6(b), but the actual magnitude
 1020 of these vortices is one-seventh times that of Fig. 5.3. Therefore, the average angular
 1021 gyration velocity is smaller than in the previous harmonic potential case.

5.2. $T_{12} = T_{21} = 0$ but T_{11} and $T_{22} \neq 0$

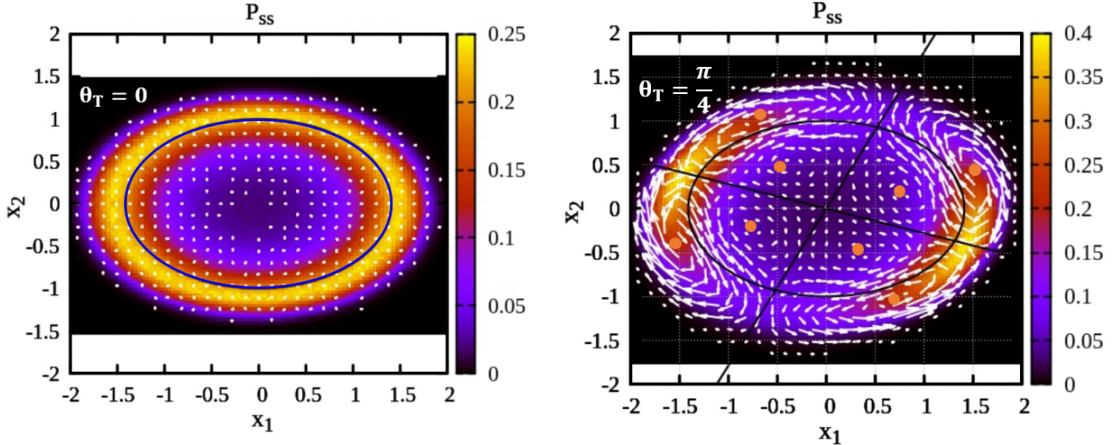


FIGURE 5.6: $E_b = 1$ and under the Mexican hat potential U_{hat} , the steady-state distribution of a Brownian particle through Langevin simulation. The black and blue curves represent $\nabla \times \vec{J} = 0$ and the lowest points of the potential. The orange dots represent the center of the vortices. Note that the \vec{J} vector field (white arrow) is amplified seven times relative to the harmonic potential well.

1022 We also found that the vortex rotation direction will be towards the origin at the
 1023 maximum value of the distribution P_{ss} , both Case A and Case B. This does not seem
 1024 to be a coincidence, and the reason requires further study in the future. In summary,
 1025 we analyze that the steady-state Fokker-Planck equation will produce the particle
 1026 flux for given $U(\vec{r})$ and $T(\vec{r})$, and there is a chance that the average trajectory of the
 1027 particle will gyrate about the origin. The direction of gyration is given by (5.47). For
 1028 the more general case of $T_{11} \neq T_{22}$, whether the zero-particle-flux condition can be
 1029 inferred is one of the directions that can be studied in the future.

CONCLUSION AND OUTLOOK

1032 We study Brownian dynamics under non-uniform temperature fields where the noise
1033 is Gaussian white. We first discuss the one-dimensional confined potential well sys-
1034 tem, which is a particle flux-free system. Then, the effective potential energy is
1035 derived to describe the probability density distribution of a one-dimensional non-
1036 uniform temperature field. The uniaxial temperature field and the single-well po-
1037 tential energy can generate unimodal or bimodal steady-state distributions, which
1038 are determined by the curvature of the potential well and the temperature field at
1039 the origin. The transition rate of the bimodal distribution cannot be directly and
1040 accurately predicted by the conventional Kramers' formula. This is because the tra-
1041 ditional Kramers' formula only applies to uniform temperature systems. To tackle
1042 this problem, we applied the saddle-point approximation to derive an appropriate
1043 approximation for the transition rate under a non-uniform temperature field. We
1044 then illustrated with an example of a harmonic potential well, and then we tried to
1045 generalize the transition rate to arbitrary single-well potential traps and unimodal
1046 temperature fields. It was found that the effective (virtual) barrier also follows the
1047 classical transition rate behavior.

1048 Furthermore, we preliminarily addressed the Landauer limit under a non-uniform
1049 temperature field. The results indicated that the Landauer limit is not simply the
1050 weighted average of the temperature the particle experienced. In the future, we
1051 intend to investigate the fundamental reason for this result, and we shall seek an
1052 optimized protocol that produces the minimum work.

1053 In addition, the reconstruction of a potential and a diffusion field is an impor-
1054 tant issue. We validated our proposed method to reconstruct a unimodal tempera-
1055 ture field by measuring only steady-state particles and diffusion distributions. Re-
1056 construction methods for more general systems will be discussed in future studies.
1057 Although there are various reconstruction methods [13], we still want to explore
1058 whether there is a simpler approach in the future.

1059 In a two-dimensional system, we studied the properties of the probability density
1060 flux \vec{J} and the drift velocity \vec{v}_{av} for a Brownian particle under a potential trap and
1061 non-uniform temperature field. One result is that a nontrivial NESS is achieved, and
1062 the non-vanishing \vec{v}_{av} must not be parallel to the equiprobability density curve. An-
1063 other finding is that we also give the conditions for the system to be non-equilibrium,
1064 and again support the argument that all one-dimensional bound potential systems
1065 are particle-flux free systems. We also found that a non-uniform temperature field
1066 can also cause the average trajectories of the Brownian particle to gyrate around the
1067 origin which is caused by the different sizes of the pairs of vortices of the \vec{J} field, and
1068 the larger pair of vortices dominates the average gyration direction of the Brownian
1069 particle. The nature of \vec{J} differs from the case of two-constant-temperature systems
1070 discussed in the autonomous Brownian gyrator (see [7]). The most prominent differ-
1071 ence, as exemplified for the case of harmonic trap, is that \vec{J} does not gyrate around
1072 the equiprobability curve in the present case, in contrast to [7].

1073 By varying the tilted angle of the potential well and/or the temperature field, the
1074 system can be changed from achieving or not achieving detailed balance. The results
1075 show that when the entropy production rate is maximum (occur at $\theta_T - \theta_U = \frac{\pi}{2}$), \vec{J}
1076 has mirror symmetry; therefore the gyration contributions of the four vortices to the
1077 Brownian particles are offset so that the particles do not gyrate around the trap center.
1078 We also proposed a formula for determining the gyration direction of a Brownian
1079 particle inside a harmonic well and under a Gaussian temperature field that peaks
1080 at the well center, with arbitrary major and minor axes, and tilted angles. Our results
1081 show that the particle does not gyrate when $T(\vec{r})$ or $U(\vec{r})$ has radial symmetry or the
1082 tilted angle difference between T and U is $\frac{n}{2}\pi$ ($n \in \mathbb{N}^+$). Finally, we also derived a
1083 formula for finding the effective potential in high dimensions for systems without
1084 particle flux. All of the above studies need to be observed through experiments in
1085 the future. For non-equilibrium steady states, the effective potential energy can be
1086 found locally (see [18]), but it is still challenging to derive the steady-state P_{ss} for

1087 general $T(\vec{x})$ and $U(\vec{x})$.

1088 For more general two non-uniform temperature fields, whether some properties
1089 of \vec{v}_{av} or \vec{J} can be deduced, and how to extract the work in the Brownian gyrator, is
1090 an interesting research direction for the future. In view of the insights in the present
1091 $T_{11} = T_{22}$ case, we speculate that any confining U under a non-uniform temperature
1092 field with $T_{11} \neq T_{22}$ will result in a non-vanishing \vec{v}_{av} with $\vec{v}_{av} \cdot \nabla \phi \neq 0$.

1093

A

1094

SOME DERIVATIONS

1095

A.1 Overview of the Stochastic Wiener Process

1096 The Wiener process (written as B_t) is a continuous but everywhere non-differentiable
1097 stochastic process, where the subscript t indicates that it is a random number that
1098 evolves over time. The Wiener process is defined to have the following properties:

1099 1. $B_0 = 0$ i.e., the probability $P(B_0 = 0) = 1$.

1100 2. $\{B_{t1} - B_{t0}, B_{t2} - B_{t1}, \dots\}$ are independent. i.e., the increments of a stochastic process
1101 are independent.

1102 3. The increment of Brownian motion obeys Gaussian distribution.

1103 A random process that satisfies these three conditions is called the Wiener process.

1104 In fact, the Wiener process is a standard Brownian motion process. Therefore, some
1105 books define the Wiener process as [22]

$$P(B_{t+\Delta t} = x | B_t = x') = \frac{1}{\sqrt{2\pi\Delta t}} \exp\left(\frac{-(x - x')^2}{2\Delta t}\right), \quad (\text{A.1})$$

1106 for any t and Δt , with the initial state as the Dirac delta function: $P(x, 0) = \delta(x)$. Or
1107 equivalently,

$$\sqrt{2\gamma k_B T} dB_t = \int_t^{t+\Delta t} \xi(s) ds, \quad (\text{A.2})$$

1108 where $\xi(t)$ is the Gaussian white noise, i.e., $\langle \xi(t) \xi(t') \rangle = \sqrt{2k_B T} \delta(t - t')$ and $\langle \xi(t) \rangle = 0$.

1109 Generally, a stochastic differential equation has the form

$$dX_t = \mu(X_t, t) dt + \sigma(X_t, t) dB_t, \quad (\text{A.3})$$

1110 where μ is called the drift term and the diffusion is given by $D = \frac{\sigma^2}{2}$. Taking the
 1111 average for (A.2), we get

$$\langle dB_t \rangle = 0. \quad (\text{A.4})$$

1112 Then, the variance is (using (A.1) when $\Delta t \rightarrow dt$)

$$(dB_t)^2 = \langle (B_t)^2 \rangle - (\langle B_t \rangle)^2 = dt. \quad (\text{A.5})$$

1113 Therefore, if we ignore orders of magnitude above dt , we get

$$(dB_t)^2 = dt, \quad (dB_t dt) = 0, \quad (dt)^2 = 0. \quad (\text{A.6})$$

1114 A.2 Derivation of the Itô Lemma

1115 The Itô lemma can be obtained through Taylor expansion. For any function

$$df(X_t) \equiv f(X_{t+dt}) - f(X_t) = f'(X_t) dX_t + \frac{f''(X_t)}{2} (dX_t)^2 + \dots \quad (\text{A.7})$$

1116 Substituting dX_t (A.3) into (A.7) and using (A.6), one get

$$df(X_t) = \left[\mu(X_t, t) f'(X_t) + \frac{\sigma(X_t, t)^2}{2} f''(X_t, t) \right] dt + \sigma(X_t, t) f'(X_t) \cdot dB_t. \quad (\text{A.8})$$

1117 This is called Itô lemma. Substituting $\sigma^2 = 2D$ into (A.8), we get the equation (2.24)
 1118 in the maintext.

1119 A.3 Derivation of the Mean First Passage Time

1120 The one-dimensional Fokker-Planck operator is defined as

$$\begin{aligned} \mathcal{L} &\equiv \frac{\partial}{\partial x} \frac{1}{\gamma(x)} \left[\frac{\partial U(x)}{\partial x} + k_B \frac{\partial}{\partial x} T(x) \right] \\ &= -\frac{\partial}{\partial x} (\mu(x) P(x, t)) + \frac{\partial^2}{\partial x^2} (D(x) P(x, t)). \end{aligned} \quad (\text{A.9})$$

A.4. Table of Integrals

¹¹²¹ Then, the Fokker-Planck equation is given by

$$\frac{\partial P(x, t|x_0, t_0)}{\partial t} = \mathcal{L}P(x, t|x_0, t_0). \quad (\text{A.10})$$

¹¹²² This is also called the Kolmogorov forward equation. The forward means the par-
¹¹²³ tial differential equations starting from initial conditions (x_0, t_0) we are given. If the
¹¹²⁴ equation given the final condition (x, t) is called the Kolmogorov backward equation
¹¹²⁵ [14].

$$\frac{\partial P(x, t|x_0, t_0)}{\partial t_0} = \mathcal{L}^\dagger P(x, t|x_0, t_0), \quad (\text{A.11})$$

¹¹²⁶ where \dagger is the adjoint operator. Now, our problem is when a particle hits the specified
¹¹²⁷ boundary Ω , its probability density is immediately set to 0. This is called absorbing
¹¹²⁸ boundary conditions, which is the final condition of $P_\Omega(x, t)$. Thus, it should satisfy
¹¹²⁹ the Kolmogorov backward equation (A.11). In addition, if we give the different initial
¹¹³⁰ x_0 ($x_0 \in \Omega$), we will get the different impact times $t_\Omega(x_0)$ to the boundary Ω . The mean
¹¹³¹ of $t_\Omega(x_0)$ is called the mean first passage time, which is given by

$$\langle t_\Omega(x_0) \rangle = \int_0^\infty dt \int_\Omega P_\Omega(x, t|x_0, t_0 = 0) dx. \quad (\text{A.12})$$

¹¹³² Now, we want to know how the $\langle t_\Omega(x_0) \rangle$ evolution therefore we action operator \mathcal{L}^\dagger
¹¹³³ on (A.12) and using (A.11).

$$\mathcal{L}^\dagger \langle t_\Omega(x_0) \rangle = \int_\Omega \partial P(x, t|x_0, t_0 = 0) = -1, \quad (\text{A.13})$$

¹¹³⁴ where -1 is because when $x \in \partial\Omega$, $P(x \in \partial\Omega, t|x_0, t_0 = 0) = 0$; when $x = x_0$,
¹¹³⁵ $P(x = x_0, t|x_0, t_0 = 0) = 1$.

¹¹³⁶ A.4 Table of Integrals

$$\int_{-1}^0 \operatorname{erf}(a(1+x)) dx = \operatorname{erf}(a) + \frac{e^{-a^2} - 1}{a\sqrt{\pi}}. \quad (\text{A.14})$$

BIBLIOGRAPHY

- 1138 [1] John AC Albay, Zhi-Yi Zhou, Chia-Hao Chang, Hsuan-Yi Chen, Jae Sung Lee,
 1139 Cheng-Hung Chang, and Yonggun Jun. Colloidal heat engine driven by engi-
 1140 neered active noise. *Physical Review Research*, 5(3):033208, 2023.
- 1141 [2] Ronald Benjamin and Ryoichi Kawai. Inertial effects in büttiker-landauer motor
 1142 and refrigerator at the overdamped limit. *Physical Review E—Statistical, Nonlin-*
 1143 *ear, and Soft Matter Physics*, 77(5):051132, 2008.
- 1144 [3] Charles H Bennett. Notes on landauer’s principle, reversible computation, and
 1145 maxwell’s demon. *Studies In History and Philosophy of Science Part B: Studies In*
 1146 *History and Philosophy of Modern Physics*, 34(3):501–510, 2003.
- 1147 [4] Antonio Celani, Stefano Bo, Ralf Eichhorn, and Erik Aurell. Anomalous ther-
 1148 modynamics at the microscale. *Physical review letters*, 109(26):260603, 2012.
- 1149 [5] Chia-Hao Chang, Chia-Jung Chang, Nian-Jhu Wu, Yonggun Jun, and Cheng-
 1150 Hung Chang. Stochastic heat engines beyond a unique definition of tempera-
 1151 ture. *Physical Review Research*, 5(4):043085, 2023.
- 1152 [6] Hsin Chang, Chi-Lun Lee, Pik-Yin Lai, and Yung-Fu Chen. Autonomous
 1153 brownian gyrators: A study on gyrating characteristics. *Physical Review E*,
 1154 103(2):022128, 2021.
- 1155 [7] K-H Chiang, C-L Lee, P-Y Lai, and Y-F Chen. Electrical autonomous brownian
 1156 gyrator. *Physical Review E*, 96(3):032123, 2017.
- 1157 [8] Raoul Dillenschneider and Eric Lutz. Memory erasure in small systems. *Physical*
 1158 *review letters*, 102(21):210601, 2009.

BIBLIOGRAPHY

- 1159 [9] DMGualtieri. Feynman-smoluchowski ratchet, 26 October, 2018.
- 1160 [10] Albert Einstein. Über die von der molekularkinetischen theorie der wärme
1161 geforderte bewegung von in ruhenden flüssigkeiten suspendierten teilchen. *Annalen der physik*, 4, 1905.
- 1162
- 1163 [11] Roger Filliger and Peter Reimann. Brownian gyrator: A minimal heat engine on
1164 the nanoscale. *Physical review letters*, 99(23):230602, 2007.
- 1165 [12] Ian J Ford and Robert W Eyre. Work relations for a system governed by tsallis
1166 statistics. *Physical Review E*, 92(2):022143, 2015.
- 1167 [13] Anna Frishman and Pierre Ronceray. Learning force fields from stochastic tra-
1168 jectories. *Physical Review X*, 10(2):021009, 2020.
- 1169 [14] Peter Hänggi, Peter Talkner, and Michal Borkovec. Reaction-rate theory: fifty
1170 years after kramers. *Reviews of modern physics*, 62(2):251, 1990.
- 1171 [15] James T Hynes. Chemical reaction rates and solvent friction. *Journal of Statistical
1172 Physics*, 42:149–168, 1986.
- 1173 [16] Yonggun Jun, Momčilo Gavrilov, and John Bechhoefer. High-precision test of
1174 landauer’ s principle in a feedback trap. *Physical review letters*, 113(19):190601,
1175 2014.
- 1176 [17] Marc TM Koper and Wolfgang Schmickler. A kramers reaction rate theory for
1177 electrochemical ion transfer reactions. *Chemical physics*, 211(1-3):123–133, 1996.
- 1178 [18] Chulan Kwon, Ping Ao, and David J Thouless. Structure of stochastic dynamics
1179 near fixed points. *Proceedings of the National Academy of Sciences*, 102(37):13029–
1180 13033, 2005.
- 1181 [19] Rolf Landauer. Motion out of noisy states. *Journal of statistical physics*, 53:233–
1182 248, 1988.
- 1183 [20] Wenqi Lin, Yi-Hung Liao, Pik-Yin Lai, Yonggun Jun, et al. Stochastic currents
1184 and efficiency in an autonomous heat engine. *Physical Review E*, 106(2):L022106,
1185 2022.

BIBLIOGRAPHY

- 1186 [21] Ignacio A Martínez, Édgar Roldán, Luis Dinis, Dmitri Petrov, Juan MR Par-
1187 rondo, and Raúl A Rica. Brownian carnot engine. *Nature physics*, 12(1):67–70,
1188 2016.
- 1189 [22] Miki Matsuo and Shin-ichi Sasa. Stochastic energetics of non-uniform temper-
1190 ature systems. *Physica A: Statistical Mechanics and its Applications*, 276(1-2):188–
1191 200, 2000.
- 1192 [23] Goran Peskir. On the diffusion coefficient: The einstein relation and beyond.
1193 2003.
- 1194 [24] Barbara Piechocinska. Information erasure. *Physical Review A*, 61(6):062314,
1195 2000.
- 1196 [25] Karel Proesmans, Jannik Ehrich, and John Bechhoefer. Finite-time landauer
1197 principle. *Physical Review Letters*, 125(10):100602, 2020.
- 1198 [26] RK Pathria RK. Statistical mechanics, 1996.
- 1199 [27] Ken Sekimoto. Stochastic energetics, 2010.
- 1200 [28] Yusheng Shen, Chengjie Luo, Yan Wen, Wei He, Pingbo Huang, Hsuan-Yi Chen,
1201 Pik-Yin Lai, and Penger Tong. Directed motion of membrane proteins under an
1202 entropy-driven potential field generated by anchored proteins. *Phys. Rev. Res.*,
1203 3:043195, Dec 2021.
- 1204 [29] Naoto Shiraishi. *An Introduction to Stochastic Thermodynamics: From Basic to Ad-
1205 vanced*, volume 212. Springer Nature, 2023.
- 1206 [30] Charles Soret. Sur l'etat d'équilibre que prend au point de vue de sa concen-
1207 tration une dissolution saline primitivement homogène dont deux parties sont
1208 portées a des températures différentes. *Arch Sci Phys Nat*, 2:48, 1879.
- 1209 [31] Yan Wen, Zhihao Li, Haiqin Wang, Jing Zheng, Jinyao Tang, Pik-Yin Lai, Xin-
1210 peng Xu, and Penger Tong. Activity-assisted barrier crossing of self-propelled
1211 colloids over parallel microgrooves. *Physical Review E*, 107(3):L032601, 2023.
- 1212 [32] Huan-Xiang Zhou. Rate theories for biologists. *Quarterly reviews of biophysics*,
1213 43(2):219–293, 2010.